

Centralized electricity generation in offshore wind farms using hydraulic networks

Jarquín Laguna, Antonio

DOI

[10.4233/uuid:9a8812d1-d152-4a68-bd17-c88261f06481](https://doi.org/10.4233/uuid:9a8812d1-d152-4a68-bd17-c88261f06481)

Publication date

2017

Document Version

Final published version

Citation (APA)

Jarquín Laguna, A. (2017). *Centralized electricity generation in offshore wind farms using hydraulic networks*. [Dissertation (TU Delft), Delft University of Technology]. <https://doi.org/10.4233/uuid:9a8812d1-d152-4a68-bd17-c88261f06481>

Important note

To cite this publication, please use the final published version (if applicable).
Please check the document version above.

Copyright

Other than for strictly personal use, it is not permitted to download, forward or distribute the text or part of it, without the consent of the author(s) and/or copyright holder(s), unless the work is under an open content license such as Creative Commons.

Takedown policy

Please contact us and provide details if you believe this document breaches copyrights.
We will remove access to the work immediately and investigate your claim.

**CENTRALIZED ELECTRICITY GENERATION
IN OFFSHORE WIND FARMS
USING HYDRAULIC NETWORKS**

CENTRALIZED ELECTRICITY GENERATION IN OFFSHORE WIND FARMS USING HYDRAULIC NETWORKS

Proefschrift

ter verkrijging van de graad van doctor
aan de Technische Universiteit Delft,
op gezag van de Rector Magnificus prof. ir. K. C. A. M. Luyben,
voorzitter van het College voor Promoties,
in het openbaar te verdedigen op dinsdag 4 april 2017 om 10:00 uur

door

Antonio JARQUÍN LAGUNA

mech ingenieur
geboren te Toluca, México.

This dissertation has been approved by the (co)promotors:

Prof. dr. A.V. Metrikine
Prof. dr. G.J.W. van Bussel
Dr. ir. J.W. van Wingerden

Composition of the doctoral committee:

Rector Magnificus,	chairperson
Prof. dr. A.V. Metrikine,	Delft University of Technology, promotor
Prof. dr. G.J.W. van Bussel,	Delft University of Technology, promotor
Dr. ir. J.W. van Wingerden,	Delft University of Technology, copromotor

Independent members:

Prof. dr. O.G. Dahlhaug,	Norwegian University of Science and Technology
Prof. dr. ir. A.S.J. Suiker,	Eindhoven University of Technology
Prof. dr. ir. W.S.J. Uijtewaal,	Delft University of Technology
Dr. ing. T. Sant,	University of Malta
Prof. dr. ir. L.J. Sluys,	Delft University of Technology, reserve member



Copyright © 2017 by A. Jarquín Laguna

All rights reserved. No part of the material protected by this copyright notice may be reproduced or utilized in any form or by any means, electronic, or mechanical, including photocopying, recording or by any information storage and retrieval system, without written permission from the copyright owner.

Printed by: Gildeprint - The Netherlands, www.gildeprint.nl

Cover design by Luz María Vergara d'Alençon and Alejandro Prieto Hoces.



ISBN 978-94-6186-778-0

An electronic version of this dissertation is available at
<http://repository.tudelft.nl/>

A mis padres y hermanos.

To my parents and brothers.

ACKNOWLEDGEMENTS

Finalizing my PhD research has certainly been one of the most challenging and rewarding experiences at both personal and professional level. This dissertation would not have been possible without the contribution and support of many people that accompanied me from the beginning of this intense journey. I would like to take the opportunity to thank them all most sincerely.

First of all, I would like to express my sincere gratitude to my supervisors Andrei Metrikine and Gerard van Bussel. Thank you Andrei for your support in the completion of this thesis and for your encouragement to continue working in the field of offshore renewables. Thank you Gerard for having accepted the supervision of my research work and for your comments and opinions given during the development of the thesis. I am also particularly grateful for the assistance given by Jan-Willem van Wingerden. Thank you for the interesting discussions and for your willingness to help and share your knowledge every time I encountered a control related challenge.

I would also like to thank Jan van der Tempel for creating the PhD position in which I had the opportunity to join the offshore wind group. A special mention goes to Niels Diepeveen, with whom I have had the most pleasant and motivating cooperation over the years. I enjoyed very much working together with my former colleagues and offshore wind enthusiasts Wybren de Vries, David Cerda Salzmänn and Maxim Segeren.

Many thanks to all my fellow colleagues and staff members from the groups of Dynamics of Solids and Structures and Offshore Engineering at TU Delft for their support and friendly working environment. I would like to thank Apostolos Tsouvalas for his advice and contribution to one of the publications, and Pim van der Male for the feedback provided during the writing process and for the Dutch translation of my summary.

I would like to thank my paranymphs Bernat Goñi Ros and Phaedra Oikonomopoulou, your friendship is worth more than I can express on paper. Many thanks to Luz María Vergara d'Alençon and Alejandro Prieto Hoces for their help with the cover design.

Special thanks go to all my friends that one way or another have been by my side throughout these years. I am very fortunate to have you all in my life.

Finally, I would like to thank my entire family for their continuous support and unconditional love which have always been with me.

Muchas gracias!

*Antonio Jarquín Laguna
Delft, February 2017*

SUMMARY

Offshore wind is becoming a competitive energy source in the future energy mix of Europe. The growth of offshore wind energy is clearly observed in the large wind farm projects being planned and constructed in the North Sea, reaching total power capacities already in the GW scale. Under the current approach, the produced electricity from each of the wind turbines in a farm is collected and conditioned in an offshore central platform before it is transmitted to shore through subsea cables. From this perspective, an offshore wind farm can be conceived as a power plant which produces electricity from hundreds of multi-MW generators. Hence, the motivation of this thesis follows the idea of producing electricity in a centralized manner from a wind farm using only one or a few large capacity generators.

The work presented in this thesis explores a new way of generation, collection and transmission of wind energy inside a wind farm, in which the electrical conversion does not occur during any intermediate conversion step before the energy has reached the offshore central platform. A centralized approach for electricity generation is considered through the use of fluid power technology. In the proposed concept the conventional geared or direct-drive power drivetrain is replaced by a positive displacement pump. In this manner the rotor nacelle assemblies are dedicated to pressurize water into a hydraulic network. The high pressure water is then collected from the wind turbines of the farm and redirected into a central offshore platform where electricity is generated through a Pelton turbine.

A numerical model is developed to describe the energy conversion process as well as the main dynamic behaviour of the proposed hydraulic wind power plant. The model is able to capture the relevant physics from the dynamic interaction between different turbines coupled to a common hydraulic network and controller. Reduced-order models are presented for the different components in the form of coupled algebraic and ordinary differential equations for their use in time-domain simulations. Special attention is given to the modelling of hydraulic networks where a semi-analytical approach is presented for transient laminar flow using a two-dimensional viscous compressible model. The model allows to analyze the steep variations in the travelling pressure waves which result from abrupt changes in flow or pressure introduced by valve closures or component failures. Furthermore, the model allows to assess the suitability of other methods such as modal approximations which are used for representing hydraulic network transients.

From the control point of view, removing the individual generators and power electronics from the turbines implies that the hydraulic drives need to replace the control actions to achieve the same or at least a similar variable-speed functionality of modern wind turbines. Both passive and active control strategies are proposed using hydraulic components for a variable-speed single wind turbine. Linear control analysis tools are used to evaluate the performance of the proposed controllers. The passive control strategy shows to be inherently stable by using a constant area nozzle for below rated wind

speed conditions. The application of this strategy requires proper dimensioning of the hydraulic components to match the optimal tip speed ratio of the rotor while having a variable pressure in the hydraulic network. The passive strategy is simple and robust but its application is limited to a single turbine. As more turbines are to be incorporated into the same hydraulic network, a constant pressure system is preferred. An active control strategy is also analyzed to obtain a variable speed rotor while keeping a constant pressure in the hydraulic network. The constant pressure control is achieved by modifying the area of the nozzle through a linear actuator. A combination of a PI control in series with a low-pass filter and notches is used to reduce the influence of the pipeline dynamics on the pressure response. In addition, a variable displacement pump operating under the controlled pressure is used to modify the transmitted torque to the rotor.

Two case studies are considered in the time-domain simulations for a hypothetical hydraulic wind farm subject to turbulent wind conditions. The performance and operational parameters of individual turbines are compared with those of a reference wind farm with conventional technology turbines, using the same wind farm layout and environmental conditions. For the presented case study, results indicate that the individual wind turbines are able to operate within the operational limits with the current pressure control concept. Despite the stochastic turbulent wind conditions and wake effects, the hydraulic wind farm is able to produce electricity with reasonable performance in both below and above rated conditions.

CONTENTS

Summary	ix
1 Introduction	1
1.1 Beyond the individual turbine	2
1.2 A new concept for a hydraulic wind power plant	2
1.2.1 Why using hydraulics?	3
1.2.2 High pressure hydraulic power transmission.	3
1.2.3 Water as hydraulic fluid	4
1.2.4 Hydro turbines to centralize electricity generation.	4
1.2.5 Hydraulic network for infield power collection and transmission	5
1.3 Review of fluid power transmissions in offshore wind turbines	6
1.4 Technical feasibility.	10
1.5 Thesis objective and scope	13
1.6 Thesis outline.	14
2 Physical modelling of hydraulic systems	15
2.1 Introduction	15
2.2 Hydraulic drives	15
2.2.1 Positive displacement pumps/motors	15
2.2.2 Hydrostatic transmission	17
2.3 Pelton turbine.	18
2.3.1 Pelton runner performance	19
2.3.2 Nozzle and spear valve.	20
2.4 Hydraulic lines	22
2.4.1 Fundamental relations and assumptions	22
2.4.2 Theoretical modelling of a single hydraulic line	23
2.4.3 Time-domain approximations	28
3 Control aspects	35
3.1 Introduction	35
3.2 Hydraulic control systems	36
3.2.1 Control strategies of hydrostatic drives.	36
3.3 Variable speed operation of wind turbines through hydraulic drives	37
3.3.1 Alternatives to replace the torque controller	40
3.4 Passive speed control analysis	43
3.4.1 Non linear reduced order model	43
3.4.2 Linearisation for control analysis	48
3.4.3 Open-loop analysis	50
3.4.4 Closed-loop response	52

3.5	Active speed control analysis	55
3.5.1	Non-linear reduced order model.	56
3.5.2	Linearisation for control analysis	56
3.5.3	Open-loop analysis	58
3.5.4	Closed-loop response	61
3.6	Other control aspects	63
3.6.1	Pitch control	63
3.6.2	Pelton speed control	63
3.7	Concluding remarks	66
4	Dynamics and performance of a single hydraulic wind turbine	67
4.1	Introduction	67
4.2	System description	67
4.2.1	NREL reference turbine	68
4.2.2	Hydraulic turbine with passive speed control (PSC)	68
4.2.3	Hydraulic turbine with active speed control (ASC)	68
4.3	Mathematical description of the physical system	70
4.3.1	Aerodynamic model	70
4.3.2	Pitch actuator model.	71
4.3.3	Structural model.	71
4.3.4	Hydraulic drivetrain model	71
4.3.5	Generator platform model	73
4.3.6	Sensors model	74
4.4	Steady-state parameters	75
4.5	Time-domain simulations	76
4.5.1	Response to an extreme operational wind gust.	76
4.5.2	Below rated wind speed conditions	78
4.5.3	Above rated wind speed conditions	81
4.6	Concluding remarks	83
5	Hydraulic network transients	85
5.1	Introduction	85
5.2	Fluid transients in hydraulic networks	85
5.3	Proposed semi-analytical method	86
5.3.1	Numerical approach and considerations.	87
5.3.2	Impulse response method for hydraulic networks	89
5.4	Case studies and model comparison	90
5.4.1	Results and discussion	92
5.5	Concluding remarks	97
6	Dynamics and performance of an offshore hydraulic wind power plant	99
6.1	Introduction	99
6.2	Extending the model to more than one turbine	100
6.2.1	Ambient wind field.	100
6.2.2	Wake effects	102
6.2.3	Incorporating the hydraulic network.	104

6.3	Simulation of two turbines	107
6.3.1	Case studies description	107
6.3.2	Time-domain results.	110
6.3.3	Performance comparison	111
6.4	Simulation of an offshore wind farm	117
6.4.1	Farm layout and environmental conditions	117
6.4.2	Time-domain results.	118
6.4.3	Performance comparison	121
6.5	Concluding remarks	122
7	Conclusions	125
	Bibliography	129
	Appendices	137
	Appendix A.	137
	Appendix B.	141
	Appendix C.	143
	Appendix D	147
	Samenvatting	149
	Publications by the author	151
	Curriculum Vitæ	153

1

INTRODUCTION

The European Union (EU) has the ambitious target to provide at least 24% of its final EU electricity consumption from wind energy by the year 2030. At the end of 2016, with a cumulative installed capacity of 12.6 Gigawatts (GW), offshore wind still represents a small fraction of the total installed wind power capacity in the EU of 154 GW (WindEurope, 2017b). Nevertheless, the growth of offshore wind is an essential aspect, which not only has been reflected in the last years by the increasing numbers of installed offshore wind farms mostly in the North Sea, but which most likely will continue in the years ahead. With 24 GW of consented offshore wind projects at present, offshore wind farms are growing in size and essentially becoming power plants in terms of the electrical output close to the GW scale (WindEurope, 2017a).

Despite improvements in technology and knowledge gained from both onshore and recent offshore practice, the cost of offshore wind energy generation needs to be further reduced. Several aspects influence the cost of energy for a particular wind farm, such as the local environmental conditions, the required support structures, the electrical infrastructure, the installation and decommissioning costs, the required maintenance and the wind turbines themselves. A total cost reduction of 40% has been recognized by the different European stakeholders as the sufficient level to secure the future of the industry (van Zuijlen et al., 2014; Det Norske Veritas and Germanischer Lloyd, 2015).

To this end, one of the preferred mechanisms of the industry to reduce the cost of offshore wind energy is aiming at the up-scaling of current technology. This trend has been a common factor since the beginning of the development of offshore wind farms around the year 2000. Since then, the turbine sizes have evolved from 0.5 Megawatts (MW) to 8 MW today, placing them among the largest existing rotating devices on earth; furthermore, commercial turbines of 10 MW are already expected by the year 2020. Fundamental basic research is without doubt needed for the realization of bigger and reliable machines which are necessary for low cost electricity generation at a power plant scale (van Kuik et al., 2016).

1.1. BEYOND THE INDIVIDUAL TURBINE

A typical offshore wind farm consists of an array of identical wind turbines several kilometers from shore. The array is organized in such way that the individual turbines are placed sufficiently far away from each other to reduce their aerodynamic interaction. This interaction, associated with the wakes that they produce while extracting energy from the flow, impacts the individual performance of the turbines and thus reduces the total energy output of the plant (Fleming et al., 2016). The turbines are designed to capture the kinetic energy from the wind and convert it into electrical power in a similar way as is done with onshore technology. From each of the individual turbines, the electrical power is collected and transmitted inside the farm to an offshore substation located inside, or on the edge of the offshore wind farm, where the electricity is collected and conditioned before it is transmitted to shore through subsea cables (Liserre et al., 2011).

Independently of the different offshore wind turbine concepts, one main characteristic of a wind farm as a collection of individual turbines, is that electricity is still generated in a distributed manner. This means that the whole process of electricity generation occurs separately and the electricity is then collected, conditioned and transmitted to shore. On the other hand, when looking at a wind farm as a power plant, it seems reasonable to consider the use of only a few electrical generators of larger capacity rather than around one hundred of generators of lower capacity. The potential benefits, challenges and limitations of a centralized electricity generation scheme for an offshore wind farm are not known yet.

1.2. A NEW CONCEPT FOR A HYDRAULIC WIND POWER PLANT

This dissertation explores a radically new concept where electricity within an offshore wind farm is generated in a centralized manner using pressurized water as power transmission medium. The working principle of using a high pressure flow of hydraulic fluid to transfer the energy captured by a single wind turbine rotor, can be applied and extrapolated to all the wind turbines in a farm. By doing so, a new way of generation, collection and transmission of wind energy is proposed, in which electrical conversion does not occur at any intermediate conversion step before the energy has reached the offshore central power collection platform.

The main idea behind this concept is to dedicate the individual rotor-nacelle assemblies to pump water into a hydraulic network instead of producing electricity. Thus, mechanical power is converted to hydraulic power without any intermediate conversion. Electricity is generated at a central offshore platform through a hydro turbine and is transmitted to shore in a similar way as in the case of conventional offshore wind farms. With this centralized approach, the gearboxes, generators and power electronics from individual turbines are removed, leaving only the rotor shaft directly coupled to a pump. The main motivation for introduction of a centralized offshore wind farm is to reduce the complexity, maintenance and capital cost for the individual rotor nacelle assemblies.

The main aspects of a hydraulic wind power plant are discussed in the following subsections. A conceptual comparison between a conventional and the proposed offshore wind farm is shown in Figure 1.1.

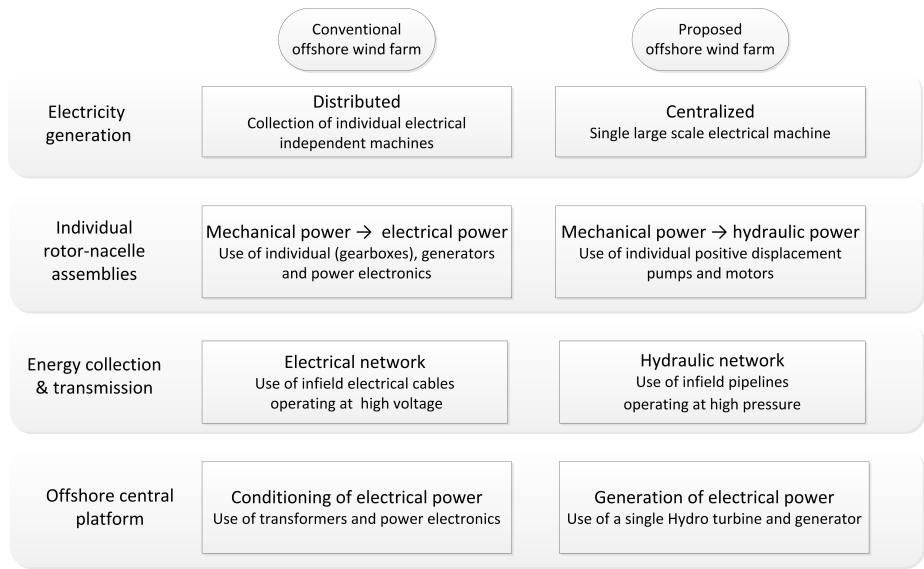


Figure 1.1: Conceptual comparison between a conventional and the proposed offshore wind farm.

1.2.1. WHY USING HYDRAULICS?

Hydraulic systems have already shown their effectiveness when used for demanding applications where performance, durability and reliability are critical aspects. In particular, the efficient and easy generation of linear movements, together with their good dynamic performance give hydraulic drives a clear advantage over mechanical or electrical solutions. Furthermore, hydraulic drives have the potential to facilitate the integration with energy storage devices such as hydraulic accumulators which are important to smooth the energy output from wind energy applications (Innes-Wimsatt and Loth, 2014). In any industry where robust machinery is required to handle large torques, hydraulic drive systems are a common choice. They have a long and successful track record of service in, for example, mobile, industrial, aircraft and offshore applications (Cundiff, 2001; Albers, 2010). Therefore, it is evident that the use of hydraulic technology is recognized as an attractive alternative solution for power conversion wind turbines (Salter, 1984).

1.2.2. HIGH PRESSURE HYDRAULIC POWER TRANSMISSION

The popularity of hydraulic drives, especially in mobile applications, is largely associated with their high power density. When compared to electrical machines, hydraulic drives have a higher torque to weight ratio which allows them to be a very compact technology. This feature is enabled by the high operating pressures that are currently handled, typically between 200 – 350 bar (20 – 35 MPa) for industrial oil hydraulics but as high as 700 bar (70 MPa) for other purpose-specific components. The maximum allowable pressure is determined by the structural limitations and properties of the materials used in the hydraulic components. If higher operating pressures were to be handled by hydraulic drives, it would result in an even more compact technology. For the proposed

concept, using high pressure makes it possible to reduce the top mass of the individual rotor-nacelle assemblies. For this reason, a high potential exists to reduce the amount of structural steel needed in the support structures as well; for a 5 MW turbine in 30 m water depth, 1.9 ton of structural steel of the monopile can be saved for every ton of top mass reduction (Segeren and Diepeveen, 2014). Using high pressures makes the use of fluid power an attractive means to transmit the captured energy from the rotor-nacelle assemblies to a central platform.

1.2.3. WATER AS HYDRAULIC FLUID

A very important aspect to be considered in fluid power technology is the selection of the hydraulic fluid. Mineral oil still remains the leading choice as hydraulic fluid in most industrial applications due to its physical properties over the whole range of operating temperatures and pressures. However, the pressure on the offshore industry to become more environmentally friendly is pushing the case for developments in water hydraulics. Furthermore, in terms of safety, water hydraulics might be preferred due to potential fire hazards or risk of leakage (Trostmann, 1995; Lim et al., 2003). Seawater is a vast resource available offshore and might also be used as hydraulic fluid. It is important to consider that seawater contains a high concentration of minerals, which give it a high degree of hardness. It also contains dissolved gases such as oxygen and chlorine which cause corrosion. Despite its corrosive nature, the use of seawater hydraulics has already been used in some industrial applications; an example in the offshore industry includes the seawater hydraulic system for deep sea pile driving incorporating high pressure water pumps (Schaap, 2012). The use of seawater requires the use of special filters which have to be cleaned more frequently.

Despite the high operating pressures, large volumetric flows of either oil or water, are required for the transmission of dozens or hundreds of MWs. Therefore, from an availability and environmental perspective, the use of water as hydraulic fluid is the preferred choice for centralizing electricity generation in an offshore wind power plant. In combination with one or more large capacity hydro turbines, the pressurized flow of water is used in this concept to generate electrical power in a central offshore platform.

1.2.4. HYDRO TURBINES TO CENTRALIZE ELECTRICITY GENERATION

Hydraulic turbines are the prime movers that transform the energy content of the water into mechanical energy and whose primary function is to drive electric generators. From the existing hydraulic turbines used in hydroelectric power plants, the Pelton turbine is the most suitable to handle high pressures (Dixon and Hall, 2014). Pelton turbines have been built up to a capacity of 423 MW for a single machine (Angehm, 2000) and with operational efficiencies above 90% (Keck et al., 2000). High rotational speed, combined with high torque, enables a compact design. Hence, a wind farm dedicated to pressurize a water flow in a central platform requires only one or a few Pelton turbines to produce electricity using similar technology to what is used in existing hydro-power plants. The same principle has been envisaged in other ocean energy technologies like wave energy farms, where flapping wave energy devices are dedicated to pressurize water into an on-shore power plant where electricity is produced via a Pelton turbine (Whittaker et al., 2007).

An important characteristic of a Pelton turbine is that the nozzle, used to create the water jet, and the runner of the turbine are not physically connected; therefore, it allows to have a physically decoupled system between the individual wind turbines and the hydraulic network at the energy capture side, from the Pelton turbine and generator at the grid side. This means that in case of an off-grid situation, the water jets can be deflected from the hydraulic turbine, while the wind turbines can still operate under normal operational conditions. The above mentioned characteristic has several advantages for the individual turbines and the hydraulic network since they are not affected by electrical disturbances. Electrical disturbances do impose difficulties with current wind farms, especially in complying with grid-fault ride-through requirements (Chen et al., 2009).

1.2.5. HYDRAULIC NETWORK FOR INFIELD POWER COLLECTION AND TRANSMISSION

One of the key aspects for having a centralized electricity generation platform is the use of hydraulic networks to collect and transport the pressurized water from the individual wind turbines to the generator. Similar to the electrical inter-array cable system for a conventional offshore wind farm, the design of the hydraulic piping lay-out should consider several practical and economical aspects, such as reducing the number and length of pipelines, operational losses and installation methods. For wind farms with a large number of turbines, it is expected that branched hydraulic networks using parallel and common pipelines will result in the most convenient configuration. A general overview of the proposed hydraulic wind farm is shown in Figure 1.2.

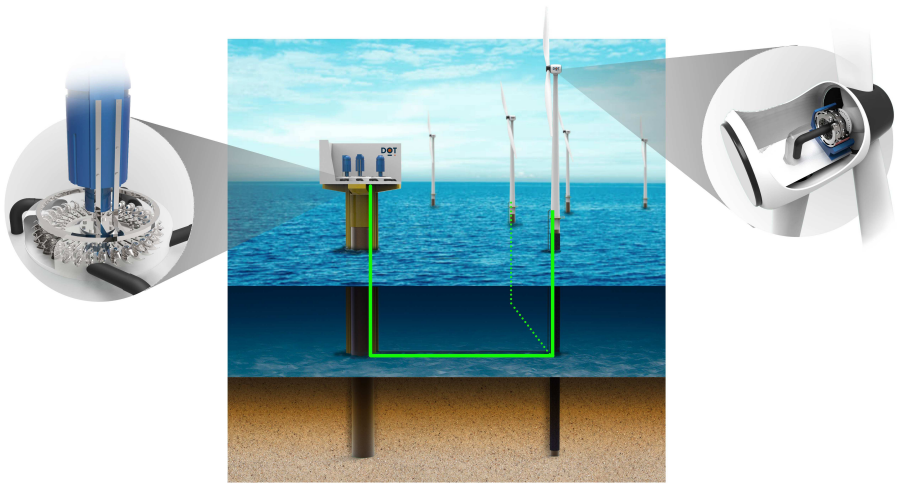


Figure 1.2: Artist impression of an offshore wind farm with centralized electricity generation using fluid power technology. Courtesy of DOT B.V. (DOT, 2016).

1.3. REVIEW OF FLUID POWER TRANSMISSIONS IN OFFSHORE WIND TURBINES

The use of hydraulic technology in modern wind turbines is found in different sub-systems such as the pitch control, the drivetrain brake, the yaw system, and the filter-cooler modules. For these applications the use of hydraulics is usually justified by their high-power density, robust design and high controllability when compared to electro-mechanical systems (Merritt, 1967; Murrenhoff and Linden, 1997). However, one of the most interesting applications of hydraulic technology is its use for the power drivetrain between the rotor and the generator. This brings yet another alternative to the existing geared and direct-drive solutions.

The working principle behind hydraulic power transmissions is that rotating mechanical power from the prime mover is converted into a fluid flow at high pressure by a positive displacement pump; this is known as the hydrostatic principle. At the other end of the hydraulic circuit, the fluid power is converted back to mechanical power and conditioned by a hydraulic motor to a higher rotational speed with a lower torque which is typically required by the electrical machines.

Another type of hydraulic power transmission is based on the hydrodynamic principle, where the momentum of the fluid flow is used to transform the hydraulic power to mechanical power. Although the hydrodynamic transmission is widely used in ground vehicles as torque converters, this particular solution it is not considered in the framework of this thesis since the hydraulic working principle of the transmission is based on hydrodynamics rather than hydrostatics, the latter being the main trend for full hydraulic transmission in wind turbines.

When compared to the commonly used geared or direct-drive transmissions, the hydrostatic transmission is particularly attractive for large offshore wind turbines for different reasons. The first reason is its compactness, as having a more compact and light transmission means less mass at the top of the tower. This mass reduction leads to a significant reduction in the required amount of support structural steel (Segeren and Diepeveen, 2014). The second reason is the possibility of having a transmission ratio between the rotor and the generator that can be modified in a continuous manner. This adds an extra degree of freedom from the control perspective and opens the opportunity to explore different control strategies or physical configurations. For example, an attractive design would be allowing the use of a synchronous generator, thereby eliminating the necessity of most power electronics.

The idea of using hydraulic transmissions in wind energy systems is not a novelty. Experimental prototypes have been developed in the 1980s, like the 6.3 kW project by the Jacobs Energy Research Inc. (JERICO, 1981) and the 3 MW BENDIX/Shackle project (Rybak, 1981). Their results reported low efficiencies and concluded that the application of hydraulic transmission was unsuited for wind turbine applications. The main reason was the lack of components specifically designed for the needs of efficient wind power generation. This argument has been the main historical cause of hydraulics being disregarded as a feasible option for wind turbines. Hence, the most challenging aspect of using hydraulics has been their lower efficiency when compared to a geared and direct-drive solution, especially when operating at conditions below rated nominal power.

The maturing of the fluid power industry together with modern production technologies, have resulted in an improved efficiency and reliability of hydraulic drives. Commercially available pumps and motors, which could be applied in wind turbines, have total efficiencies up to 96% for a broad range of operation (Häggblunds Drive Systems, 2014; Bosch-Rexroth, 2015). Furthermore, with the development of the digital technology, more advanced pumps and motors have achieved efficiencies up to 98%. At the moment, these advanced pumps and motors are in the process of being scaled close to the power ratings of modern wind turbines (Payne et al., 2007). In parallel, efforts from research institutes have focused on a different approach. Researchers from IFAS have used available off-the-shelf components and different control strategies to improve the efficiency and dynamic behaviour, reaching up to 85% efficiency at nominal conditions in their full 1 MW test bench (Schmitz et al., 2010, 2011, 2012). An overview of the main hydraulic transmission systems used in wind turbines is shown in Figure 1.3, where the maturity of each developer's technology is shown according to the technology readiness level (TRL). The main characteristics of these developments are summarized in Table 1.1.

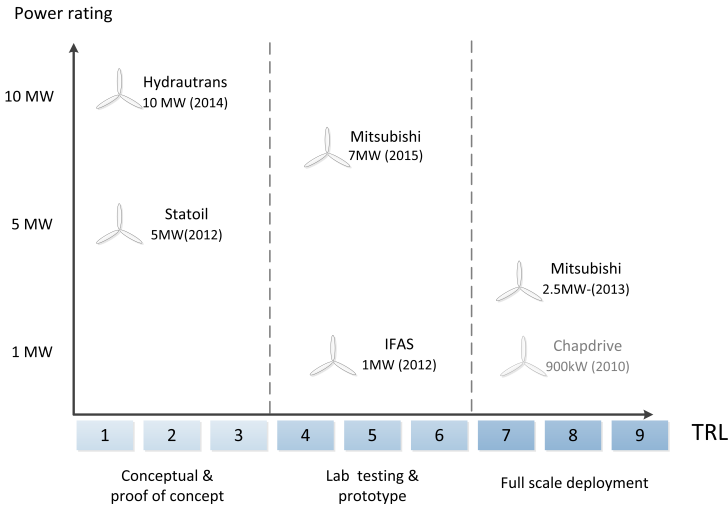


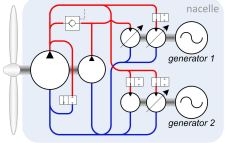
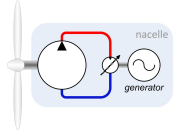
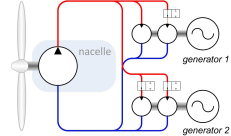
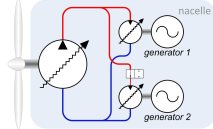
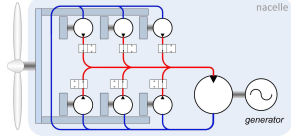
Figure 1.3: Overview of hydraulic transmissions used in wind turbines according to their power rating and technology readiness level (TRL).

Regarding the configuration and the functionality of the motor and pump, not all the concepts have opted for a continuous variable transmission. An alternative idea is based on a two-speed hydraulic transmission using fixed displacement pumps and motors, as proposed by Statoil (Skaare et al., 2011, 2012). The central reasoning of this concept, is to avoid the use of less efficient variable displacement motors. Instead, it uses two highly efficient radial motors that can be switched on/off to allow the rotor to operate close to the optimal rotational speed. The aerodynamic efficiency will be slightly reduced for the greater part of the envelope, but the overall transmission efficiency will be increased. Since 1994, the desire for a highly efficient hydraulic transmission with variable ratio, led the Scottish company Artemis to develop a new type of hydraulic machine. The original

idea was intended for wave and tidal energy applications, but this technology is a good fit for wind energy developments too. Their multi-stroke radial piston pump and motor uses computer controlled valves to engage or idle each of the individual pistons, thereby yielding a high efficiency over the entire range of operation (Payne et al., 2007). This innovation was taken over by Mitsubishi Heavy Industries and implemented into a 2.5 MW onshore wind turbine prototype in 2013. Despite their initial plans to enter the offshore wind market with a 7 MW turbine (Mitsubishi-Heavy-Industries, 2015), it is more likely that this drivetrain technology will only be offered as an option to the 8 MW offshore turbine from the MHI Vestas platform.

On the other hand, other companies foresee a combination of geared and hydraulic components in the drivetrain as a better solution. For instance, Hydrautrans proposes a 10 MW concept using a single stage gearbox with crown-gears in combination with six hydraulic pumps of smaller size (Hydrautrans, 2014). A different 'hybrid' solution is the commercial drivetrain WinDrive developed by Voith (Höhn, 2011). Their technology is based on a hydrodynamic torque converter combined with a planetary gear. This solution also requires a two stage gearbox coupled to the main rotor.

Table 1.1: Main characteristics of fluid power transmissions used in wind turbines.

Developer	Configuration	Hydraulic concept	Electrical concept	Power rating	Technology	Schematic
IFAS (Schmitz et al., 2010, 2011, 2012)	Nacelle based	Hydrostatic with variable transmission ratio	Synchronous without power electronics	1 MW	Commercially available components	
Chapdrive (no longer in business) (Jensen et al., 2012)	Ground based	Hydrostatic with variable transmission ratio	Synchronous without power electronics	2 MW	Commercially available components	
Statoil (Skaare et al., 2011, 2012)	Ground based	Hydrostatic with two fixed ratios	(A)synchronous without power electronics	5 MW	Commercially available components	
Mitsubishi (Mitsubishi-Heavy-Industries, 2015) (Artemis Intelligent Power, 2016) (Taylor, 2012)	Nacelle based	Hydrostatic with variable transmission ratio	Synchronous without power electronics	7 MW	Technology developed by Artemis	
Hydrautrans (Hydrautrans, 2014)	Nacelle based	Hydrostatic with one fixed ratio	Asynchronous with power electronics	10 MW	Technology developed by INNAS	

1.4. TECHNICAL FEASIBILITY

The technical feasibility of a hydraulic offshore wind farm using centralized electricity generation depends on the convergence of three main aspects: the physical principles of wind energy conversion, the available technology in the fluid-power industry and the control strategies employed. From the conceptual to the preliminary design of the proposed idea, a number of technical aspects have to be taken into account before considering the idea of centralized generation as a feasible solution. This thesis builds on with previous research, where the use of available hydraulic technology for offshore wind energy conversion is discussed (Diepeveen, 2013). A graphical representation of the main technical aspects and their interactions is shown in Figure 1.4.

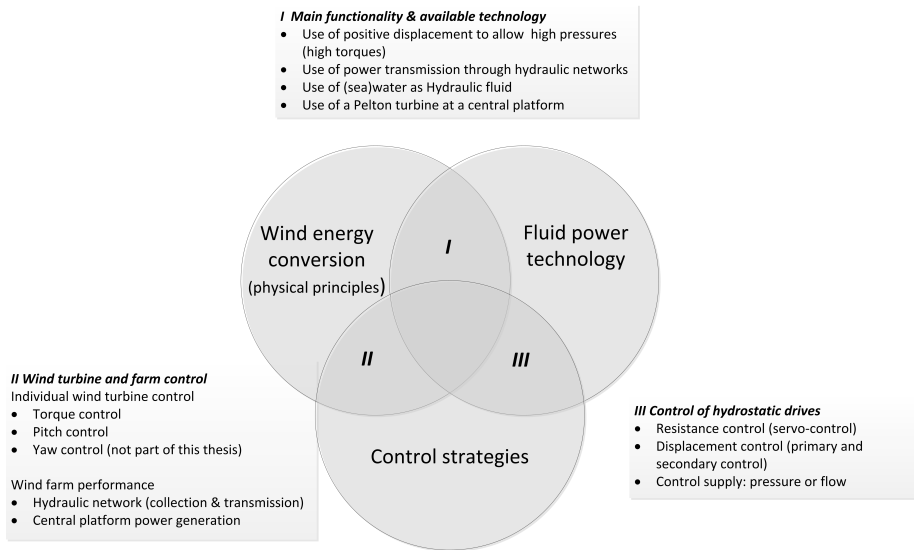


Figure 1.4: Interaction of the technical aspects for centralized electricity generation in an offshore wind farm using fluid power technology.

One of the main challenges is the lack of specific components designed for the required operating conditions, particularly the availability of multi-MW pumps and motors able to work efficiently with water as hydraulic fluid at high pressures. In order to demonstrate the physical principle and feasibility of the proposed concept using available technology, an intermediate solution has been proposed using a hydrostatic transmission between the individual rotors and the water pumps of each turbine. The hydrostatic transmission uses high pressure oil and operates in a similar manner as the drivetrains presented in Section 1.3.

The reasoning behind using a hydrostatic transmission as part of an intermediate solution is based on the following capabilities that this transmission offers:

- It allows to adjust the operational conditions, mainly pressures and rotational speeds, such that commercially available components can be used.
- It gives the opportunity to explore different control strategies by using additional degrees of freedom in the control of hydraulic drives.
- It takes advantage of the current knowledge and best practices from hydrostatic transmissions employed in wind turbines.

On the other hand, the complexity of the concept is significantly increased by introducing extra components which has a direct impact on the reliability and efficiency of the whole system. Nevertheless, this solution should be regarded as a step to demonstrate the feasibility and potential advantages of the concept, before the extension to using hydraulic power collection from a large amount of wind turbines is considered in a complete hydraulic wind farm. A comparison between the conceptual design and a feasible intermediate solution, considering the available technology and operating conditions, is shown in Figure 1.5, with the most important technical aspects is summarized in Table 1.2.

Table 1.2: Comparison between the conceptual design and an intermediate solution in terms of component functionality and technical limitations.

	Component	Motivation	Note
Conceptual design	Seawater pump	Variable displacement drive to allow for variable-speed operation of the rotor.	Non-existing component for the required operating conditions and efficiencies: low speed, high pressures (> 200 bars).
	High pressure water line	Compact design and minimization of friction losses.	Best practice of fluid power industry is to design for a specific range of fluid velocities.
	Adjustable nozzle	A spear valve is used to keep the hydraulic network at constant pressure to allow for collection of flows from different turbines.	A proper control strategy should be included to reduce fluid transients.
	Seawater as hydraulic fluid	Freely available and environmental friendly transmission medium.	Composition of seawater contains many particles and elements which may be harmful due to their corrosive and erosive nature.
	Pelton turbine	Operation at constant speed and variable flow rates.	Power ratings available but maximum pressure is limited to ≈ 200 bars.
Intermediate solution	Radial pump	Fixed displacement drive for high pressure oil hydraulics.	Available component with efficiencies > 94%.
	Hydraulic motor	Variable displacement drive to allow for variable-speed operation of the rotor and drive the water pump at medium/high speed.	Available component.
	Water pump	Fixed displacement unit at medium or high speed.	Available component with lower efficiencies than oil hydraulics.
	Adjustable nozzle	A spear valve is used to keep the hydraulic network at constant pressure to allow for collection of flows from different turbines.	A proper control strategy should be included to reduce fluid transients.
	Water as hydraulic fluid	Freely available and environmental friendly transmission medium.	Use of a closed-loop might be required using filtered seawater.
	Pelton turbine	Operation at constant speed.	Available component.

1

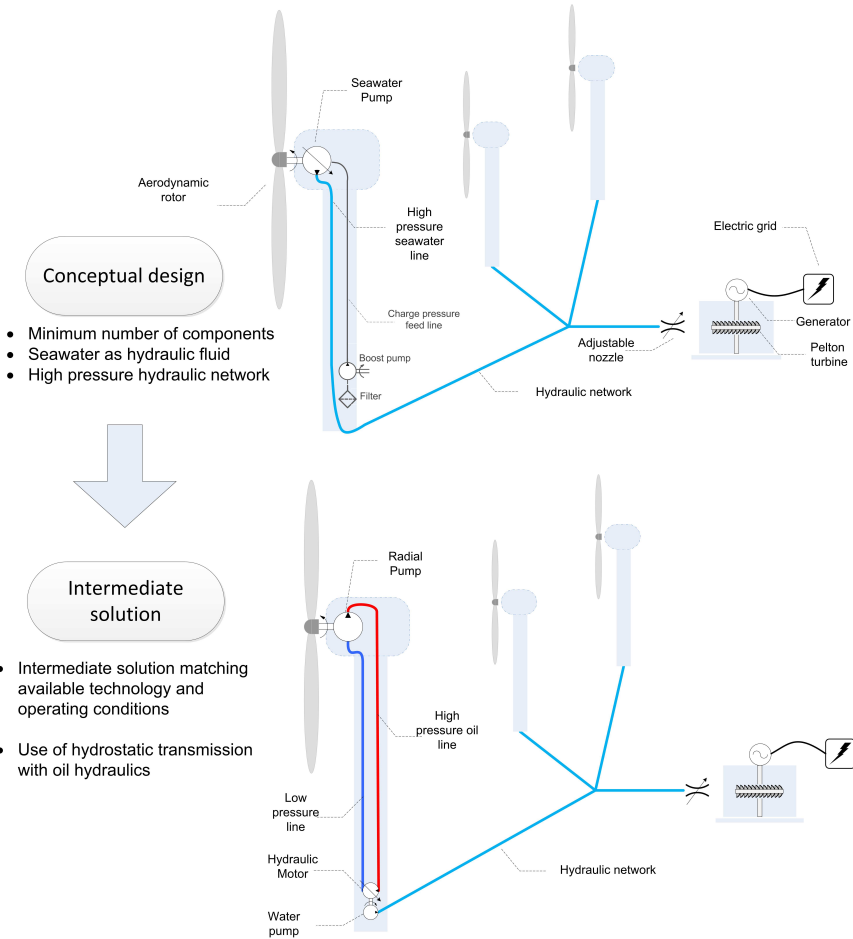


Figure 1.5: Schematics showing the development from the conceptual design to the intermediate solution.

1.5. THESIS OBJECTIVE AND SCOPE

This work focuses on a new concept of wind power plant, where individual wind turbines are used in a hydraulic network to generate electricity in a centralized way. In Sections 1.1 and 1.2, the motivation and the main aspects of a hydraulic wind power plant were presented. Section 1.3 gave an overview of current applications of hydraulic drivetrains that have been explored for its use in wind turbines. Finally Section 1.4 showed how available technology and control strategies could be combined to achieve a feasible technical solution of the initially proposed concept.

As with any new idea, the concept itself has raised several discussions regarding the feasibility and claimed benefits and/or problems when compared to the current technology. Before the proposed concept can be regarded or disregarded as a potential solution, the working principle and operational behaviour of the system have to be better understood. Therefore, in order to contribute to the existing body of work, the objective of this thesis is to understand the influence of a hydraulic network on the operational behaviour of the individual turbines of a hydraulic wind power plant with centralized electricity generation.

Since this concept has not been considered before, the main original contribution of this thesis is the creation of a numerical model that is able to describe and quantify the energy conversion process, as well as the main dynamic behaviour of a hydraulic wind power plant, without the necessity of developing a detailed design or the need for detailed information. In this process, the knowledge from different disciplines such as aerodynamics, hydraulics and control will be brought together and will be used to build a numerical model of the proposed concept. The model will be used to perform time-domain simulations of a hypothetical wind farm under typical wind conditions. Based on the obtained results, this thesis will provide a better basis to compare the main advantages, limitations and challenges of the proposed concept with respect to the current solutions which generate electricity in a distributed manner.

The analysis presented for the wind turbines is being based on modifications to the NREL 5MW baseline rotor, which is used in the field of wind energy research as a representative utility-scale offshore turbine (Jonkman et al., 2009). With respect to the control theory, the performance and design of the controllers is limited to the framework of linear control.

Because of the large flexibility in design and functionality that is offered by fluid power technology, this work only discusses the results of a particular proposed concept. The author expects that the presented work serves as an inspiration, and provides the framework to analyze similar concepts or applications where both wind energy and fluid power technology are combined.

1.6. THESIS OUTLINE

The thesis is composed of seven chapters, the content of which is outlined as follows.

Chapter 2 presents a discussion of the physical modelling of the hydraulic components comprised in a hydraulic wind farm. These components are used as building blocks in the following chapters. Special attention is paid to the dynamics and modelling of the flow characteristics inside the hydraulic lines. All the models are presented in terms of a set of algebraic and ordinary differential equations (ODEs).

In Chapter 3 the main control aspects are addressed for the individual turbines. It is shown how hydraulic technology can be used as a power drivetrain to achieve the optimal aerodynamic performance of modern wind turbines. Both passive and active control strategies are proposed for a variable-speed turbine and reduced order models are used in combination with linear control analysis tools to evaluate the performance of the proposed controllers.

Chapter 4 describes the numerical model of two fictitious offshore wind turbines with hydraulic transmission based on the control strategies defined in the preceding chapter. The hydraulic transmission models are presented using the building blocks from Chapter 2. Time-domain simulation are performed and the results are compared to that of a conventional turbine for both below and above rated wind conditions.

In Chapter 5 a semi-analytical method is proposed to study the hydraulic network transients. The method is based on the impulse response of laminar flow through a hydraulic line and includes the exact solution of a two-dimensional viscous problem in the frequency domain with various interface and boundary conditions. A comparison with existing numerical models for laminar flow dynamics is presented in three time-domain examples.

In Chapter 6 the approach is extended from a single wind turbine towards a hydraulic offshore wind power plant. The first part of the chapter includes a description of the tools used to model the wind field interactions inside the offshore wind farm. Next, simulation results of a simple configuration using only two turbines are presented for different hydraulic networks and control options. The last part of the chapter presents the simulation results of a small hydraulic wind power plant comprising five turbines.

Finally Chapter 7 gives the main findings and the overall conclusions of this thesis.

2

PHYSICAL MODELLING OF HYDRAULIC SYSTEMS

2.1. INTRODUCTION

This chapter addresses the physical modelling of different hydraulic components to be used in combination with various wind turbine subsystems. Reduced-order models are presented in the form of algebraic and ordinary differential equations (ODEs) for their use in time-domain simulations. The chapter is organized as follows. In Sections 2.2 and 2.3, the working principle of different hydraulic systems and their mathematical models is shown. Then, Section 2.4 describes the theory and modelling of the hydraulic line dynamics. The line models will be used in following chapters to interconnect different components and to form hydraulic networks. The chapter is concluded with an example of numerical implementation and comparison of a single blocked line using modal approximations.

2.2. HYDRAULIC DRIVES

2.2.1. POSITIVE DISPLACEMENT PUMPS/MOTORS

In fluid-power technology, the positive displacement principle refers to a fixed volume of fluid that is trapped and forced to move into a separate confined space. In hydraulic systems, this method has been the most efficient way of creating high pressures and therefore the preferred option for handling large forces.

In the framework of this work, the focus is limited to rotating devices, where the physical principle is mostly based on reciprocating pistons. In this way hydraulic pumps and motors are used to convert rotational mechanical energy into hydraulic energy and viceversa. Positive displacement pumps and motors are characterized by a volumetric displacement, which describes the volume of fluid obtained per rotational displacement of the driving shaft. In the case of an ideal pump where no leakages occur, the volumetric displacement V_p relates the volumetric flow rate Q obtained at a certain shaft rotational velocity ω_p (Merritt, 1967):

$$Q = V_p \omega_p \quad (2.1)$$

The ideal torque τ_p required to obtain the pressure difference Δp is given by the following expression:

$$\tau_p = V_p \Delta p \quad (2.2)$$

Hence, for an ideal hydraulic drive (no energy losses), the mechanical power given by the product of the torque and rotational speed is equal to the hydraulic power given by the product of the volumetric flow and the pressure difference across the machine,

$$\tau_p \omega_p = Q \Delta p \quad (2.3)$$

A hydraulic pump or motor is not an ideal machine, there are energy losses that should be considered. In practice, two different efficiencies are defined to describe the nature of the energy losses. A volumetric efficiency is introduced in Equation 2.1 to describe the energy losses that are associated with the volumetric flow rate such as internal or external leakages and compressibility of the fluid. In the same manner, a mechanical efficiency is introduced in Equation 2.2 to account for the energy losses mostly associated with friction forces. The total efficiency of a hydraulic machine is given by the product of both the volumetric and mechanical efficiencies.

A more realistic but still simplified model of a pump is described by the following quasi-static relations which describe the net generated volumetric flow Q_p and transmitted torque τ_p (Merriitt, 1967).

$$Q_p = V_p \omega_p - C_s \Delta p \quad (2.4)$$

$$\tau_p = V_p \Delta p + B_p \omega_p + C_f V_p \Delta p \quad (2.5)$$

The internal leakage losses are described as a function of the pressure difference across the pump through the laminar leakage coefficient C_s . For the transmitted torque, a friction torque is described with a viscous and a dry component defined with the damping coefficient B_p and a friction coefficient C_f , respectively.

For the case of a hydraulic motor the volumetric flow and transmitted torque are:

$$Q_m = V_m \omega_m + C_s \Delta p \quad (2.6)$$

$$\tau_m = V_m \Delta p - B_m \omega_m - C_f V_m \Delta p \quad (2.7)$$

Some of the hydraulic drives are capable of continuously modifying their volumetric displacement per rotational cycle. An adjustable volumetric displacement is physically obtained in different ways, where the combination of a linear actuator and a swash plate is the most commonly used. To account for the variable displacement, Equations 2.4 and 2.5 are modified in the following manner:

$$Q_p = V_p(e) \omega_p - C_s \Delta p \quad (2.8)$$

$$\tau_p = V_p(e) \Delta p + B_p \omega_p + C_f V_p(e) \Delta p \quad (2.9)$$

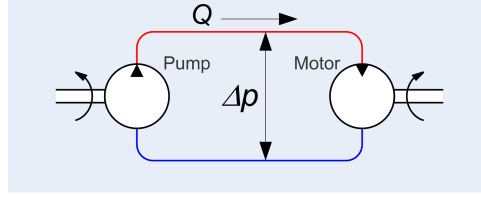


Figure 2.1: Ideal hydrostatic transmission with fixed transmission ratio (Diepeveen, 2013).

where a factor e is introduced as the ratio of the current volumetric displacement and its nominal value per rotational cycle such that:

$$V_p = e V_{p,max} \quad (2.10)$$

The variable e from Equation 2.10 can be used as a control variable to modify either the volumetric flow or the transmitted torque of the pump or motor.

The dynamics of a general actuator used to modify the volumetric displacement of a pump or motor are approximated by a first order differential equation. The constant T_e characterizes the actuator response rate to an arbitrary reference value input e_{dem} according to the following equation:

$$\dot{e} = \frac{1}{T_e} (e_{dem} - e) \quad (2.11)$$

2.2.2. HYDROSTATIC TRANSMISSION

A hydrostatic transmission is created between a prime mover and a secondary mover when two or more hydraulic drives are connected in a hydraulic circuit. Assume that a hydraulic transmission consists of an ideal pump and motor with volumetric displacement V_p and V_m , respectively, as shown in Figure 2.1. Neglecting energy losses in the hydraulic lines, the rotational speed and torque conversion between the prime mover and the load is obtained from Equations 2.1 and 2.2 as:

$$\omega_m = \frac{Q}{V_m} = \frac{V_p}{V_m} \omega_p \quad (2.12)$$

$$\tau_m = \Delta p V_m = \frac{V_m}{V_p} \tau_p \quad (2.13)$$

Hence, the transmission ratio between the prime mover and the load is determined by the ratio of the volumetric displacements of the hydraulic drives. In the case of using a pump or motor with a variable displacement functionality, a variable transmission ratio is achieved, which inherently allows to have a variable-speed operation.

In general, a hydraulic drive circuit can be designed as an open-loop system or closed-loop system. Figure 2.2 shows an example of these two different configurations using hydraulic motors as rotatory actuators. It is important to mention that linear actuators, such as hydraulic cylinders, are very commonly used for the generation of linear movement.

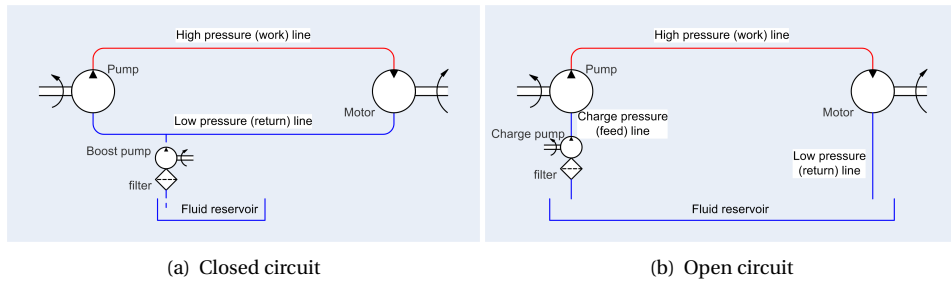


Figure 2.2: Diagrams of closed and open circuit hydraulic transmission systems (Diepeveen, 2013).

2.3. PELTON TURBINE

Once the energy content of the wind is transferred to a pressurized flow of water, it is collected from multiple turbines and transmitted to a central offshore platform. Here, the kinetic energy is extracted from the water through a hydraulic turbine and delivered as mechanical energy to the generator shaft. In this way, centralized electricity generation takes place with the help of an electrical machine.

From the different hydroturbines, the Pelton turbine is particularly suited to high pressure applications and power ratings up to 500 MW (Dixon and Hall, 2014). The Pelton wheel, named after its American inventor Lester A. Pelton, was brought into use in the second half of the 19th century and its appearance has not changed much since then (Doble, 1899). The runner consists of a series of double spoon shaped buckets spaced uniformly along the periphery of a large disc. The water jets are directed to the center of the buckets and tangent to the runner Pitch Circle Diameter (PCD) as shown in the static framework of Figure 2.3. As the water jet hits the runner, a splitter inside the buckets redirects the flow as it leaves in almost opposite direction as the original jet. In this way, the momentum of the water jet is transferred to the runner and this water impulse exerts a torque on the Pelton turbine. The driving energy is supplied only by the kinetic energy contained in the water jet.

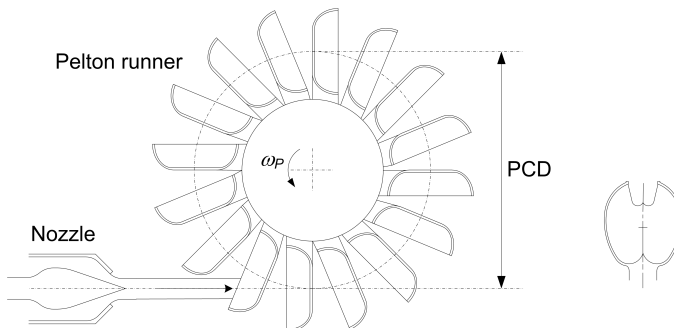


Figure 2.3: Schematized view of a Pelton turbine (left) and a single elliptical bucket from the runner (right).

2.3.1. PELTON RUNNER PERFORMANCE

The hydraulic efficiency of the Pelton runner η_P is obtained from momentum theory according to different geometrical and operational parameters as described in (Thake, 2000) and (Zhang, 2007):

$$\eta_P = 2k(1-k)(1-\xi \cos \gamma) \quad (2.14)$$

where γ is defined as the angle between the circumferential and relative velocities of the flow as shown in Figure 2.4. ξ is an efficiency factor to account for the friction of the flow in the bucket and k is the runner speed ratio defined by the ratio between the tangential velocity of the runner at PCD and the jet speed. R_{PCD} is the radius of the pitch circle, ω_P is the angular velocity of the runner and U_{jet} is the water jet velocity.

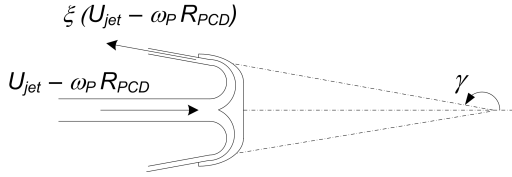


Figure 2.4: Simplified diagram of flow in a Pelton seen from a reference frame fixed to the bucket (only one half of the emergent velocity diagram is shown).

$$k = \frac{\omega_P R_{PCD}}{U_{jet}} \quad (2.15)$$

The theoretical Pelton efficiency is shown in Figure 2.5 for different friction factors and constant bucket angle. Optimal efficiency is obtained when the water jet velocity is twice the tangential velocity of the runner at PCD.

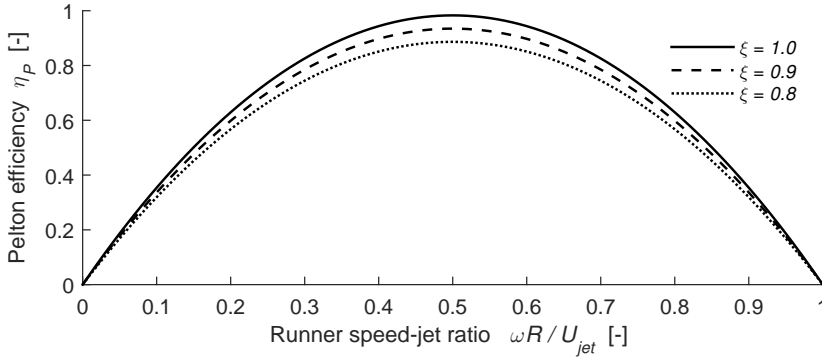


Figure 2.5: Theoretical Pelton efficiency for different values of friction factor ξ and $\gamma = 165$ degrees.

The mechanical torque produced by the Pelton runner τ_P , is then obtained from the hydraulic efficiency calculated in Equation 2.14 and the rotational speed of the runner according to the following expression:

$$\tau_P = \frac{\eta_P P_{hyd}}{\omega_P} \quad (2.16)$$

The electrical power conversion is obtained by considering the hydraulic power contained in the water jet P_{hyd} and the mechanical and electrical efficiencies given by η_P and η_{el} .

$$P_{el} = \eta_P \eta_{el} P_{hyd} \quad (2.17)$$

2.3.2. NOZZLE AND SPEAR VALVE

Nozzle. It is in the nozzles of a Pelton turbine where the pressurized flow is converted into one or more high velocity water jets. The Bernoulli equation is commonly employed to obtain the static pressure-flow relation. Hence, the pressure drop across the nozzle, Δp , is proportional to the square of the velocity or volumetric flow rate Q_{nz} according to the following equation:

$$\Delta p = \frac{1}{2} \frac{\rho_{hyd}}{C_d^2 A_{nz}^2} Q_{nz} |Q_{nz}| \quad (2.18)$$

where ρ_{hyd} is the density of the hydraulic fluid, A_{nz} is the nozzle cross sectional area determined by the position of the spear valve, and C_d is the discharge coefficient to account for pressure losses due to the geometry and flow regime at the nozzle exit (Al'tshul' and Margolin, 1968).

For numerical purposes, it is more convenient to describe the nozzle characteristics as a first order differential equation by taking the momentum equation of fluid particle into account along the nozzle length L_{nz} as described in the following equation (Makinen et al., 2010):

$$\rho_{hyd} L_{nz} \dot{Q}_{nz} = \Delta p A_{nz} - \frac{1}{2} \frac{\rho_{hyd}}{C_d^2 A_{nz}} Q_{nz} |Q_{nz}| \quad (2.19)$$

The hydraulic power at the nozzle P_{hyd} is given by the product of the volumetric flow rate and the pressure of the seawater at this location. The water jet velocity U_{jet} is simply the volumetric flow rate divided by the cross sectional area and multiplied by a *vena contracta* coefficient C_v to account for the change in velocity immediately after the water jet exits the nozzle (Thake, 2000).

$$P_{hyd} = Q_{nz} \Delta p \quad (2.20)$$

$$U_{jet} = C_v \frac{Q_{nz}}{A_{nz}} \quad (2.21)$$

Spear valve. According to Equation 2.18, one way of adapting the pressure and flow characteristics of the nozzle is by modifying its cross sectional area A_{nz} . A variation of this geometrical characteristic is achieved through the use of a spear valve. A conical frustrum geometry is considered where the nozzle cross sectional area is described by

the linear position of the spear valve h_s according to Equation 2.22 (Buhagiar et al., 2016). It is assumed that the spear valve position is smaller than the fixed nozzle diameter ($h_s < d_s$). The geometric characteristics of the spear valve are included through the spear cone angle α as shown in Figure 2.6.

$$A_{nz}(h_s) = \min\left(\pi \left[h_s d_s \sin\left(\frac{\alpha}{2}\right) - h_s^2 \sin^2\left(\frac{\alpha}{2}\right) \cos\left(\frac{\alpha}{2}\right) \right], \frac{\pi}{4} d_s^2\right) \quad (2.22)$$

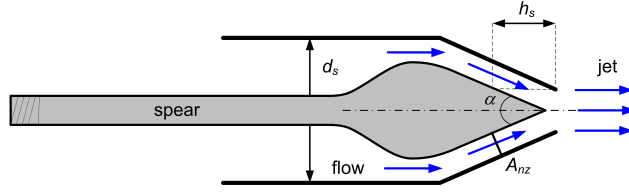


Figure 2.6: Schematic of the spear valve and nozzle.

Figure 2.7 shows the normalized cross sectional area of the nozzle as function of the spear valve linear position for different spear cone angles.

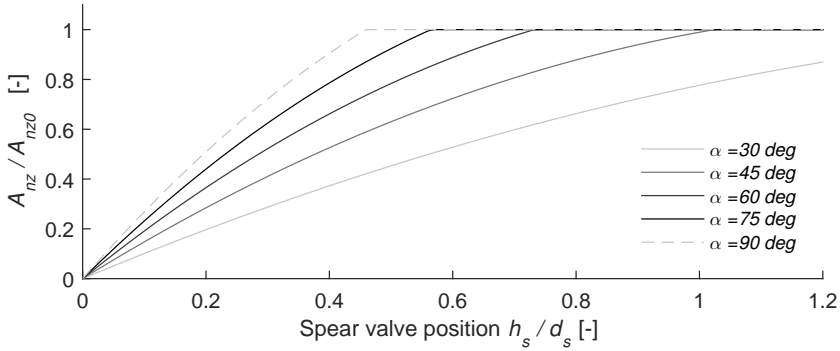


Figure 2.7: Cross sectional area of the nozzle as function of the spear valve linear position for different spear cone angles where $A_{nz0} = \frac{\pi}{4} d_s^2$.

The dynamics of the spear valve linear actuator are approximated by a first order differential equation in which a constant T_h characterizes how slow or fast the spear valve position responds to reference value input $h_{s,dem}$ according to the following equation:

$$\dot{h}_s = \frac{1}{T_h} (h_{s,dem} - h_s) \quad (2.23)$$

2.4. HYDRAULIC LINES

2.4.1. FUNDAMENTAL RELATIONS AND ASSUMPTIONS

In the study of viscous, compressible flows, the unknown quantities to be determined are the three velocity components of the vector \mathbf{u} , the pressure p , density ρ and temperature of the fluid Θ , all of which are functions of the spatial coordinates and time t . For a homogeneous fluid, the equations relating these unknowns are commonly known as the Navier-Stokes equations and are based on the basic principles of conservation of mass, momentum and energy together with a state equation. For single-phase liquid flows in particular, thermal effects can be neglected; this allows the energy equation to be excluded from consideration. Hence, five remaining fundamental equations are required to obtain a solution. The simplified Navier-Stokes equations for a single-phase, compressible Newtonian fluid with laminar flow and constant viscosity become:

The continuity equation or conservation of mass (one equation)

$$\frac{\partial \rho}{\partial t} + \rho_o \nabla \cdot \mathbf{u} = 0 \quad (2.24)$$

The equation of motion or conservation of momentum (three equations)

$$\rho_o \left[\frac{\partial \mathbf{u}}{\partial t} + \mathbf{u} \cdot (\nabla \mathbf{u}) \right] = -\nabla p + \mu_o \nabla^2 \mathbf{u} + \frac{1}{3} \mu_o \nabla (\nabla \cdot \mathbf{u}) \quad (2.25)$$

The state-equation for liquids (one equation)

$$\frac{d\rho}{\rho_o} = \frac{dp}{K} \quad (2.26)$$

where the fluid properties are designated through the fluid density ρ_o , the fluid dynamic viscosity μ_o and the fluid bulk modulus of elasticity K . The derivation of the previous equations from the general Navier-Stokes equations can be found in Appendix A. The underlying assumptions in the previous equations are summarized below.

No bulk viscosity. This is based on the Stokes assumption that there is a relation between the first and second coefficients of viscosity, making the overall bulk viscosity ξ zero.

$$\xi = \left(\lambda + \frac{2}{3} \mu \right) = 0 \quad (2.27)$$

This implies that when the fluid is at rest, the hydrostatic pressure is equal to the thermodynamic pressure. This consideration is true for liquids and removes the bulk viscosity term from the equations of motion.

Constant coefficients. The fluid properties which depend on pressure and temperature are assumed constant. Their average values are used for the physical properties of the fluid at the relevant pressure and temperature. If the pressure variations are relatively small when compared to the bulk modulus of the fluid, then the density variations can be neglected when compared to the average density. As a result, spatial density variations are removed, i.e. $\rho(t)$, and the average density is used as coefficient.

Laminar flow. For steady flow, the criteria for occurrence of turbulence is simply given by the Reynolds number; however, for unsteady flow neither the criteria used to predict

flow instability, nor the manner in which it occurs is well understood. In the case of an oscillating flow component which is superimposed on a mean turbulent flow, the laminar flow solutions might be still applicable over a limited turbulent flow range. Both physical and empirical-based corrections to the shear stress model have been proposed for turbulent pipe transients (Vardy et al., 1993; Vardy and Brown, 1995). The correct modelling of turbulence in transient flows is an ongoing research topic; it is not addressed in this work.

2.4.2. THEORETICAL MODELLING OF A SINGLE HYDRAULIC LINE

Consider a laminar flow, of a Newtonian fluid, through a straight rigid line with a constant diameter, in which the mean fluid velocity is considerably less than the acoustic velocity. The velocities in the axial x -coordinate and radial r -coordinate are denoted by $u_x(x, r, t)$ and $u_r(x, r, t)$, respectively as shown in Figure 2.8.

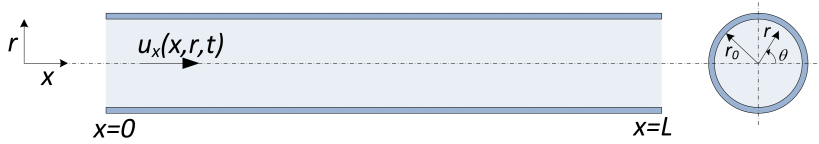


Figure 2.8: Schematic of a single hydraulic line.

With the following assumptions, the Navier-Stokes equations are further simplified for the case of liquid flow through a pipeline; the underlying details are given in Appendix B.

Axisymmetric flow. Due to rotational symmetry, the change of all dependent variables in the circumferential (azimuthal) direction are neglected. This assumption is also applied to pipes with a relatively small curvature radius.

Disturbance propagate isentropically. This implies that the walls of the conduit are perfectly rigid. The isentropic acoustic speed c_o is introduced into the state equation according to $c_o^2 = (K_e / \rho_o)$. The effective bulk modulus of the fluid K_e takes into account the compressibility of the hydraulic fluid and the effect of any entrapped air into the system.

No radial pressure distribution. Assuming that the motion in the radial direction is negligible compared to the motion in the axial direction $u_x \gg u_r$, the radial pressure distribution is constant across the cross-sectional area, i.e. $p(x, t)$. This is only true when the radius of the conduit is smaller than the wavelength of the propagating disturbance.

Non-linear convective acceleration terms are neglected. This is true if the mean fluid velocity is considerably less than the acoustic velocity.

Relevant viscous terms in the equation of motion. The only important viscous terms are those involving the radial distribution of the axial velocity component, other viscous terms can be neglected.

The expanded partial differential equations corresponding to the mass conservation and the momentum equilibrium in the axial direction are reduced to the following two linear partial differential equations (D'Souza and Oldenburger, 1964):

$$\frac{\partial p(x, t)}{\partial t} + c_o^2 \rho_o \left[\frac{\partial u_x(x, r, t)}{\partial x} + \frac{\partial u_r(x, r, t)}{\partial r} + \frac{u_r(x, r, t)}{r} \right] = 0 \quad (2.28)$$

$$\rho_o \frac{\partial u_x(x, r, t)}{\partial t} + \frac{\partial p(x, t)}{\partial x} = \mu_o \left[\frac{\partial^2 u_x(x, r, t)}{\partial r^2} + \frac{1}{r} \frac{\partial u_x(x, r, t)}{\partial r} \right] \quad (2.29)$$

The cross-sectional volumetric flow Q , is obtained through the integration of the axial velocity across the cross-sectional area of the line with finite radius r_0 . The volumetric flow is also defined as the product of the average axial velocity $\bar{u}(x, t)$ and the cross-sectional area:

$$Q(x, t) = \pi r_0^2 \bar{u}(x, t) = \int_0^{r_0} u_x(x, r, t) 2\pi r \, dr \quad (2.30)$$

Equations 2.28 to 2.30 correspond to what is known as a two-dimensional viscous compressible model or dissipative friction model (Goodson and Leonard, 1972; Stecki and Davis, 1986).

2

GENERAL SOLUTION FOR A SINGLE LINE IN THE FREQUENCY DOMAIN

The solution of Equations 2.28 and 2.29 can be obtained in the frequency domain by using the Fourier transform with respect to time according to the following transformation pair,

$$\tilde{f}(\omega) = \mathcal{F}[f(t)] = \int_{-\infty}^{\infty} f(t) e^{-i\omega t} \, dt \quad (2.31)$$

$$f(t) = \mathcal{F}^{-1}[\tilde{f}(\omega)] = \frac{1}{2\pi} \int_{-\infty}^{\infty} \tilde{f}(\omega) e^{i\omega t} \, d\omega \quad (2.32)$$

where ω represents the frequency and $i = \sqrt{-1}$ is the imaginary unit. Let $\bar{U}(x, \omega) = \mathcal{F}[\bar{u}(x, t)]$ and $\bar{P}(x, \omega) = \mathcal{F}[\bar{p}(x, t)]$. The average velocity and the pressure are then given in the frequency domain by the following two equations (D'Souza and Oldenburger, 1964):

$$\bar{U}(x, \omega) = \left[A(\omega) \cos \frac{i\omega\beta}{c_o} x + B(\omega) \sin \frac{i\omega\beta}{c_o} x \right] \frac{J_0 \left[i \left(\frac{i\omega r_0^2}{\nu_o} \right)^{\frac{1}{2}} \right]}{\beta^2} \quad (2.33)$$

$$\bar{P}(x, \omega) = \left[A(\omega) \sin \frac{i\omega\beta}{c_o} x - B(\omega) \cos \frac{i\omega\beta}{c_o} x \right] \frac{\rho_o c_o}{\beta} J_0 \left[i \left(\frac{i\omega r_0^2}{\nu_o} \right)^{\frac{1}{2}} \right] \quad (2.34)$$

in which $A(\omega)$ and $B(\omega)$ are the unknown integration constants to be obtained from the applied boundary conditions, $\nu_o = \mu_o / \rho_o$ is the kinematic viscosity of the fluid and the constant β is expressed through the Bessel functions of the first kind $J_0(z)$ and $J_1(z)$.

$$\beta = \left(\frac{2}{i \left(\frac{i\omega r_0^2}{\nu_o} \right)^{\frac{1}{2}}} \frac{J_1 \left[i \left(\frac{i\omega r_0^2}{\nu_o} \right)^{\frac{1}{2}} \right]}{J_0 \left[i \left(\frac{i\omega r_0^2}{\nu_o} \right)^{\frac{1}{2}} \right]} - 1 \right)^{-\frac{1}{2}} \quad (2.35)$$

Using the boundary conditions at the upstream section where $x = 0$, and at the downstream section with $x = L$, the integration constants $A(\omega)$ and $B(\omega)$ are obtained for a single pipeline. Hence the velocity and pressure at the upstream side $\bar{U}_u(\omega)$ and $\bar{P}_u(\omega)$, can be expressed in terms of the downstream velocity and pressure $\bar{U}_d(\omega)$ and $\bar{P}_d(\omega)$. If the volumetric flow is used instead of the average velocity using Equation 2.30, the following relations can be formulated in the matrix form as follows:

$$\begin{bmatrix} P_u(\omega) \\ Q_u(\omega) \end{bmatrix} = \begin{bmatrix} \cos \frac{i\omega\beta L}{c_o} & -\frac{\beta\rho_o c_o}{\pi r_0^2} \sin \frac{i\omega\beta L}{c_o} \\ \frac{\pi r_0^2}{\beta\rho_o c_o} \sin \frac{i\omega\beta L}{c_o} & \cos \frac{i\omega\beta L}{c_o} \end{bmatrix} \begin{bmatrix} P_d(\omega) \\ Q_d(\omega) \end{bmatrix} \quad (2.36)$$

The solution for a single line can also be expressed in terms of the complex Laplace variable $s = \sigma + i\omega$; where σ is a decay factor and ω represents the frequency. Hence, for $\sigma = 0$ Equation 2.36 is rewritten as,

$$\begin{bmatrix} P_u(s) \\ Q_u(s) \end{bmatrix} = \begin{bmatrix} \cos \frac{s\beta L}{c_o} & -\frac{\beta\rho_o c_o}{\pi r_0^2} \sin \frac{s\beta L}{c_o} \\ \frac{\pi r_0^2}{\beta\rho_o c_o} \sin \frac{s\beta L}{c_o} & \cos \frac{s\beta L}{c_o} \end{bmatrix} \begin{bmatrix} P_d(s) \\ Q_d(s) \end{bmatrix} \quad (2.37)$$

The previous equations are expressed more commonly in terms of hyperbolic functions instead of trigonometric functions using the relations: $\sin ix = -i \sinh x$, and $\cos ix = \cosh x$. The hyperbolic notation is the most usual way to show the solution for a single line as it is expressed only in terms of the line characteristic impedance $Z_c(s)$ and the propagation operator $\Gamma(s)$ (Goodson and Leonard, 1972; Stecki and Davis, 1986):

$$\begin{bmatrix} P_u(s) \\ Q_u(s) \end{bmatrix} = \begin{bmatrix} \cosh \Gamma(s) & Z_c(s) \sinh \Gamma(s) \\ \frac{1}{Z_c(s)} \sinh \Gamma(s) & \cosh \Gamma(s) \end{bmatrix} \begin{bmatrix} P_d(s) \\ Q_d(s) \end{bmatrix} \quad (2.38)$$

This general notation allows to use the solution for the different distributed parameters models, i.e. a 1D inviscid model, or a 1D linear friction model, depending on the expression used for the terms $Z_c(s)$ and $\Gamma(s)$. Using the normalized Laplace variable $\bar{s} = s/\omega_c$, where $\omega_c = \nu_o/r_0^2$ is the viscosity frequency, the line characteristic impedance $Z_c(\bar{s})$ and the propagation operator $\Gamma(\bar{s})$ are given by Table 2.1. Two constants based on the physical properties of the fluid line are introduced, the line impedance Z_0 and the dissipation number of the line D_n which are defined respectively as:

$$Z_0 = \frac{\rho_o c_o}{\pi r_0^2} \quad (2.39)$$

$$D_n = \frac{v_o L}{r_0^2 c_o} \quad (2.40)$$

The value of the dissipation number is important for the transient response, as it gives an indication of the attenuation and distortion along the line. It is given by the ratio of the wave travel time along a line to a term indicative of the transient decay.

Table 2.1: Propagation operator Γ and line characteristic impedance Z_c for different distributed parameter models.

	$\Gamma(\bar{s})$	$Z_c(\bar{s})$
Lossless model (1D inviscid compressible)	$D_n \bar{s}$	Z_0
Linear friction model (1D inviscid compressible)	$D_n \bar{s} \left(1 + \frac{8}{\bar{s}}\right)^{\frac{1}{2}}$	$Z_0 \left(1 + \frac{8}{\bar{s}}\right)^{\frac{1}{2}}$
Dissipative friction model (2D viscous compressible)	$D_n \bar{s} \left(1 - \frac{2}{i(\bar{s})^{\frac{1}{2}}} \frac{J_1 \left[i(\bar{s})^{\frac{1}{2}}\right]}{J_0 \left[i(\bar{s})^{\frac{1}{2}}\right]}\right)^{-\frac{1}{2}}$	$Z_0 \left(1 - \frac{2}{i(\bar{s})^{\frac{1}{2}}} \frac{J_1 \left[i(\bar{s})^{\frac{1}{2}}\right]}{J_0 \left[i(\bar{s})^{\frac{1}{2}}\right]}\right)^{-\frac{1}{2}}$

As an example consider the case of a ‘blocked pipeline’, where the downstream flow rate is zero, $Q_d(s) = 0$. Hence, the downstream pressure is expressed as a function of the upstream pressure according to

$$P_d(s) = \frac{1}{\cosh \Gamma(s)} P_u(s) \quad (2.41)$$

A comparison between the different models is shown in Figure 2.9. The frequency response of the downstream pressure of a blocked line is shown for certain pipeline characteristics.

CAUSALITY AND PHYSICAL REALIZATION

The solution presented in Equation 2.38 is a non-causal representation which gives a good insight in the pipeline dynamics. However, for simulation purposes, it is a primary requirement to establish the causality of the model representation according to different boundary conditions. The physical realization of the pipeline dynamics is a combination of two propagation effects, one in forward direction at the upstream line end boundary, and one in backward direction at the downstream line end boundary. This means, that in terms of the physical variables p and Q , one of them should be chosen as input variable at the upstream end, and one of them should also be chosen as an input at the downstream end.

Therefore, there are four possible input-output configurations corresponding to the four possible sets of physically realizable boundary conditions:

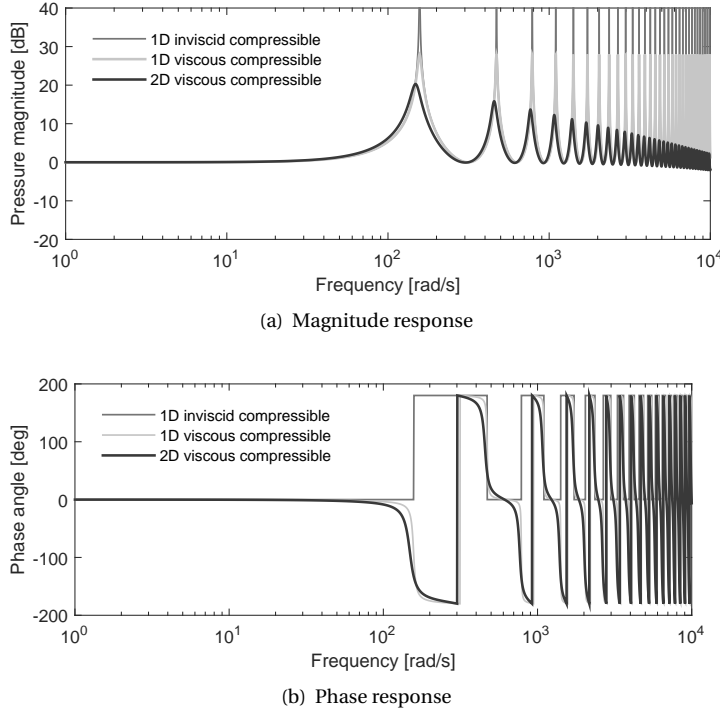


Figure 2.9: Frequency domain comparison for the downstream pressure response of a blocked line for an upstream pressure input $D_n = 0.01$.

Impedance model. The impedance model of a pipeline is defined when the inputs of the model are specified as the flow rates at the two ends of the pipeline. The outputs from the model are the pressures at the upstream and downstream side of the pipeline. This model will be referred as Q-model.

$$\begin{bmatrix} P_u(s) \\ P_d(s) \end{bmatrix} = \begin{bmatrix} \frac{Z_c(s) \cosh \Gamma(s)}{\sinh \Gamma(s)} & -\frac{Z_c(s)}{\sinh \Gamma(s)} \\ \frac{Z_c(s)}{\sinh \Gamma(s)} & -\frac{Z_c(s) \cosh \Gamma(s)}{\sinh \Gamma(s)} \end{bmatrix} \begin{bmatrix} Q_u(s) \\ Q_d(s) \end{bmatrix} \quad (2.42)$$

Admittance model. The admittance model with pressures as input and flow rates as output. The admittance model is defined using the pressures at the two ends of the pipeline as inputs. The outputs from the model are the flow rates at the upstream and downstream side of the pipeline. This model will be referred as P-model.

$$\begin{bmatrix} Q_u(s) \\ Q_d(s) \end{bmatrix} = \begin{bmatrix} \frac{\cosh \Gamma(s)}{Z_c(s) \sinh \Gamma(s)} & -\frac{1}{Z_c(s) \sinh \Gamma(s)} \\ \frac{1}{Z_c(s) \sinh \Gamma(s)} & -\frac{\cosh \Gamma(s)}{Z_c(s) \sinh \Gamma(s)} \end{bmatrix} \begin{bmatrix} P_u(s) \\ P_d(s) \end{bmatrix} \quad (2.43)$$

Pressure-flow model. This model uses mixed boundary conditions with the upstream pressure and downstream flow rate as input, and the downstream pressure and upstream flow rate as output. This model will be referred as PQ-model.

$$\begin{bmatrix} P_d(s) \\ Q_u(s) \end{bmatrix} = \begin{bmatrix} \frac{1}{\cosh \Gamma(s)} & -\frac{Z_c(s) \sinh \Gamma(s)}{\cosh \Gamma(s)} \\ \frac{\sinh \Gamma(s)}{Z_c(s) \cosh \Gamma(s)} & \frac{1}{\cosh \Gamma(s)} \end{bmatrix} \begin{bmatrix} P_u(s) \\ Q_d(s) \end{bmatrix} \quad (2.44)$$

Flow-pressure model Similarly to the previous model, the flow-pressure model uses mixed boundary conditions with upstream flow rate and downstream pressure as input, and downstream flow rate and upstream pressure as output. This model will be referred as QP-model.

$$\begin{bmatrix} Q_d(s) \\ P_u(s) \end{bmatrix} = \begin{bmatrix} \frac{1}{\cosh \Gamma(s)} & -\frac{\sinh \Gamma(s)}{Z_c(s) \cosh \Gamma(s)} \\ \frac{Z_c(s) \sinh \Gamma(s)}{\cosh \Gamma(s)} & \frac{1}{\cosh \Gamma(s)} \end{bmatrix} \begin{bmatrix} Q_u(s) \\ P_d(s) \end{bmatrix} \quad (2.45)$$

2

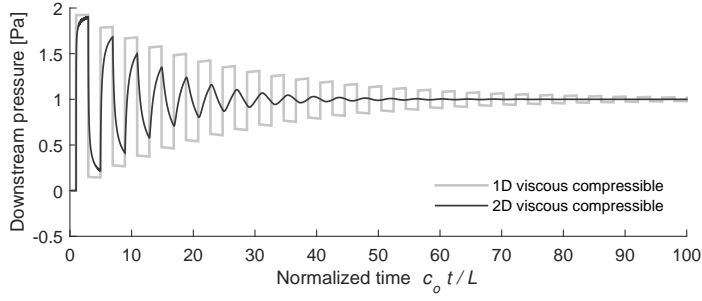
2.4.3. TIME-DOMAIN APPROXIMATIONS

Several numerical methods, which approximate the governing partial differential equations, exist to model fluid transients (Goodson and Leonard, 1972; Stecki and Davis, 1986). To date, the method of characteristics (MOC) is frequently used because of its accuracy, simplicity and ability to include different boundary conditions in the one dimensional case (Wylie et al., 1993a). This method has also been adapted for two dimensional cases to account for the frequency dependence of the friction forces (Zielke, 1968; Trikha, 1975). Figure 2.10 shows the results of using this method for both 1D and 2D approaches; the time-domain response corresponds to the time-domain representation of Equation 2.41.

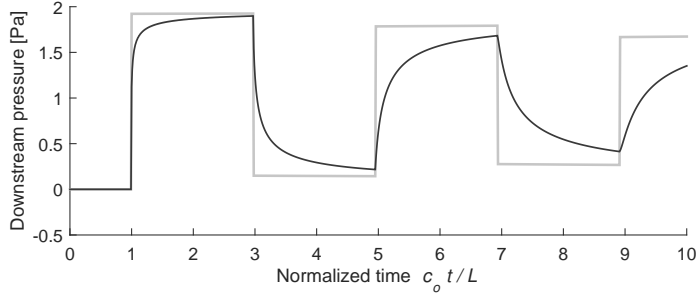
MODAL APPROXIMATIONS

As an alternative to the MOC and other formulations, such as finite differences or finite volumes, the modal method allows to approximate the fluid transients for laminar flow, in both frequency and time-domain, without spatial discretization of the hydraulic line. This modal method has certain advantages when used in time domain simulations, not only because it is easily coupled to other mechanical or hydraulic subsystems, but additionally because it can be implemented and solved numerically with a variable time step ODE solver. Furthermore, several studies have shown that modal methods are more convenient and numerically stable when compared, for example, with discrete methods (Watton and Tadmori, 1988; Soumelidis et al., 2005).

The idea behind this technique is to represent the transcendental expressions in the frequency domain, as a finite summation of low-order rational polynomial transfer functions. Thus, it is possible to approximate each mode of the transmission line in the time domain by a second order linear differential equation (Hsue and Hullender, 1983; Yang and Tobler, 1991; Van Schothorst, 1997; Ayalew and Kulakowski, 2005). These quadratic modal forms are possible by using the infinite product representation of the hyperbolic functions as described by (Hsue and Hullender, 1983), where:



(a) Downstream pressure response of a blocked line subject to an upstream step pressure



(b) Close-up of the unit step response

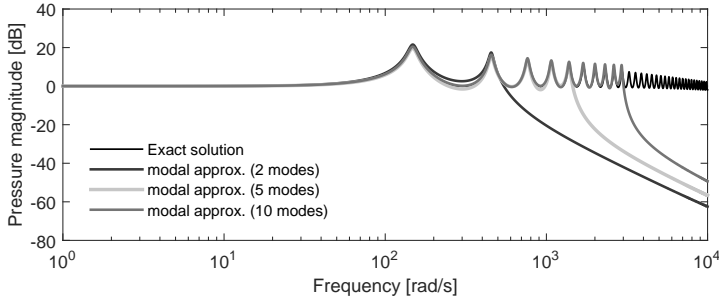
Figure 2.10: Comparison between the response of two distributed parameter models for a pipeline with $D_n = 0.01$. Results obtained using the method of characteristics.

$$\cosh \Gamma(s) = \prod_{n=1}^{\infty} \left[1 + \frac{4\Gamma^2(s)}{(2n-1)^2 \pi^2} \right] \quad (2.46)$$

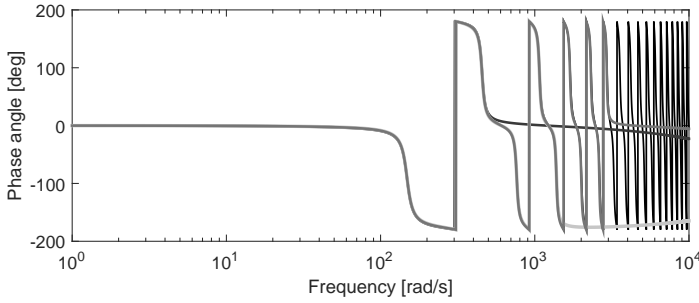
$$\sinh \Gamma(s) = \Gamma(s) \prod_{n=1}^{\infty} \left[1 + \frac{\Gamma^2(s)}{n^2 \pi^2} \right] \quad (2.47)$$

For the dissipative friction model, a product series representation of the Bessel functions is also required to approximate the propagation operator Γ and the line characteristic impedance Z_c . After using the partial fraction expansion of the product series, the transcendental transfer functions from Equations 2.42, 2.43, 2.44 and 2.45 can be approximated in a rational polynomial form; for example the transfer function from Equation 2.41 can be approximated with the following expression:

$$\frac{1}{\cosh \Gamma(s)} = \sum_{i=1}^n \frac{a_i s + b_i}{s^2 + 2\zeta_i \omega_{ni} s + \omega_{ni}^2} \quad (2.48)$$



(a) Magnitude response



(b) Phase response

Figure 2.11: Frequency domain comparison for the downstream pressure response of a blocked line using the modal method $D_n = 0.01$.

Similar formulations of the modal method have also been proposed by (Piché and Ellman, 1995) and (Mäkinen et al., 2000). It is important to mention that this method requires a finite number of modes or truncated terms of the series which will result in an oscillatory response known as Gibbs' phenomenon. One means of reducing or smoothing these oscillations is to use the Lanczos sigma factor technique (Scheid, 1988). An example of the modal approximation is given in Figure 2.11, where the downstream pressure is shown in the frequency domain for a blocked line.

APPROXIMATION OF THE TRANSFER FUNCTIONS

The continuous time models representation based on the modal approximations of Equations 2.42, 2.43, 2.44 and 2.45 have been formulated as a time invariant systems in (Mäkinen et al., 2000). The proposed distributed parameter models are a two-port model based on volumetric flow rates and pressures at the upstream and downstream side of the pipeline.

The formulation is derived from the transfer functions based on a trigonometric basis. In this approach a change of variables is used for the pressures and flow rates, in which they are decomposed into a 'symmetric' and 'antisymmetric' components:

$$P_s = \frac{P_u + P_d}{2}, \quad Q_s = \frac{Q_u + Q_d}{2} \quad (2.49)$$

$$P_a = \frac{P_u - P_d}{2}, \quad Q_a = \frac{Q_u - Q_d}{2} \quad (2.50)$$

In this way the symmetric and antisymmetric pressures are written in the following manner for the Q-model,

$$P_s = Z_0 H_s Q_s, \quad P_a = Z_0 H_a Q_a \quad (2.51)$$

where the symmetric and antisymmetric transfer functions H_s and H_a are defined in terms of the normalized variable $\bar{s} = Ts$. The physical parameter T , represents the wave travel time and is defined as:

$$T = \frac{L}{c_o} \quad (2.52)$$

$$H_s(\bar{s}) = \frac{2}{\bar{s}} + \sum_{i=2,4,\dots}^n \frac{4\Gamma^2/\bar{s}}{\Gamma^2 + (i\pi)^2}, \quad H_a(\bar{s}) = \sum_{i=1,3,\dots}^{n-1} \frac{4\Gamma^2/\bar{s}}{\Gamma^2 + (i\pi)^2} \quad (2.53)$$

The approximation of the propagation operator from the definitions of Table 2.1 lead to the following approximations of the transfer functions:

$$H_s(s) = \frac{2}{Ts} + \sum_{i=2,4,\dots}^n \frac{4\sigma_i Ts + 4\sigma_i (8D_n)}{T^2 s^2 + \epsilon_i Ts + \omega_i^2}, \quad H_a(s) = \sum_{i=1,3,\dots}^{n-1} \frac{4\sigma_i Ts + 4\sigma_i b_n (8D_n)}{T^2 s^2 + \epsilon_i Ts + \omega_i^2} \quad (2.54)$$

The modal natural frequency ω_i and the modal damping coefficient ϵ_i are given by:

$$\omega_i = \alpha_i - \frac{1}{2}\sqrt{2\alpha_i D_n} + \frac{1}{2}D_n \quad (2.55)$$

$$\epsilon_i = \sqrt{2\alpha_i D_n} + D_n \quad (2.56)$$

$$\alpha_i = i\pi, \quad i = 1, 2, 3, \dots, n \quad (2.57)$$

As mentioned before, the following attenuation factors σ_i , might be used to reduce the spurious oscillations due to the finite number of modes used. Similarly, the factor b_n , is used to obtain the correct steady-state pressure drop value due to the finite number of modes used.

$$\sigma_i = \frac{\sin\left(\frac{i\pi}{n+1}\right)}{\frac{i\pi}{n+1}}, \quad (2.58)$$

$$b_n = \left(8 \sum_{i=1,3,\dots}^{n-1} \frac{\sigma_i}{\omega_i^2}\right)^{-1} \quad (2.59)$$

STATE-SPACE REPRESENTATION OF THE IMPEDANCE MODEL

For the impedance model, the transfer functions from Equations 2.53 are represented by single order linear differential equations:

$$\begin{aligned}
 \dot{p}_0 &= \frac{2}{T} Z_0 Q_s \\
 \dot{p}_1 &= \frac{4\sigma_1 b_n (8D_n)}{T^2} Z_0 Q_a - \frac{\omega_1^2}{T^2} p_1, & \dot{p}_1 &= \frac{4\sigma_1}{T} Z_0 Q_a - \frac{\epsilon_1}{T} p_1 + r_1 \\
 \dot{p}_2 &= -\frac{\omega_2^2}{T^2} p_2, & \dot{p}_2 &= \frac{4\sigma_2}{T} Z_0 Q_s - \frac{\epsilon_2}{T} p_2 + r_2 \\
 \dot{p}_3 &= \frac{4\sigma_3 b_n (8D_n)}{T^2} Z_0 Q_a - \frac{\omega_3^2}{T^2} p_3, & \dot{p}_3 &= \frac{4\sigma_3}{T} Z_0 Q_a - \frac{\epsilon_3}{T} p_3 + r_3 \\
 \dot{p}_4 &= -\frac{\omega_4^2}{T^2} p_4, & \dot{p}_4 &= \frac{4\sigma_4}{T} Z_0 Q_s - \frac{\epsilon_4}{T} p_4 + r_4 \\
 &\vdots & & \\
 \dot{p}_n &= -\frac{\omega_n^2}{T^2} p_n, & \dot{p}_n &= \frac{4\sigma_n}{T} Z_0 Q_s - \frac{\epsilon_n}{T} p_n + r_n
 \end{aligned} \tag{2.60}$$

$$\begin{aligned}
 p_u &= p_0 + p_1 + p_2 + p_3 + p_4 + \dots + p_n \\
 p_d &= p_0 - p_1 + p_2 - p_3 + p_4 - \dots + p_n
 \end{aligned}$$

In a more general manner, this representation is known as the state-space form such that:

$$\dot{\mathbf{x}} = \mathbf{A}\mathbf{x} + \mathbf{B}\mathbf{u} \tag{2.61}$$

$$\mathbf{y} = \mathbf{C}\mathbf{x} + \mathbf{D}\mathbf{u} \tag{2.62}$$

where, \mathbf{x} is the state vector, \mathbf{u} is the input vector and \mathbf{y} is the output vector. Matrices \mathbf{A} , \mathbf{B} , \mathbf{C} and \mathbf{D} are known as state-space matrices. Hence, the state-space formulation of Equation 2.42 or Q-model is given by

$$\text{Q-model} \left\{ \begin{aligned} \dot{\mathbf{x}} &= \mathbf{A}_Q \mathbf{x} + \mathbf{B}_Q \begin{bmatrix} Q_u \\ Q_d \end{bmatrix} \\ \begin{bmatrix} \Delta p_u \\ \Delta p_d \end{bmatrix} &= \mathbf{C}_Q \mathbf{x} \end{aligned} \right. \tag{2.63}$$

Here, \mathbf{x} is the state vector given by:

$$\mathbf{x} = [p_0, r_1, p_1, r_2, p_2, \dots, r_n, p_n]^T \tag{2.64}$$

The matrices \mathbf{A}_Q , \mathbf{B}_Q and \mathbf{C}_Q are defined in terms of the physical parameters of the hydraulic line:

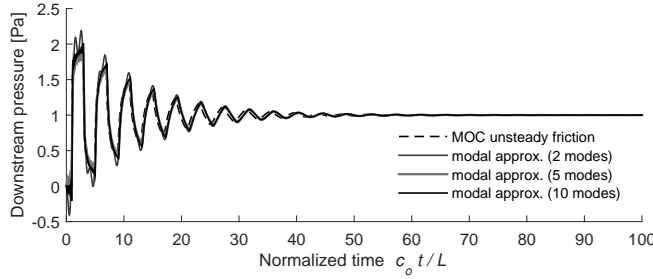
$$\mathbf{A}_Q = \text{diag} [0, \mathbf{A}_1, \mathbf{A}_2, \dots, \mathbf{A}_n], \quad \mathbf{A}_i = \begin{bmatrix} 0 & -\frac{\omega_i^2}{T^2} \\ 1 & -\frac{\xi_i}{T} \end{bmatrix} \quad (2.65)$$

$$\mathbf{B}_Q = \begin{bmatrix} \mathbf{B}_0 \\ \mathbf{B}_1 \\ \vdots \\ \mathbf{B}_n \end{bmatrix}_{(2n+1) \times 2} \quad \left\{ \begin{array}{l} \mathbf{B}_0 = \frac{Z_0}{T} \begin{bmatrix} 1 & -1 \end{bmatrix} \\ \mathbf{B}_{2i-1} = \frac{2Z_0 \sigma_{2i-1}}{T^2} \begin{bmatrix} 8D_n b_n & 8D_n b_n \\ T & T \end{bmatrix} \\ \mathbf{B}_{2i} = \frac{2Z_0 \sigma_{2i}}{T^2} \begin{bmatrix} 8D_n & -8D_n \\ T & -T \end{bmatrix} \end{array} \right. \quad (2.66)$$

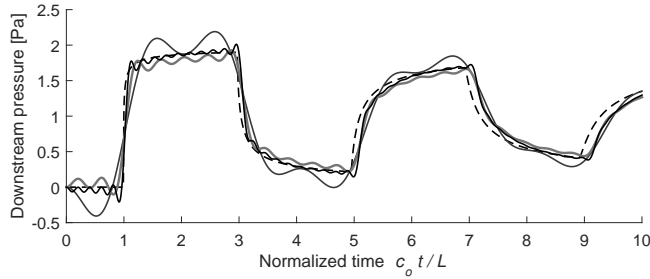
$$\mathbf{C}_Q = \begin{bmatrix} 1 & 0 & 1 & 0 & 1 & 0 & \dots \\ 1 & 0 & -1 & 0 & -1 & 0 & \dots \end{bmatrix}_{2 \times (2n+1)} \quad (2.67)$$

An example of the time-domain implementation is shown in Figure 2.12, where the downstream pressure response of a blocked line is presented using this approximation. The state-space representation of the remaining models from Equations 2.43, 2.44 and 2.45 is presented in (Makinen et al., 2010) and reproduced in Appendix C.

2



(a) Downstream pressure response of a blocked line subject to an upstream step pressure



(b) Close-up of the unit step response

Figure 2.12: Time domain comparison for the downstream pressure response of a blocked line using the modal method $D_n = 0.01$.

3

CONTROL ASPECTS

3.1. INTRODUCTION

For an offshore wind farm, it is essential that the proper operation of every single turbine is maintained independently of the technology used for the energy transmission. To this end, active control actions are required by every single turbine to comply with the different objectives such as power regulation and load mitigation among others. The term ‘active control’, refers to the general manipulation of the turbine properties or settings during operation.

In modern wind turbines, mainly three independent control actions are used to ensure a proper aerodynamic performance for the different operating regions. The first one is to orient the whole rotor-nacelle assembly towards the main wind direction in such a way that it perpendicularly faces the wind stream; this action is referred as *yaw control*. The second one is to change the orientation of the blades to influence the aerodynamic loads acting on the rotor; this action is known as *pitch control*. The third action is commonly referred to as variable-speed operation and consists in adjusting the rotational velocity of the rotor between certain limits. This last control operation can be achieved in two different manners: by modifying the blades pitch angle, or by applying a torque to accelerate or decelerate the rotor through the electrical generator and power electronics; this control action is known as *generator torque control*.

The so-called variable-speed operation is of particular interest in the framework of this thesis because by removing the individual generators and power electronics from the turbines, as stated in the motivation of this work, the hydraulic drives need to replace the control actions to achieve the same or at least a similar variable-speed functionality. Therefore, this chapter explores alternative solutions and limitations of the rotor-speed control for both active and passive hydraulic configurations. Both the yaw and pitch control strategies will remain unchanged with respect to conventional modern wind turbines.

Parts of this chapter have been published in *Journal of Physics: Conference Series*, 555(1) (Diepeveen and Jarquin Laguna, 2014) and are reproduced here with permission of the co-author.

The chapter is organized as follows. Section 3.2 gives a general overview and classification of the hydraulic control systems. In Section 3.3 it is shown how the hydraulic systems can be used to achieve a variable speed operation of the wind turbines. The following sections, make use of linear control analysis tools to evaluate the performance of two different variable-speed control options: a passive control strategy is analyzed in Section 3.4, and an active control strategy is evaluated in Section 3.5. Finally, Section 3.6 presents other control aspects relevant to the proposed hydraulic concept like the Pelton turbine speed control.

3.2. HYDRAULIC CONTROL SYSTEMS

3.2.1. CONTROL STRATEGIES OF HYDROSTATIC DRIVES

In general, hydraulic drives can be used to control different mechanical quantities:

- position (x or θ) or velocity (\dot{x} or $\dot{\theta}$)
- acceleration (\ddot{x} or $\ddot{\theta}$)
- force F or torque τ

In order to achieve the control objectives, different control actions are required. Hence, the hydraulic systems are classified according to the kind of control actions carried out by the hydraulic components (Murrenhoff, 1999):

3

Resistance-controlled drives. They make use of a control valve or servo-valve in the main circuit. This kind of control inherently induces energy losses in the system due to the throttling action of the valves. The energy losses are dissipated as thermal energy leading to the heating of the hydraulic fluid. Thus, resistance-control drives are not very suitable for efficient power transmission; they are typically used for power classes below 10 kW.

Displacement-controlled drives. They make use of a linear actuator to modify the volumetric displacement of the rotary drives. The linear actuator might still use a servo valve but the power losses are avoided in the main circuit. However, the efficiency of variable-displacement drives themselves is typically lower than that of the fixed-displacement drives depending on the operating pressures and rotational speeds. For the supply of hydraulic systems, pressure controls or flow control are mainly used in the fluid power industry. Hydrostatic drives with either a resistance control or a displacement control with flow supply are also called '*primary controlled*'. One characteristic of primary controlled drives, is that each drive needs its own supply.

Displacement controlled systems with a pressure supply are often referred as '*secondary controlled drives*'. In contrast to primary controlled drives, a secondary control allows parallel drives fed by one main pressure supply but it also requires variable displacement motors. Thus, linear actuators cannot be used easily for secondary control. An overview of the different control strategies according to the kind of control actions and hydraulic supply is shown in Figure 3.1.

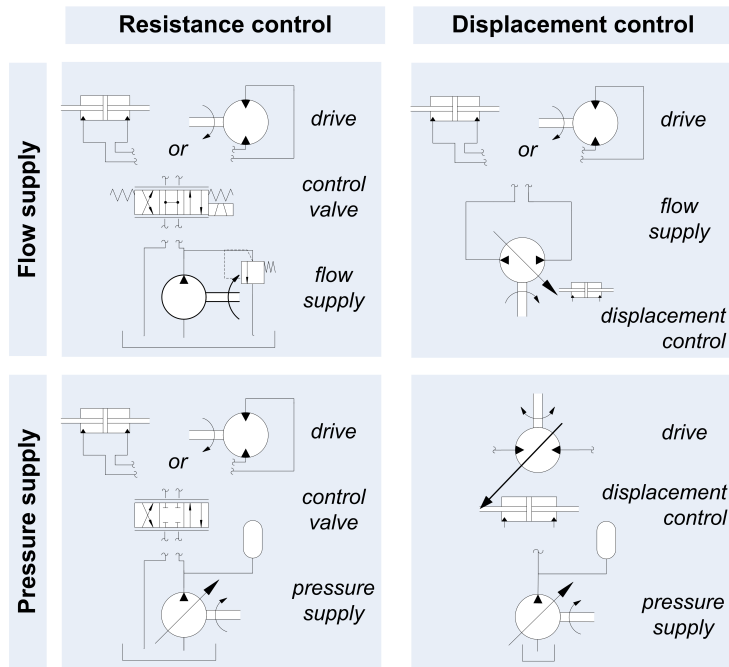


Figure 3.1: Diagram of hydraulic control strategies, reproduced from (Murrenhoff, 1999). For efficient power transmission, displacement control strategies are preferred over resistance control.

3.3. VARIABLE SPEED OPERATION OF WIND TURBINES THROUGH HYDRAULIC DRIVES

A wind turbine is typically characterized by the power that can be extracted from the different operating wind speeds. This is represented through a so-called power curve, where three separate regions are mainly distinguished based on different wind speed thresholds as shown in Figure 3.2.

Region 1 corresponds to wind speeds below U_{cut-in} . In this region, the energy content of the wind is relatively low and generation of electricity is not worthy, therefore the rotor is in idle operation without producing electrical power. For wind speeds between U_{cut-in} and rated wind speed U_{rated} , the turbine operates in region 2. In this below-rated region the main objective is to maximize the energy extraction from the wind. In region 3, the operating wind speeds are above U_{rated} , here the main objective is to maintain a constant nominal power capture P_{rated} , while keeping the turbine within its design limits. Above the cut-out wind speed $U_{cut-out}$, the turbine is shut down to avoid potential structural overload. The choice by a wind turbine manufacturer of the cut-in, cut-out, rated wind speed and nominal power is the result of different physical and economic constraints.

The aerodynamic characteristics of a horizontal axis wind turbine rotor is a function of its rotational speed ω_r , the pitch angle of the blades β and the relative velocity of the up-

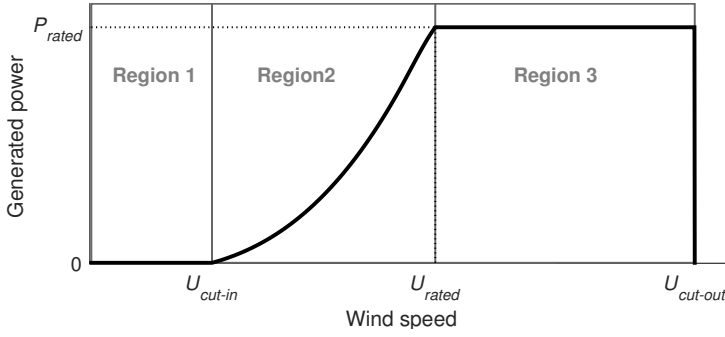


Figure 3.2: Ideal power curve of an individual wind turbine.

stream wind speed U_{rel} with respect to the rotor. Typically, the torque, thrust and power performance are described through their non-dimensional steady-state coefficients as a function of the upstream wind speed (Burton et al., 2011):

$$\tau_{aero} = C_T(\lambda, \beta) \frac{1}{2} \rho_{air} \pi R^3 U_{rel}^2 \quad (3.1)$$

$$F_{thrust} = C_{Fax}(\lambda, \beta) \frac{1}{2} \rho_{air} \pi R^2 U_{rel}^2 \quad (3.2)$$

$$P_{aero} = C_P(\lambda, \beta) \frac{1}{2} \rho_{air} \pi R^2 U_{rel}^3 \quad (3.3)$$

where the following relation is satisfied for the torque and power coefficients

$$C_P = \lambda C_T \quad (3.4)$$

These aerodynamic coefficients are generally expressed as a function of the tip speed ratio λ and the blades pitch angle. The tip speed ratio is a non-dimensional parameter which relates the tangential velocity of the blade tip and the upstream undisturbed wind speed.

$$\lambda = \frac{\omega_r R}{U_{rel}} \quad (3.5)$$

During normal operation of a horizontal axis wind turbine in the region 2, below-rated wind speed, the power capture is maximized by modifying the rotational speed of the rotor while keeping a constant pitch-angle of the blades. Hence, the aerodynamic loading of the rotor is described through quasi-static relations for the torque, thrust and power only as a function of the tip-speed ratio. Figure 3.3 shows an example of the torque and power coefficients of a three-bladed turbine with a fixed pitch angle.

The main idea of a variable speed wind turbine is that in order to operate at maximum aerodynamic performance in region 2, the rotor should be able to operate with a constant tip speed ratio where the maximum power coefficient $C_{p,max}$ is achieved for the required range of wind speeds. The optimal static relationship between the aerodynamic

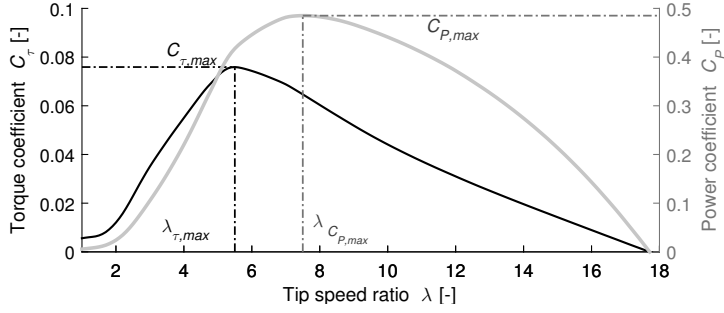


Figure 3.3: Torque and power coefficients at rated pitch angle $\beta = 0$.

torque as a function of the rotor speed is described with the following equation by inserting Equations 3.4 and 3.5 into 3.1,

$$\tau_{aero} = K_1 \omega_r^2 \quad (3.6)$$

$$K_1 = \frac{C_{Pmax}}{\lambda_{Pmax}^3} \frac{1}{2} \rho_{air} \pi R^5 \quad (3.7)$$

The theoretical location of the optimal performance for the different wind speeds and rotational speeds of a wind turbine described by Equation 3.6 is shown in Figure 3.4.

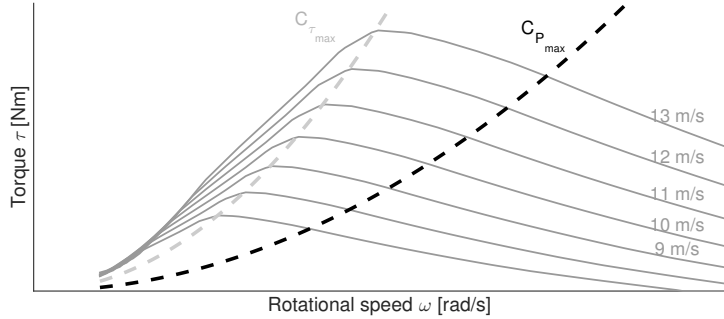


Figure 3.4: The optimal aerodynamic performance follows a quadratic relation between the aerodynamic torque and the rotational speed of the rotor denoted by the dashed black line.

In a conventional drivetrain, the reaction torque at the generator side should be in equilibrium with the aerodynamic torque described in Equation 3.6. Hence, the required steady-state torque from the generator side is expressed as a function of the generator speed, which is often measured. The transmission ratio of the gearbox G is included to relate both the torque and speed of the rotor to the torque and speed of the generator. Under the assumption of a rigid shaft, the following control strategy is used to define the generator torque:

$$\tau_{gen} = K_2 \omega_{gen}^2 \quad (3.8)$$

$$K_2 = \frac{C_{pmax}}{G^3 \lambda_{pmax}^3} \frac{1}{2} \rho_{air} \pi R^5 \quad (3.9)$$

From above equations, it can be observed that for maximum aerodynamic performance, the ideal steady-state relation between the torque and the rotational speed follows a quadratic function. A simple but satisfactory way of incorporating a variable speed operation, is to use this quadratic relation to set the torque demand of the generator as a function of the measured generator speed.

The quadratic relation based on the measured generator speed is widely used because of its simplicity, stability and smoothness. However in turbulent winds, the large rotational inertia of the rotor prevents it from changing its speed fast enough, resulting in small deviations from the optimal point of operation with a reduced C_p . In this case, other control strategies, such as Proportional-Integral (PI) control with an indirect estimation of the wind speed have also been used to improve the performance of the variable-speed rotor (Bossanyi, 2000; Bianchi et al., 1997). Furthermore, additional controllers might be added to the reference generator-torque control to account for structural vibrations. These vibrations are caused by the excitation of certain structural modes of the turbine. In particular, the first tower fore-aft vibrational mode and the drivetrain torsional mode are important as they have a direct impact on the turbine response and the available measurements (Bossanyi and Witcher, 2009).

3

3.3.1. ALTERNATIVES TO REPLACE THE TORQUE CONTROLLER

In order to achieve a variable speed operation in wind turbines using hydraulic drives, the generator torque control strategy has to be replaced. Two different modes of operation have been explored in this work: a passive or compliant control, and an active control strategy.

PASSIVE TORQUE CONTROL STRATEGY

It is possible to configure the fluid power transmission system in such a way that no form of active control is required to adjust the rotor speed below rated wind speed conditions. From this perspective, the passive control is an inherent property or compliant characteristic of the system. The idea behind the passive control is to couple the rotor to a fixed displacement pump and a nozzle. A high pressure line is used to conduct the pressurized flow of hydraulic fluid into a nozzle. The flow through the nozzle induces a pressure in the pump which determines the transmitted torque. As can be seen from Equation 2.18, the pressure difference along the nozzle is proportional to the square of the flow rate. The flow rate, is directly proportional to the rotational speed of the pump according to Equation 2.1, thus:

$$\begin{aligned} \Delta p &\propto Q_{nz}^2 \\ &\propto \omega_p^2 \end{aligned} \quad (3.10)$$

The final torque transmitted by the pump to the rotor, which is directly proportional to the pressure difference, see Equation 2.2, can also be expressed as a quadratic function of the flow rate or rotor speed:

$$\begin{aligned}\tau_p &\propto \Delta p \\ &\propto \omega_p^2\end{aligned}\quad (3.11)$$

Therefore, the quadratic relation from Equation 3.6 is closely matched by the torque transmitted by the pump when both pump and rotor have the same rotational speed. The flow rate and the cross sectional area of the nozzle at the end of the circuit determine the pressure in the high pressure line.

For a constant tip speed ratio, both the rotor torque and the nozzle induced pressure (and therefore pump torque) are functions of the wind velocity squared. Therefore, by correctly sizing the pump and nozzle, the operating curve of the transmission is matched to the optimal static relation. Further elaboration and analysis of this passive control strategy is carried out in Section 3.4.

Two different passive control configurations are shown in Figure 3.5. The difference between both solutions is the presence of an intermediate closed-loop oil circuit shown in Figure 3.5(b). As mentioned in Section 1.4, this intermediate solution allows to match the operational characteristics of the hydraulic drives with available commercial technology. Both concepts make use of a variable-speed Pelton turbine through the use of power electronics to operate at maximum efficiency depending on the pressure at the nozzle.

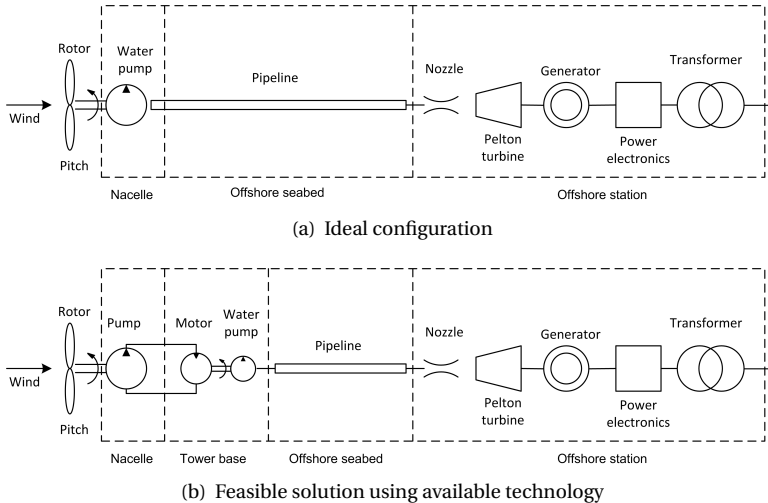


Figure 3.5: Passive control strategies for centralized generation.

ACTIVE TORQUE CONTROL STRATEGIES

Hydraulic drives with displacement control strategy can also be used to replace the generator torque control. For the case of a positive displacement pump directly coupled to the rotor, the transmitted torque can be manipulated in two different ways. According to Equation 2.2, the torque can be modified through the pressure difference across the pump or by adjusting the volumetric displacement.

In the first alternative, the pump has a fixed volumetric displacement. The pressure is controlled by adjusting the flow supply with a variable displacement motor (primary control). The 1 MW hydrostatic transmission developed by IFAS presented in Section 1.3 gives an example of primary torque control strategy (Schmitz et al., 2011, 2012).

The second alternative requires the volumetric displacement of the pump to be controlled under a constant pressure supply. A variable displacement motor is also required to keep a constant pressure difference across the drive (secondary control). An example of this secondary torque control strategy is used by the hydrostatic transmission developed by Artemis, now MHI (Payne et al., 2007; Silva et al., 2014). Other strategies for wind turbines have been studied using a resistance control alternative (Deldar et al., 2015), however as mentioned in the previous section, the associated losses to this kind of strategy are relatively large and clearly considered impractical for efficient power transmission.

A nozzle with an active-control spear valve can also be used instead of the variable displacement motor to adjust the pressure in both primary and secondary control strategies. For centralized electricity generation the nozzle with a spear valve is preferred to keep a constant pressure in the hydraulic line. With a constant pressure, the Pelton turbine is able to operate in the optimal region without need of modifying its rotational

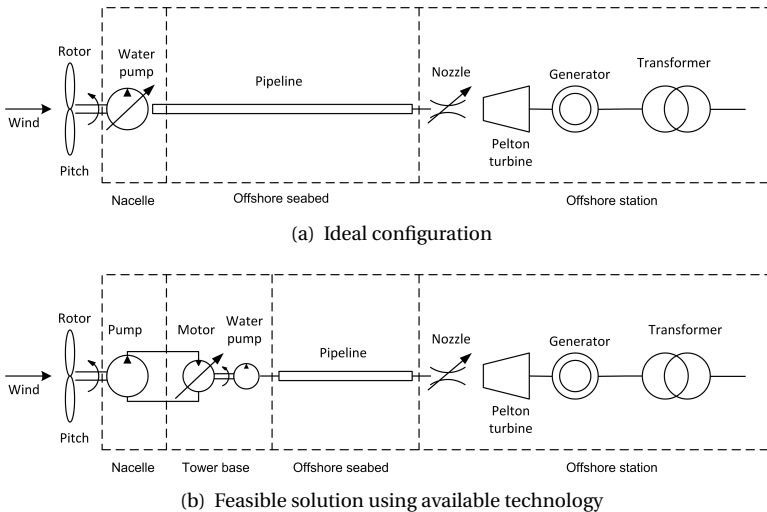


Figure 3.6: Active control strategies for centralized generation. Components designated with a diagonal arrow are used to indicate active-control.

speed as opposed to the passive control strategies. A Pelton turbine operating with a constant rotational speed considerably simplifies the integration with the electrical grid. The constant rotational speed is realized by using a grid-connected synchronous generator, similar to most large scale hydroelectric generation plants. A schematic of these configurations is shown in Figure 3.6.

3.4. PASSIVE SPEED CONTROL ANALYSIS

This section uses linear control tools to analyse the operation below rated wind speed of a horizontal axis variable speed wind turbine with a fluid power drivetrain. There is particular interest to analyse stability of a passive control method using fluid power technology. In order to illustrate the passive control operation, let us consider the ideal case where no friction, flow leakages or pressure losses occur. In this case, the final torque transmitted by the pump to the rotor is also expressed as a quadratic function of the rotor speed by using Equations 2.1 and 2.18 in Equation 2.2 according to:

$$\tau_p = K_3 \omega_r^2 \quad (3.12)$$

$$K_3 = \frac{1}{2} \rho_{hyd} \frac{V_p^3}{C_d^2 A_{nz}^2} \quad (3.13)$$

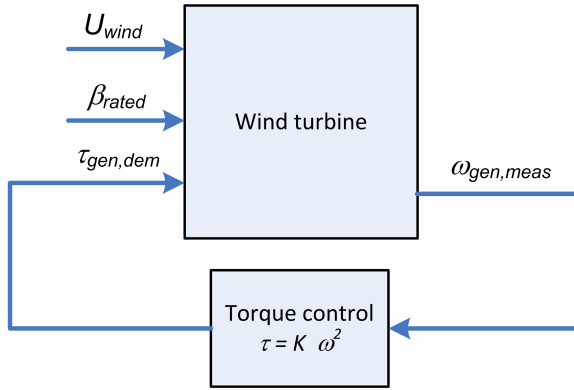
By making equal the terms K_1 and K_3 from Equations 3.7 and 3.13 it is possible to match both curves by proper dimensioning of the components given the aerodynamic performance of the rotor. Hence, the nozzle is used as a hydraulic component which induces a feedback pressure into the rotor and pump arrangement as shown in Figure 3.7.

If all the different losses in the fluid power transmission are included, the quadratic relation in Equation 2.2 is no longer valid. However, deviations from the optimal quadratic relation are rather small if components are properly dimensioned based on the required characteristics and ranges of operation. An experimental validation of this concept was described in (Diepeveen and Jarquin Laguna, 2014). In general, when a design wind speed and tip speed ratio is selected, a constant value of the nozzle area can be found such that the resulting torque-speed curve of the power transmission closely matches the maximal aerodynamic performance of the rotor for different wind speeds. For low wind speeds, this will result in a slightly lower tip speed ratio and for higher wind speeds the tip speed ratio will be slightly higher. In order to select the proper nozzle area, other design parameters should be taken into account like maximum tip speed velocity and rated wind speed.

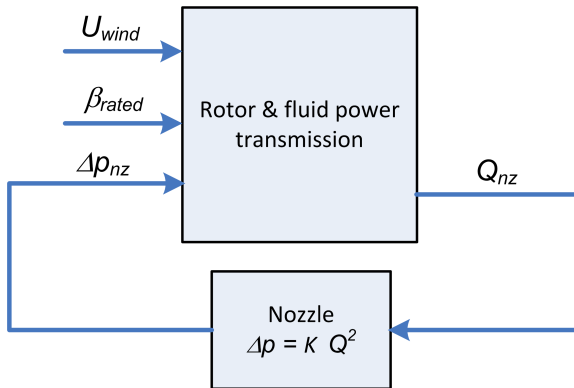
3.4.1. NON LINEAR REDUCED ORDER MODEL

The rotor and fluid power transmission can be modeled by including the rotational dynamics of the rotor, the design characteristics of the pump, the fluid flow dynamics from the pipeline and the nozzle. A schematic showing the subsystem level modelling is shown in Figure 3.8.

A first equation of the governing set of equations describes the rotor speed acceleration by the balance of the aerodynamic torque and the transmitted torque of the pump. Ig-



(a) Conventional active control based on the measured generator speed



(b) Passive control based on induced pressure feedback for the proposed hydraulic concept

Figure 3.7: Schematic showing the variable-speed control analogy between a conventional wind turbine and the proposed hydraulic concept.

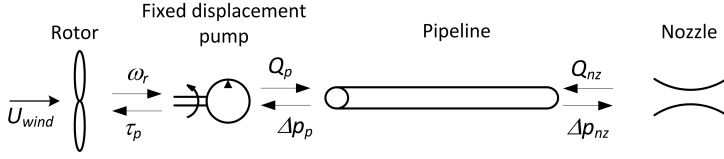


Figure 3.8: Schematic with the input-output variables of the passive control model.

noring the stiffness of the rotor shaft and assuming a constant pitch angle of the blades, such equation can be written as:

$$J_r \dot{\omega}_r - \tau_{aero}(U, \omega_r) + \tau_p(\omega_r, \Delta p_p) = 0 \quad (3.14)$$

The aerodynamic torque is obtained based on Equations 3.1 and 3.4 where the steady-state characteristics of the turbine are justified due to the large mass moment of inertia of the rotor.

$$\tau_{aero}(U, \omega_r) = \frac{C_p(\lambda)}{\lambda} \frac{1}{2} \rho_{air} \pi R^3 U^2 \quad (3.15)$$

The pump characteristics are given by the quasi-static relations as described by Equations 2.4 and 2.5. Under the assumption that the rotor and the pump are directly connected through a rigid shaft, both components have the same rotational velocity ω_r .

$$Q_p = V_p \omega_r - C_s \Delta p_p \quad (3.16)$$

$$\tau_p = V_p \Delta p_p + B_p \omega_r + C_f V_p \Delta p_p \quad (3.17)$$

To account for the dynamics of hydraulic lines, a modal approximation of the dissipative model is used as described in Section 2.4. The model gives a description of 1D laminar viscous flow which describe the dynamics of the pressure and volumetric flow at the upstream and downstream ends of the pipeline. Fluid inertia, compressibility and frequency dependent friction effects are included in the model. These are particularly important for lines with high dissipation numbers; this means either relatively long lines or for lines with high viscosity hydraulic fluids (Yang and Tobler, 1991). The equations of the model are given in a linear state-space representation assuming a finite number of modes (Mäkinen et al., 2000). Regarding the model causality, volumetric flow rates are used as an input and pressures at both upstream and downstream side of the line as an output.

$$\text{Q-model} \begin{cases} \dot{\mathbf{x}} = \mathbf{A_Q} \mathbf{x} + \mathbf{B_Q} \begin{bmatrix} Q_p \\ Q_{nz} \end{bmatrix} \\ \begin{bmatrix} \Delta p_p \\ \Delta p_{nz} \end{bmatrix} = \mathbf{C_Q} \mathbf{x} \end{cases} \quad (3.18)$$

The state vector \mathbf{x} , the matrices \mathbf{A}_Q , \mathbf{B}_Q and \mathbf{C}_Q are shown in Equations 2.64 to 2.67. To illustrate the pipeline dynamics, the frequency response of the downstream pressure is shown in Figure 3.9; the parameters of the water line used in the model are given in Table 3.1.

Table 3.1: Pipeline parameters used in the impedance or Q-model.

Parameter	Symbol	value
Line length	L	1000 m
Internal diameter	D	0.5 m
Fluid density	ρ_0	1020 kg/m ³
Fluid kinematic viscosity	ν_0	1e-6 m ² /s
Effective sound speed	c_0	1400 m/s
Number of modes	n	8

To describe the nozzle, Equation 2.18 is rewritten to express the flow rate at Q_{nz} as a function of the pressure drop Δp_{nz} .

$$Q_{nz} = C_d A_{nz} \sqrt{\frac{2 \Delta p_{nz}}{\rho_{hyd}}} \quad (3.19)$$

An important remark regarding stability should be made. The turbine operation will be stable as long as the torque-speed curve of the fluid power transmission matches the envelope curves of the rotor where it has a negative slope ($d\tau_{aero}/d\omega < 0$). If the wind speed increases, the rotor will exert a higher torque than the transmission torque and the rotor speed will increase. Increasing the rotor speed will also decrease the aerodynamic torque for the given wind speed and increase the transmission torque, leading to a point where a new equilibrium is reached.

On the other hand, the turbine operation will be unstable in the region where the slope of the rotor torque curve is positive ($d\tau_{aero}/d\omega > 0$). Following the same reasoning, if the wind speed increases, the rotor will exert less torque than the transmission, therefore the rotor will stall and eventually stop. Therefore it is important to correctly size the nozzle in order to operate in the stable region of the rotor.

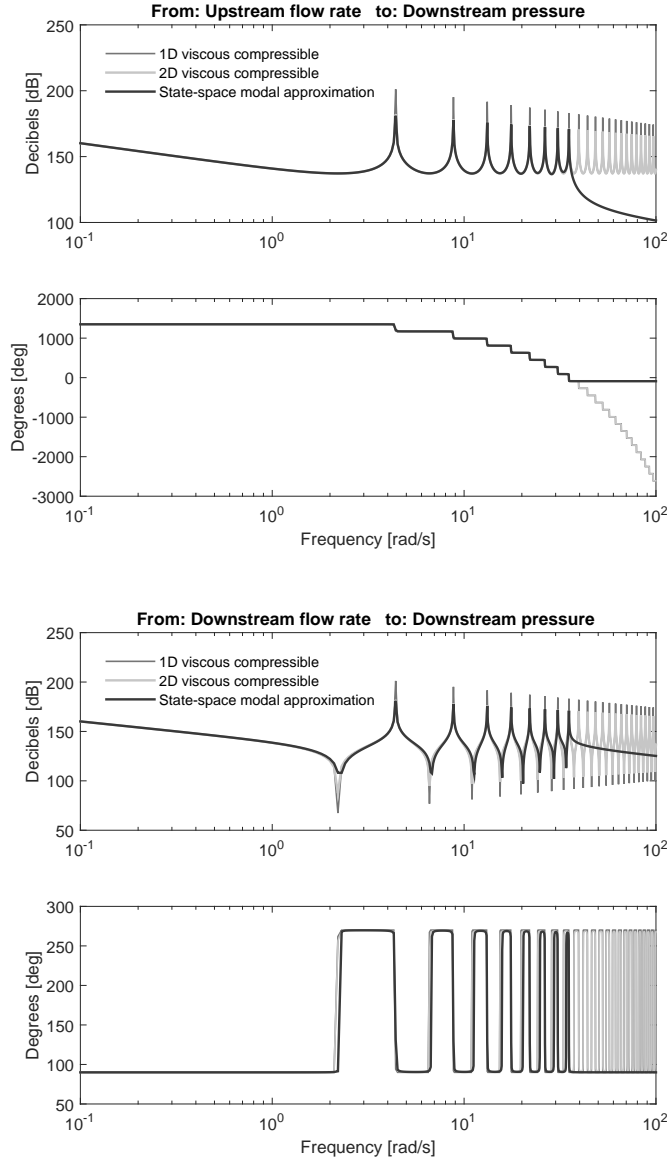


Figure 3.9: Frequency response of the downstream pressure of a water pipeline subject to a harmonic flow rate input. Eight modes are used for the state-space approximation. $D_n = 1.14e - 5$ and $Z_0 = 7.3e6 \text{ kgm}^4\text{s}^{-1}$.

3.4.2. LINEARISATION FOR CONTROL ANALYSIS

The passive control system will be analyzed from the perspective of feedback-control design of linear systems. To this aim, the system will be linearised around the different operating points.

AERODYNAMIC TORQUE LINEARISATION

As observed in Equations 3.1, the total torque and thrust are non-linear due to the wind turbine aerodynamics. For a fixed pitch operation, the aerodynamic torque coefficient C_τ is only function of the tip-speed-ratio λ . Thus, the linearisation of the aerodynamic torque is done around its operating point $(\bar{\omega}_r, \bar{U})$, according to (Bianchi et al., 1997).

$$\hat{\tau}_{aero} = -B_r (\bar{\omega}_r, \bar{U}) \hat{\omega}_r + k_{r,U} (\bar{\omega}_r, \bar{U}) \hat{U} \quad (3.20)$$

In this notation, the bars $()$ and hats $()$ over the variables mean ‘steady-state value’ and ‘variation with respect to the steady state value’. For example, the tip speed ratio at the operating point is $\bar{\lambda} = R \bar{\omega}_r / \bar{U}$.

$$B_r (\bar{\omega}_r, \bar{U}) = - \left. \frac{\partial \tau_{aero}}{\partial \omega_r} \right|_{(\bar{\omega}_r, \bar{U})} = - \frac{\tau_{aero}(\bar{\lambda}, \bar{U})}{\bar{\omega}_r} \left. \frac{\partial C_\tau / \partial \lambda}{C_\tau / \lambda} \right|_{(\bar{\omega}_r, \bar{U})} \quad (3.21)$$

The constant B_r plays an important role in the stability problem as it shows the intrinsic speed feedback of the turbine. This coefficient can be viewed as a sort of damping, taking positive values above $\lambda_{\tau, max}$ where C_τ is a decreasing function of λ . Negative values of B_r are also possible for operating conditions below $\lambda_{\tau, max}$ where C_τ increases with λ .

$$k_{r,U} (\bar{\omega}_r, \bar{U}) = \left. \frac{\partial \tau_{aero}}{\partial U} \right|_{(\bar{\omega}_r, \bar{U})} = \frac{\tau_{aero}(\bar{\lambda}, \bar{U})}{\bar{U}} \left(2 - \left. \frac{\partial C_\tau / \partial \lambda}{C_\tau / \lambda} \right|_{(\bar{\omega}_r, \bar{U})} \right) \quad (3.22)$$

The gain between the wind speed and the aerodynamic torque is given by $k_{r,U}$. In normal operation this gain is positive but it might also become negative at low values of λ when the turbine stalls. The numerical values of both B_r and $k_{r,U}$ are shown in Figure 3.10 for the NREL 5 MW turbine (Jonkman et al., 2009).

LINEARISED NOZZLE

Assuming that the cross-sectional area of the nozzle is constant, the linearised equation for the nozzle flow rate as a function of pressure difference is described by

$$\hat{Q}_{nz} = C_{nz} (\Delta \bar{p}) \Delta \hat{p} \quad (3.23)$$

$$C_{nz} (\Delta \bar{p}_{nz}) = \left. \frac{\partial Q_{nz}}{\partial \Delta p} \right|_{(\Delta \bar{p})} = \frac{C_d A_{nz}}{\sqrt{2 \rho_{hyd} \Delta \bar{p}}} \bigg|_{\Delta \bar{p}} \quad (3.24)$$

In this equation C_{nz} is a function of the operating pressure $\Delta \bar{p}$. Figure 3.11 illustrates this coefficient for a range of operating pressure differences and a constant cross-sectional area of the nozzle.

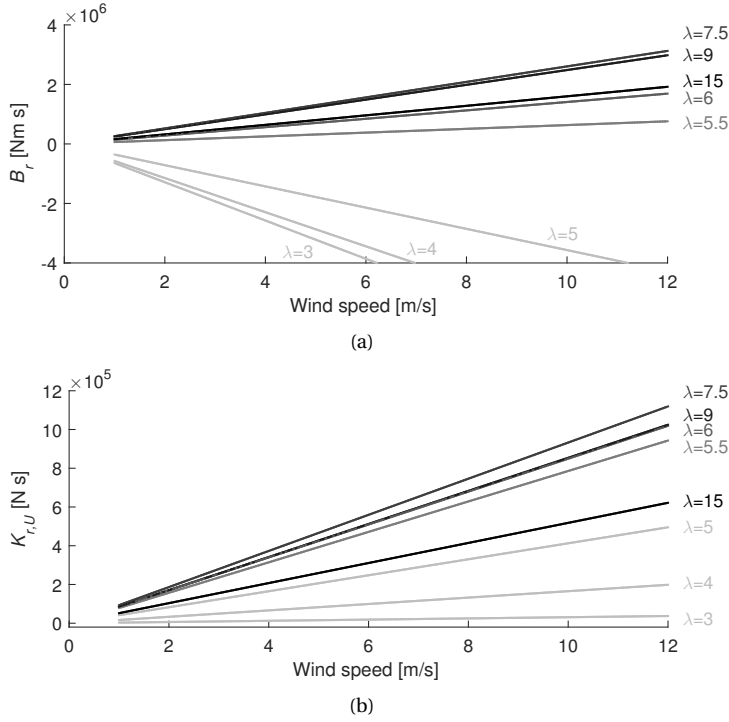


Figure 3.10: Linearized aerodynamic torque gains with respect to: 3.10(a) Rotor speed, 3.10(b) Wind speed. The values are obtained for the NREL 5 MW reference turbine (Jonkman et al., 2009).

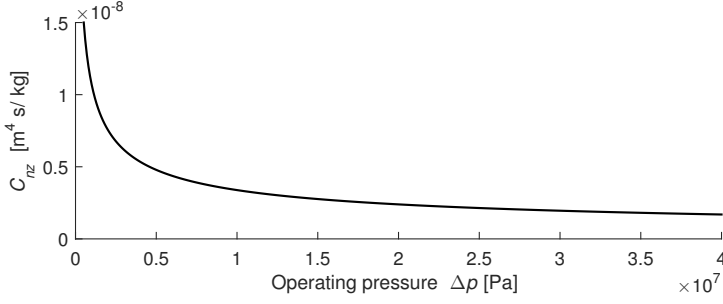


Figure 3.11: Linearized gain of the nozzle flow rate with respect to the operating pressure; $\rho_{hyd} = 1000 \text{ kgm}^{-3}$, $C_d = 0.95$ and $A_{nz} = 19e-4 \text{ m}^2$.

3.4.3. OPEN-LOOP ANALYSIS

A schematic representation of the passive control system is shown in Figure 3.12, where the nozzle feedback effect can be considered as a control action to the pump and rotor. From this perspective, the linear models can be represented in the frequency domain through their respective transfer functions.

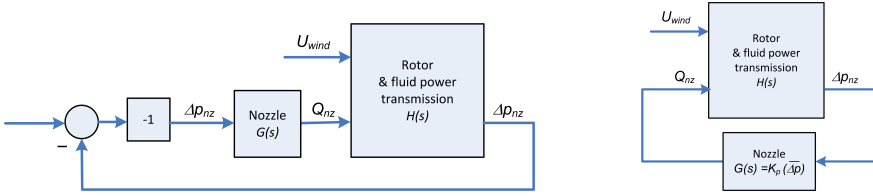


Figure 3.12: Schematic representation of the system using feedback control from the nozzle.

The linear model of the rotor and fluid power transmission is obtained from Equations 3.14, 3.16 and 3.18 in the following state space form:

$$\begin{bmatrix} \dot{\omega}_r \\ \dot{\mathbf{x}} \end{bmatrix} = \mathbf{A}_{ol}(\bar{\omega}_r, \bar{U}) \begin{bmatrix} \omega_r \\ \mathbf{x} \end{bmatrix} + \mathbf{B}_{ol}(\bar{\omega}_r, \bar{U}) \begin{bmatrix} U \\ Q_{nz} \end{bmatrix} \quad (3.25)$$

$$\Delta p_{nz} = \mathbf{C}_{ol} \begin{bmatrix} \omega_r \\ \mathbf{x} \end{bmatrix} \quad (3.26)$$

$$\mathbf{A}_{ol}(\bar{\omega}_r, \bar{U}) = \begin{bmatrix} -\frac{B_r(\bar{\omega}_r, \bar{U}) + B_p}{J_r} & -\frac{V_p(1+C_f)\mathbf{c}_1^T}{J_r} \\ V_p \mathbf{b}_1 & \mathbf{A}_Q - C_v \mathbf{b}_1 \mathbf{c}_1^T \end{bmatrix} \quad (3.27)$$

$$\mathbf{B}_{ol}(\bar{\omega}_r, \bar{U}) = \begin{bmatrix} \frac{k_{r,U}(\bar{\omega}_r, \bar{U})}{J_r} & 0 \\ 0 & \mathbf{b}_2 \end{bmatrix} \quad (3.28)$$

$$\mathbf{C}_{ol} = \begin{bmatrix} 0 & \mathbf{c}_2^T \end{bmatrix} \quad (3.29)$$

The numerical subscripts in vectors and matrices indicate column vectors (i.e. \mathbf{b}_1 is the first column of matrix \mathbf{B}_Q ; \mathbf{c}_2^T indicates the second row vector of matrix \mathbf{C}_Q).

The transfer function for the pressure difference at the nozzle with the nozzle flow rate as an input is obtained in the frequency domain from the following expression:

$$H(s) = \frac{\Delta p_{nz}(s)}{Q_{nz}(s)} = \mathbf{C}_{01}(s\mathbf{I} - \mathbf{A}_{01})^{-1} \mathbf{B}_{01} \quad (3.30)$$

For the transfer function of the linearized nozzle, the following equations are used

$$Q_{nz}(s) = \frac{C_d A_{nz}}{\sqrt{2\rho_{hyd}\Delta\bar{p}}} \Delta p_{nz}(s) \quad (3.31)$$

$$G(s) = \frac{Q_{nz}(s)}{\Delta p_{nz}(s)} = \frac{C_d A_{nz}}{\sqrt{2\rho_{hyd}\Delta\bar{p}}} \quad (3.32)$$

Stability analysis based on the frequency response. Stability analysis is based on the transfer function $GH(s)$. From this open-loop response it is possible to give an indication of the degree of stability of the system. It is well-known from feedback theory, that the degree of stability is related to the closeness of $GH(i\omega)$ to the $-1 + i0$ point on a conformal mapping of the s plane onto the $GH(s)$ plane (Ogata, 2001). The amount of additional phase lag required to reach the $-1 + i0$ point can be used as indication of the degree of stability. The so-called *phase margin* is obtained at the points where the magnitude of the open-loop transfer function, $|GH(i\omega)|$, reaches a unity value which is equivalent to 0 dB.

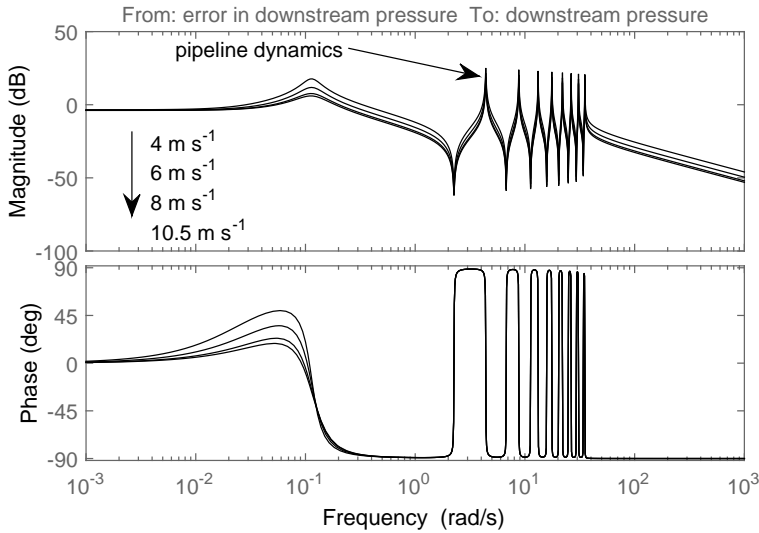


Figure 3.13: Open loop frequency response for different operating wind speeds.

From the frequency response shown in Figure 3.13 it is observed that the phase of the system does not go below -90 degrees. This means that the system will be unconditionally stable as instability requires a phase of -180 degrees. This result implies that the proposed passive control strategy using a constant area nozzle is stable for the considered operating points. On the other hand, the pipeline dynamics are slightly damped. From the frequency response it is observed that the magnitude of the error reaches the unity value at the resonant frequencies of the pipeline which might introduce high oscillations in the pressure response for frequencies above 3 rad/s.

3.4.4. CLOSED-LOOP RESPONSE

For the closed loop response, the nozzle is integrated into the system, and the response of the rotational speed is obtained with respect to a wind speed input as observed in Figure 3.14

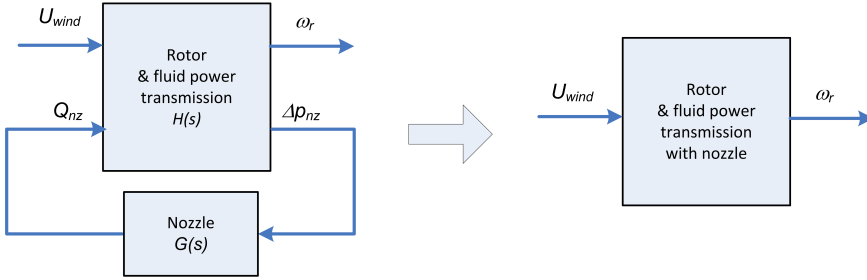


Figure 3.14: Closed-loop schematic.

in this case, the state space representation is given by the following equations:

$$\begin{bmatrix} \dot{\omega}_r \\ \dot{\mathbf{x}} \end{bmatrix} = \mathbf{A}_{cl}(\bar{\omega}_r, \bar{U}, \Delta \bar{p}_{nz}) \begin{bmatrix} \omega_r \\ \mathbf{x} \end{bmatrix} + \mathbf{B}_{cl}(\bar{\omega}_r, \bar{U}) U \quad (3.33)$$

$$\begin{bmatrix} \omega_r \\ \Delta p_{nz} \end{bmatrix} = \mathbf{C}_{cl} \begin{bmatrix} \omega_r \\ \mathbf{x} \end{bmatrix} \quad (3.34)$$

in which the closed-loop state-space matrices \mathbf{A}_{cl} and \mathbf{B}_{cl} are defined as:

$$\mathbf{A}_{cl}(\bar{\omega}_r, \bar{U}, \Delta \bar{p}_{nz}) = \begin{bmatrix} -\frac{B_r(\bar{\omega}_r, \bar{U}) + B_p}{J_r} & -\frac{V_p(1+C_f)\mathbf{c}_1^T}{J_r} \\ V_p \mathbf{b}_1 & \mathbf{A}_Q - C_v \mathbf{b}_1 \mathbf{c}_1^T + C_{nz}(\Delta \bar{p}_{nz}) \mathbf{b}_2 \mathbf{c}_2^T \end{bmatrix} \quad (3.35)$$

$$\mathbf{B}_{cl}(\bar{\omega}_r, \bar{U}) = \begin{bmatrix} \frac{k_r U(\bar{\omega}_r, \bar{U})}{J_r} \\ 0 \end{bmatrix} \quad (3.36)$$

$$\mathbf{C}_{cl} = \begin{bmatrix} 1 & \mathbf{0} \\ 0 & \mathbf{c}_2^T \end{bmatrix} \quad (3.37)$$

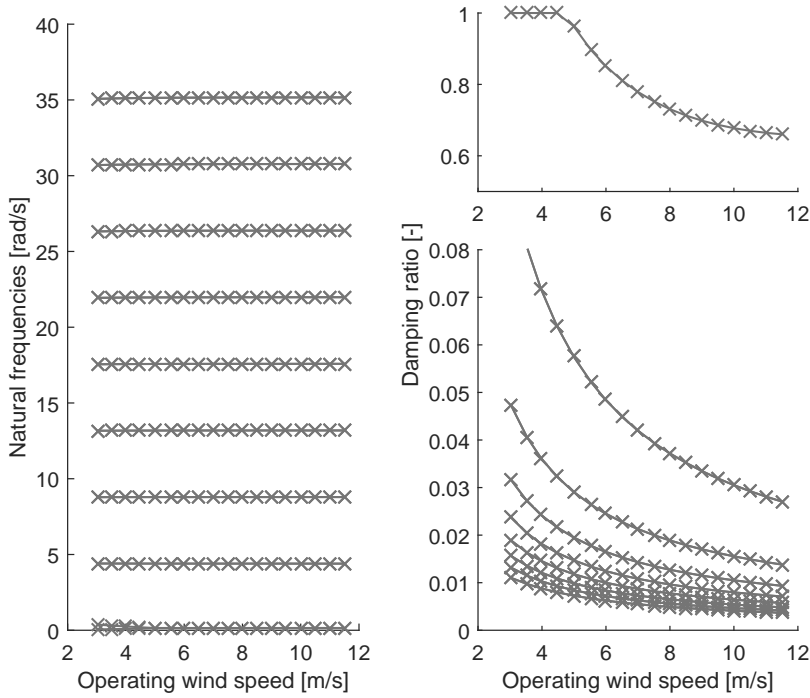


Figure 3.15: Natural frequencies and damping ratios for different operating wind speeds.

From the closed loop system, the natural frequencies and damping ratios of the system are computed for different operating wind speeds, see Figure 3.15. From the frequency response of the closed-loop system to different wind speed inputs, see Figures 3.16 and 3.17, it is seen that the rotational speed behaves as a highly damped second order system with very little oscillations; the pipeline dynamics are not present at all in the rotor speed response as a consequence of the high inertia of the rotor.

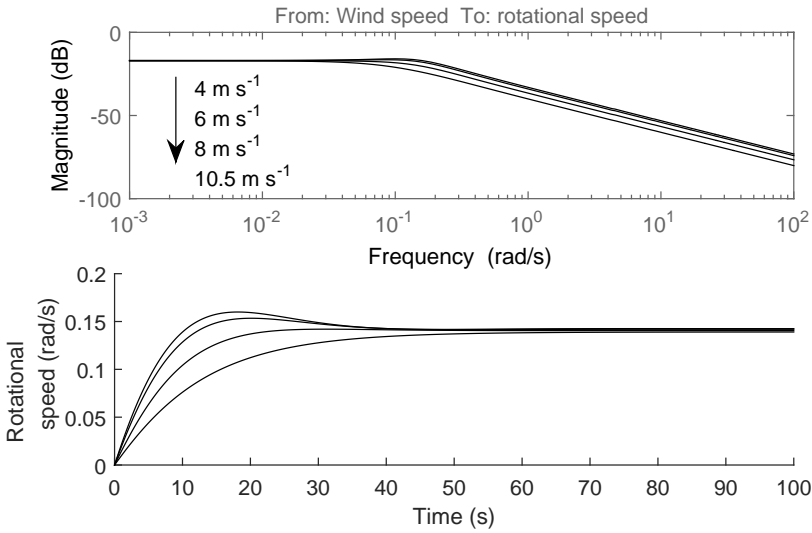


Figure 3.16: Closed loop frequency response (top) and time domain step response (bottom) of the rotational speed to wind speed input.

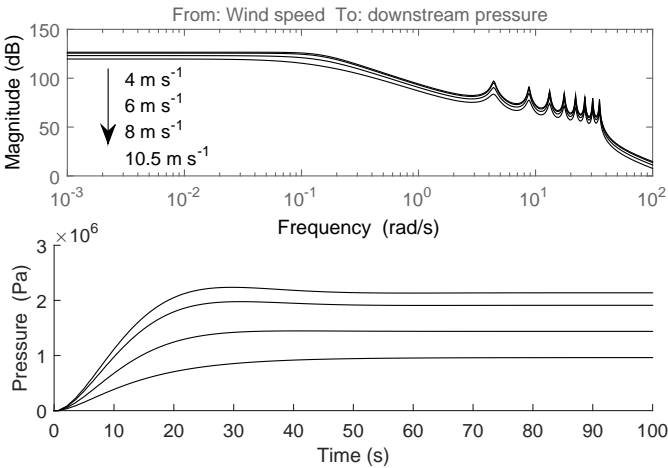


Figure 3.17: Closed loop frequency response (top) and time domain step response (bottom) of the nozzle pressure to wind speed input.

3.5. ACTIVE SPEED CONTROL ANALYSIS

As shown in Equation 2.9, it is possible to manipulate the transmitted torque of the pump by modifying the pressure difference across it and/or the volumetric displacement of the pump. Hence, when active control is introduced, two extra degrees of freedom might be added with respect to the passive configuration: the first one, is the linear motion of a spear valve which allows to change the area of the nozzle and therefore modify the induced pressure at the downstream side of the line. The control objective of this sub-system is to maintain a relatively constant pressure level. The second degree of freedom is the adjustment of the volumetric displacement of the pump. Thus, the transmitted torque from the pump to the rotor is adapted to comply with the variable-speed operation required for different operating wind speeds below rated conditions.

Pump controller. In this case, the volumetric displacement of the pump from each turbine is controlled under a relatively constant pressure supply. Hence, the rotational speed of each rotor is able to be modified independently according to the local wind speed conditions. This strategy is commonly known in hydraulic systems as ‘secondary control’ as mentioned in Section 3.2. The required volumetric displacement of the pump e_{dem} is obtained from Equation 2.9 as a function of the measured rotational speed of the rotor $\omega_{r,meas}$ and the measured pressure at the pump location $\Delta p_{p,meas}$ as follows:

$$e_{dem} = \frac{\tau_{ref}(\omega_{r,meas}) - B_p \omega_{r,meas}}{V_p(1 + C_f) \Delta p_{p,meas}} \quad (3.38)$$

A low pass filter on the pressure measurement is employed to prevent actuation from the fluid transient fluctuations in the hydraulic network. The reference torque τ_{ref} is obtained from the steady-state torque-speed curves defined for different operating regions as in conventional variable-speed control strategies.

Spear valve controller. In order to achieve a constant pressure in the hydraulic network, the linear actuation of the spear valve is used to constrict or release the flow rate through the nozzle area. The pressure control is based on a PI feedback controller and a cascade controller compensation to modify the linear position of the spear valve. A similar pressure control loop has been proposed in (Buhagiar et al., 2016); a schematic of the proposed controller is shown in Figure 3.18.

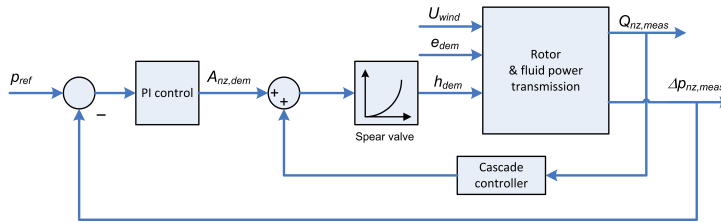


Figure 3.18: Pressure control schematic based on the spear valve position of the nozzle.

3.5.1. NON-LINEAR REDUCED ORDER MODEL

In addition to the rotational dynamics of the rotor and the pipeline dynamics described by Equations 3.14 and 3.18, the dynamics of the variable displacement pump and nozzle with spear valve are included. A schematic showing the subsystem level modelling is shown in Figure 3.19.

To account for the variable displacement pump, the flow rate and transmitted torque equations are modified according to:

$$Q_p = V_p(e) \omega_r - C_s \Delta p_p \quad (3.39)$$

$$\tau_p = V_p(e) \Delta p_p + B_p \omega_r + C_f V_p(e) \Delta p_p \quad (3.40)$$

In the case of the nozzle with spear valve, the flow characteristics of the nozzle are also modified:

$$Q_{nz} = C_d A_{nz}(h_s) \sqrt{\frac{2 \Delta p_{nz}}{\rho_{hyd}}} \quad (3.41)$$

According to Equations 2.10 and 2.22, both volumetric displacement of the pump and nozzle area, are dependent on the volumetric displacement ratio e and the position of the spear valve h_s respectively. In addition, the dynamics of the linear actuators to control both the volumetric displacement ratio and the spear valve position are described through a first order system. From Equations 2.11 and 2.23:

$$\dot{e} = \frac{1}{T_e} (e_{dem} - e) \quad (3.42)$$

$$\dot{h}_s = \frac{1}{T_h} (h_{s,dem} - h_s) \quad (3.43)$$

3.5.2. LINEARISATION FOR CONTROL ANALYSIS

In order to design the controller in the frequency domain, both the pump and nozzle are linearized around their operating points. Linearising Equations 3.39 and 3.40, the following equations are obtained:

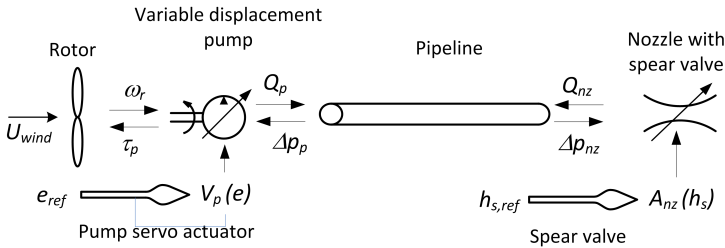


Figure 3.19: Schematic with the input-output variables of the active control model.

$$\hat{Q}_p = \left(\frac{\partial Q_p}{\partial \omega_p} \bigg|_{(\bar{\omega}_p, \bar{e})} \hat{\omega}_p + \frac{\partial Q_p}{\partial e} \bigg|_{(\bar{\omega}_p, \bar{e})} \hat{e} \right) - C_s \Delta p_p \quad (3.44)$$

$$= V_p \bar{e} \hat{\omega}_p + V_p \bar{\omega}_p \hat{e} - C_s \Delta p_p \quad (3.45)$$

$$\hat{\tau}_p = \left(\frac{\partial \tau_p}{\partial \Delta p_p} \bigg|_{(\bar{\omega}_p, \Delta \bar{p}_p)} \Delta \hat{p}_p + \frac{\partial \tau_p}{\partial e} \bigg|_{(\bar{\omega}_p, \Delta \bar{p}_p)} \hat{e} \right) + B_p \omega_p \quad (3.46)$$

$$= V_p (1 + C_f) \bar{e} \Delta \hat{p}_p + V_p (1 + C_f) \Delta \bar{p}_p \hat{e} + B_p \omega_p \quad (3.47)$$

Linearization of the nozzle flow rate as a function of both pressure and nozzle area gives:

$$\hat{Q}_{nz} = C_{nz1} (\Delta \bar{p}, \bar{A}_{nz}) \Delta \hat{p}_{nz} + C_{nz2} (\Delta \bar{p}) \hat{A}_{nz} \quad (3.48)$$

where the nozzle constants are evaluated according to the operating characteristics of the system:

$$C_{nz1} (\Delta \bar{p}_{nz}, \bar{A}_{nz}) = \frac{\partial Q_{nz}}{\partial \Delta p} \bigg|_{(\Delta \bar{p}, \bar{A}_{nz})} = \frac{C_d A_{nz}}{\sqrt{2 \rho_{hyd} \Delta p}} \bigg|_{(\Delta \bar{p}, \bar{A}_{nz})} \quad (3.49)$$

$$C_{nz2} (\Delta \bar{p}_{nz}) = \frac{\partial Q_{nz}}{\partial A_{nz}} \bigg|_{(\Delta \bar{p}, \bar{A}_{nz})} = C_d \sqrt{\frac{2 \Delta p_{nz}}{\rho_{hyd}}} \bigg|_{(\Delta \bar{p}, \bar{A}_{nz})} \quad (3.50)$$

The last equation corresponds to the linearisation of the nozzle area with respect to the spear valve position, this relation is described in Equation 2.22. Assuming that the geometrical parameters of the nozzle are constant, the nozzle area is described only as a function of the spear valve position. This relation is linearized according to Equation 3.51. The pressure control schematic for the linearized model of the nozzle is shown in Figure 3.20.

$$\hat{A}_{nz} = K_{nz} (\bar{h}) \hat{h} \quad (3.51)$$

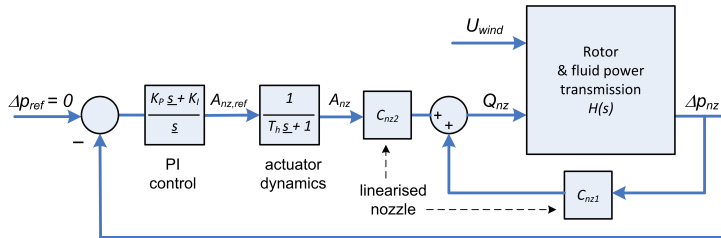


Figure 3.20: Pressure control schematic using the linearized model of the nozzle.

3.5.3. OPEN-LOOP ANALYSIS

For the open-loop analysis, the so-called 'plant' is considered to include the actuator dynamics such that the input variables to the system are the wind speed U , the reference value for the volumetric displacement ratio of the pump e_{ref} and the reference value for the nozzle spear valve h_{ref} . The state-space representation of the system is given by:

$$\begin{bmatrix} \dot{\omega}_r \\ \dot{e} \\ \dot{\mathbf{x}} \\ \dot{h} \end{bmatrix} = \mathbf{A}_{\text{plant}}(\bar{\omega}_r, \bar{U}, \Delta\bar{p}_p, \Delta\bar{p}_{nz}, \bar{e}, \bar{h}) \begin{bmatrix} \omega_r \\ e \\ \mathbf{x} \\ h \end{bmatrix} + \mathbf{B}_{\text{plant}}(\bar{\omega}_r, \bar{U}) \begin{bmatrix} U \\ e_{ref} \\ h_{ref} \end{bmatrix} \quad (3.52)$$

$$\begin{bmatrix} \Delta p_{nz} \\ \omega_r \\ Q_{nz} \end{bmatrix} = \mathbf{C}_{\text{plant}}(\Delta\bar{p}_{nz}, \bar{h}) \begin{bmatrix} \omega_r \\ e \\ \mathbf{x} \\ h \end{bmatrix} \quad (3.53)$$

$$\mathbf{A}_{\text{plant}} = \begin{bmatrix} -\frac{B_r(\bar{\omega}_r, \bar{U}) + B_p}{J_r} & -\frac{V_p(1+C_f)\Delta\bar{p}_p}{J_r} & -\frac{V_p\bar{e}(1+C_f)\mathbf{c}_1^T}{J_r} & 0 \\ 0 & -\frac{1}{T_e} & \mathbf{0} & 0 \\ V_p\bar{e}\mathbf{b}_1 & V_p\bar{\omega}_r\mathbf{b}_1 & \mathbf{a}_{33} & \mathbf{a}_{34} \\ 0 & 0 & \mathbf{0} & -\frac{1}{T_h} \end{bmatrix} \quad (3.54)$$

$$\mathbf{B}_{\text{plant}} = \begin{bmatrix} \frac{k_{r,U}(\bar{\omega}_r, \bar{U})}{J_r} & 0 & 0 \\ 0 & \frac{1}{T_e} & 0 \\ 0 & 0 & 0 \\ 0 & 0 & \frac{1}{T_h} \end{bmatrix} \quad (3.55)$$

$$\mathbf{C}_{\text{plant}} = \begin{bmatrix} 0 & 0 & \mathbf{c}_2^T & 0 \\ 1 & 0 & \mathbf{0} & 0 \\ 0 & 0 & \mathbf{c}_{33} & K_{nz}(\bar{h})C_{nz2}(\Delta\bar{p}_{nz}) \end{bmatrix} \quad (3.56)$$

$$\mathbf{a}_{33} = \mathbf{A}\mathbf{Q} - C_v\mathbf{b}_1\mathbf{c}_1^T + C_{nz1}(\Delta\bar{p}_{nz}, \bar{A}_{nz})\mathbf{b}_2\mathbf{c}_2^T \quad (3.57)$$

$$\mathbf{a}_{34} = K_{nz}(\bar{h})C_{nz2}(\Delta\bar{p}_{nz})\mathbf{b}_2 \quad (3.58)$$

$$\mathbf{c}_{33} = C_{nz1}(\Delta\bar{p}_{nz}, \bar{A}_{nz})\mathbf{c}_2^T \quad (3.59)$$

The frequency response of the downstream pressure to the spear valve displacement is shown in Figure 3.21 for different operating wind speeds. A great influence of the pipeline dynamics is observed above 1 rad/s at the resonant frequencies of the pipeline. The Proportional-Integral (PI) controller acting on the error of the nozzle's pressure is determined by the following equation:

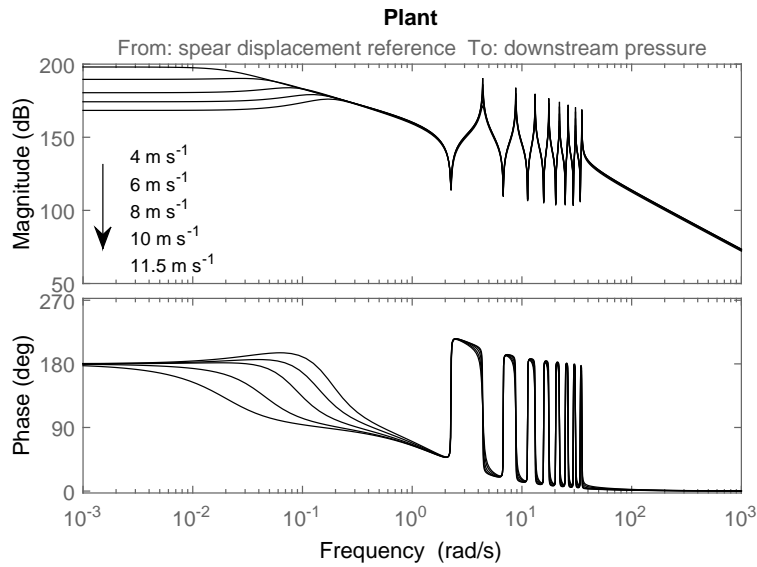


Figure 3.21: Plant frequency response for different operating wind speeds.

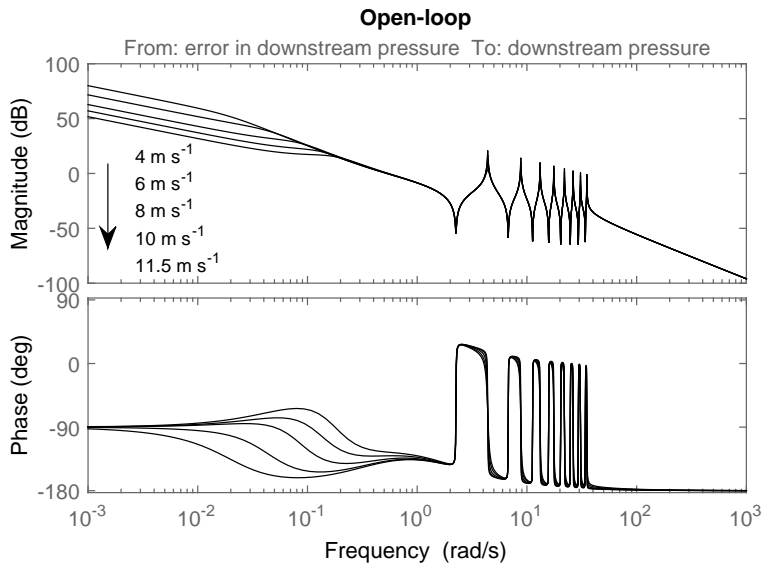


Figure 3.22: Open loop frequency response for different operating wind speeds.

$$h_{dem} = K_P p_{nz,error} + K_I \int_0^t p_{nz,error} dt \quad (3.60)$$

$$p_{nz,error} = p_{ref} - p_{nz} \quad (3.61)$$

where $p_{nz,error}$ represents the error between the desired pressure level p_{ref} value and the measured pressure at the nozzle p_{nz} . The proportional action of the controller is given by the constant K_P , while the integral action is carried out through the constant K_I . The dynamics of the PI controller can also be described in a state-space representation using $p_{nz,error}$ as an input and h_{dem} as an output:

$$h_{dem} = K_P p_{nz,error} + K_I \chi \quad (3.62)$$

where the state variable χ is used to describe the integral of the pressure error with respect to time. This can be expressed as a first order differential equation

$$\dot{\chi} = p_{ref} - p_{nz} \quad (3.63)$$

The frequency response of the downstream pressure can now be extended with the PI controller such that the frequency response of the open-loop system is given by the Figure 3.22. From the open-loop response, the magnitude of the downstream pressure reaches the unity value at several resonant frequencies of the pipeline. In order to reduce the influence of the pipeline dynamics, the PI controller is augmented with a second order low pass filter and a series of notch filters. A schematic showing the structure of the augmented controller is shown in Figure 3.23.

The low pass filter and the notch filters are described in the frequency domain according to Equations 3.64 and 3.65. The values of the different control parameters are displayed in Table 3.2. The negative values of the proportional and integral gain show that if the reference pressure is higher than the measured pressure at the nozzle (positive error input to the controller), the controller action should reduce the nozzle area to constrict the flow rate and induce a higher pressure. This inverse relation is reflected in the negative values of the controller gains.

$$LPF(s) = \frac{\omega_{LPF}^2}{s^2 + 2\omega_{LPF}\zeta_{LPF}s + \omega_{LPF}^2} \quad (3.64)$$

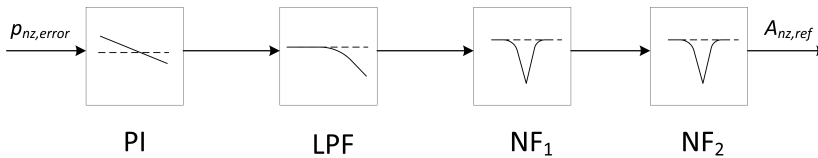


Figure 3.23: Schematic overview of the structure of the controller. The control blocks from left to right: Proportional-integral (PI), low-pass filter (LPF), notch filter 1 (NF1), notch filter 2 (NF2).

$$NF_i(s) = \frac{s^2 + 2\omega_{ni}\zeta_{ni}s + \omega_{ni}^2}{s^2 + 2\omega_{ni}\beta_{ni}s + \omega_{ni}^2} \quad (3.65)$$

Table 3.2: Controller parameters of the augmented controller.

Description	Symbol	value
Proportional gain	K_p	$-2.7898 \cdot 10^{-10} \text{ m}^2 \text{ Pa}^{-1}$
Integral gain	K_I	$-1.0565 \cdot 10^{-10} \text{ m}^2 \text{ Pa}^{-1} \text{ s}$
Low-pass filter frequency	ω_{LPF}	$1 \cdot 2\pi \text{ rad s}^{-1}$
Low-pass filter parameter	ζ_{LPF}	0.7
Notch filter 1 frequency # 1	ω_{n1}	$0.7 \cdot 2\pi \text{ rad s}^{-1}$
Notch filter 2 frequency # 2	ω_{n2}	$1.4 \cdot 2\pi \text{ rad s}^{-1}$
Notch filter 1 parameter # 1	ζ_{n1}	0.01
Notch filter 1 parameter # 2	β_{n1}	0.7
Notch filter 2 parameter # 1	ζ_{n2}	0.01
Notch filter 2 parameter # 2	β_{n2}	0.7

The resulting open-loop response of the plant with augmented controller is presented in Figure 3.24. In the figure it is observed that the augmented controller with the low-pass and notches filters have an effect on both the magnitude and phase of the error response. The magnitude of the error is kept below the unity value for frequencies above 0.5 rad/s, effectively reducing the influence of the pipeline dynamics on the error response. The phase is affected differently at the resonance frequencies for the considered operating wind speeds without significant influence on the error response. After the open-loop analysis the closed-loop response is used to verify both the stability and performance of the proposed controller.

3.5.4. CLOSED-LOOP RESPONSE

The closed-loop response of the system and the step response for different operating wind speeds are shown in Figure 3.25. The time domain response shows the transient behavior of the downstream pressure to a step change in the reference pressure. It is observed that with the augmented controller, the pressure tracking shows a damped behaviour and takes between 30 to 40 s to reach the reference value.

By introducing the combination of low pass filter in series with the notches, the effect of the pipeline dynamics is reduced. The oscillations observed in the time domain response are attributed to the first closed-loop mode located between 0.4 and 0.8 rad/s. From this closed-loop analysis it is concluded that the designed controller system is able to track a reference pressure for a single turbine operating in below rated wind speed conditions.

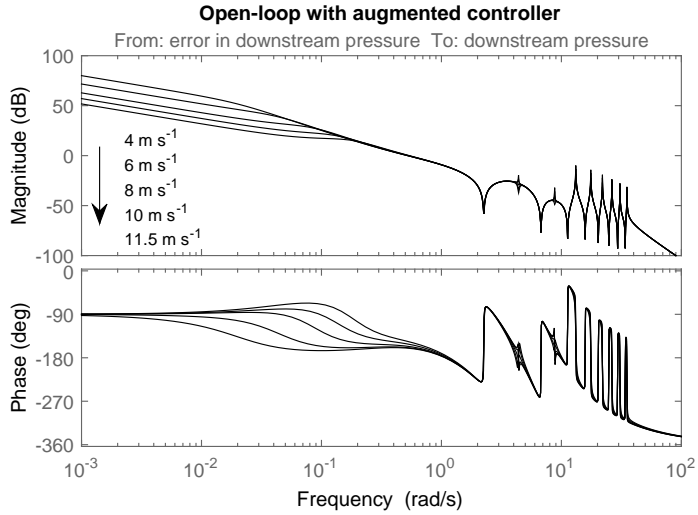


Figure 3.24: Open loop frequency response with augmented controller for different operating wind speeds.

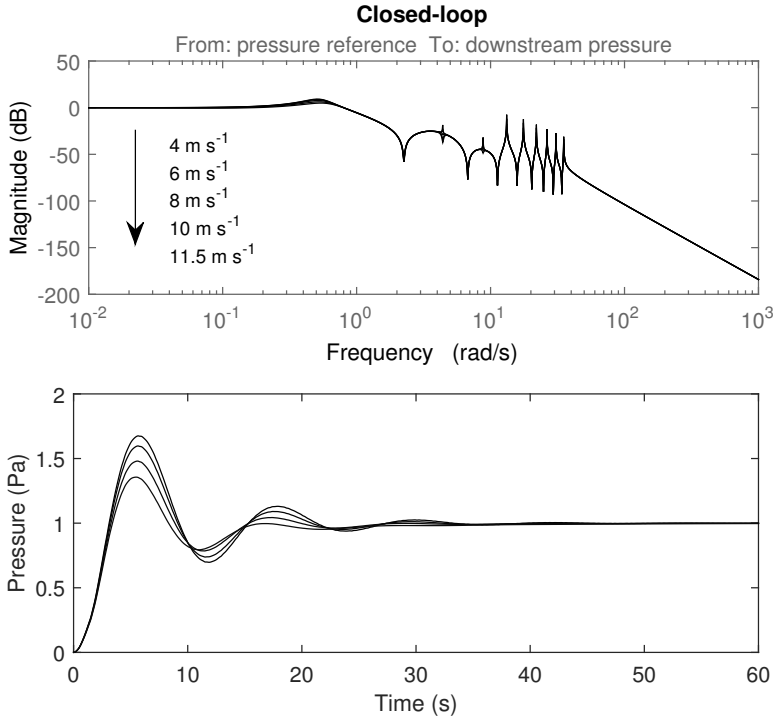


Figure 3.25: Closed loop frequency response (top) and time domain step response (bottom) for different operating wind speeds.

3.6. OTHER CONTROL ASPECTS

3.6.1. PITCH CONTROL

Above rated wind speed, the rated rotor speed is maintained by pitching collectively the rotor blades. A conventional PI pitch controller is proposed using the rotor speed error instead of the generator speed error. Due to the sensitivity of the aerodynamic response of the rotor to the pitch angle, the value of the controller gains are modified as a function of the pitch angle through a gain-scheduled approach. The gain scheduled PI controller is shown in the next equations, where $K_{P/I}$ are the proportional and integral gains respectively, $K_{P/I,0}$ is the gain at rated pitch angle $\beta = 0$, and β_K is the blade pitch angle at which the pitch sensitivity of aerodynamic power to rotor collective blade pitch has doubled from its value at the rated operating point.

$$\beta_{dem} = K_P(\beta) \omega_{r,error} + K_I(\beta) \int_0^t \omega_{r,error} dt \quad (3.66)$$

$$K_{P/I}(\beta) = K_{P/I,0} \frac{\beta_K}{\beta_K + \beta} \quad (3.67)$$

$$\omega_{r,error} = \omega_{r,rated} - \omega_{r,meas} \quad (3.68)$$

The values of the different gains are obtained in a similar way as described in (Jonkman et al., 2009), taking into account the drivetrain inertia relative to the low speed shaft. Assuming a rigid shaft and a transmission ratio set to one, this drivetrain inertia is given by the summation of the rotational mass moments of inertia of the rotor, the pump and the low speed shaft. To get rid of high frequency excitation, a low pass filter on the rotor speed measurement is used to prevent high frequency pitch action.

Table 3.3: Controller parameters of the pitch controller.

Description	Symbol	value
Proportional gain at rated pitch angle	$K_{P,0}$	-18.6288 s
Integral gain at rated pitch angle	$K_{I,0}$	-7.9838
Blade pitch angle for gain scheduling	β_K	0.0082 rad

3.6.2. PELTON SPEED CONTROL

In order to keep an optimal runner speed ratio, defined by k_{opt} , the Pelton rotational velocity is controlled by using the generator torque. A speed control strategy based on nozzle pressure measurement is proposed using a PI controller. From the measurement of the pressure difference across the nozzle, a maximum power point tracking (MPPT) is derived from static relations based on Equations 2.18 and 2.15 to determine the reference runner speed for maximum hydraulic efficiency. The optimal runner speed ratio for maximum runner efficiency is derived from Equation 2.14 and has a theoretical value of $k_{opt} = 0.5$ (Zhang, 2007). In reality as a result of bearing friction and 'windage' losses

inside the casing of the runner, the optimal runner speed ratio has a lower value typically between 0.46 and 0.48 (Dixon and Hall, 2014).

$$\omega_{P,ref} = \frac{k_{opt}}{R_{PCD}} C_v C_d \sqrt{\frac{2|\Delta p_{nz,meas}|}{\rho_{sw}}} \quad (3.69)$$

The PI controller for the Pelton runner speed is given by:

$$\tau_{dem} = K_P \omega_{P,error} + K_I \int_0^t \omega_{P,error} dt \quad (3.70)$$

$$\omega_{P,error} = \omega_{P,ref} - \omega_{P,meas} \quad (3.71)$$

A low pass filter applied to the pressure measurement at the nozzle is also used to get rid of high frequency excitation due to pressure transients.

Pelton torque. The mechanical torque obtained from the Pelton runner is obtained by considering its mechanical efficiency resulting in the following expression in terms of water jet velocity U_{jet} and the rotational speed of the Pelton runner ω_P . Inserting Equations 2.14, 2.15, 2.18 and 2.20 into Equation 2.16, we obtain:

$$\tau_P = K_4 \left(U_{jet}^2 - \omega_P R_P U_{jet} \right) \quad (3.72)$$

where constant K_4 is given by:

$$K_4 = (1 - \xi \cos \gamma) \rho A_{nz} R_P \quad (3.73)$$

Pelton control. The equation of motion for the rotational speed of the Pelton turbine is formulated as:

$$J_P \frac{d\omega_P}{dt} + B_P \omega_P = \tau_P + \tau_{ctrl} \quad (3.74)$$

It is desirable that the controller is able to track a reference rotational speed where maximum efficiency is achieved. Therefore a controller with integral action is a reasonable choice. The required torque from the control action is then given by a PI controller:

$$\tau_{ctrl} = K_P e + K_I \int_0^t e dt \quad (3.75)$$

$$e = \omega_{P,ref} - \omega_P \quad (3.76)$$

Assuming that $\omega_{P,ref}$ is constant and taking the first and second time derivative of Equation 3.76 we obtain:

$$\frac{de}{dt} = -\frac{d\omega_P}{dt} \quad (3.77)$$

$$\frac{d^2e}{dt^2} = -\frac{d^2\omega_P}{dt^2} \quad (3.78)$$

In order to avoid dealing with both derivatives and integrals, the derivatives of Equations 3.72 and 3.75 with respect to time are taken:

$$\frac{d\tau_P}{dt} = K_A (2U_{jet} - \omega_P R_P) \frac{dU_{jet}}{dt} - K_A R_P U_{jet} \frac{d\omega_P}{dt} \quad (3.79)$$

$$\frac{d\tau_{ctrl}}{dt} = K_P \frac{de}{dt} + K_I e \quad (3.80)$$

Similarly, equation of motion 3.74 is also time differentiated to give:

$$J_P \frac{d^2\omega_P}{dt^2} + B_P \frac{d\omega_P}{dt} = \frac{d\tau_P}{dt} + \frac{d\tau_{ctrl}}{dt} \quad (3.81)$$

Equations 3.77, 3.78 and 3.80 can be substituted in Equation 3.81 and the following second order differential equation can be obtained:

$$J_P \frac{d^2e}{dt^2} + (B_P + K_P) \frac{de}{dt} + K_I e = -\frac{d\tau_P}{dt} \quad (3.82)$$

Inserting Equations 3.76, 3.77 and 3.79 into Equation 3.82 we obtain:

$$J_P \frac{d^2e}{dt^2} + (B_P + K_P + K_A R_P U_{jet}) \frac{de}{dt} + \left(K_I + K_A R_P \frac{dU_{jet}}{dt} \right) e = K_A (\omega_{P,ref} R_P - 2U_{jet}) \frac{dU_{jet}}{dt} \quad (3.83)$$

From the assumption that $\omega_{P,ref}$ is constant, it follows that U_{jet} is also constant, which simplifies Equation 3.83 to:

$$J_P \frac{d^2e}{dt^2} + (B_P + K_P + K_A R_P U_{jet}) \frac{de}{dt} + K_I e = 0 \quad (3.84)$$

the characteristic equation corresponding to Equation 3.84 can be rewritten as:

$$\lambda^2 + 2\zeta\omega_0\lambda + \omega_0^2 = 0 \quad (3.85)$$

where the natural frequency and damping ratio are given by:

$$\omega_0^2 = \frac{K_I}{J_P} \quad (3.86)$$

$$\zeta = \frac{B_P + K_P + K_A R_P U_{jet}}{2\sqrt{J_P K_I}} \quad (3.87)$$

Hence, the controller gains K_P and K_I can be chosen in terms of the desired parameters for ζ and ω_0 using the following relations:

$$K_P = J_P 2\zeta\omega_0 - (B_P + K_A R_P U_{jet}) \quad (3.88)$$

$$K_I = J_P \omega_0^2 \quad (3.89)$$

3.7. CONCLUDING REMARKS

This chapter showed that it is possible to use hydraulic technology to replace the variable speed functionality of wind turbines. Both a passive and active control strategies were analyzed for a single wind turbine using feedback control tools in both the frequency and time domain. The passive control strategy showed to be inherently stable by using a constant area nozzle for below rated wind speed conditions. In this strategy, the size of the diameter of the nozzle can be chosen to match the optimal tip speed ratio of the rotor while having a variable pressure in the hydraulic network. The passive strategy is simple and robust but is limited for a single turbine. As more turbines are to be incorporated into the same hydraulic network, a constant pressure system would be preferred.

An active control strategy was also analyzed to obtain a variable speed rotor while keeping a constant pressure in the hydraulic network. The constant pressure control was achieved by modifying the area of the nozzle through a linear actuator. A combination of a PI control in series with a low-pass filter and notches was used to reduce the influence of the pipeline dynamics on the pressure response. In addition a variable displacement pump operating under the controlled pressure was used to modify the transmitted torque to the rotor. Since the controllers were designed under the framework of linear-control theory, it is expected that other control methods can lead to a more effective and robust variable speed functionality.

4

DYNAMICS AND PERFORMANCE OF A SINGLE HYDRAULIC WIND TURBINE

4.1. INTRODUCTION

Before evaluating the performance of a hydraulic wind farm, it is desirable to understand the performance and dynamic response of a single turbine subject to a stochastic wind. This chapter presents the modelling and analysis of two fictitious offshore wind turbines using pressurized water as transmission medium. In order to evaluate their performance, their performance is compared with that of a conventional offshore wind turbine. Each of these turbines will be considered as a single operating unit of a hydraulic wind farm at a later stage, in the simulations of Chapter 6.

The chapter is organized as follows. Section 4.2 provides the operational principle and the main design aspects of two concepts of turbines. In Section 4.3, the hydraulic models and control strategies described in Chapter 2 and Chapter 3 are incorporated into the model, while the operational steady-state characteristics are shown in Section 4.4. Finally, time domain simulations are used in Section 4.5 to analyze the dynamic performance and transient response of a single turbine under different operational conditions.

4.2. SYSTEM DESCRIPTION

Two different concepts of offshore wind turbines will be evaluated as potential solutions for a hydraulic wind farm. The design parameters of both hydraulic concepts were obtained using as a basis the operating conditions and the same rotor as the 5 MW NREL offshore turbine (Jonkman et al., 2009). The rotor is rigidly interconnected to the fluid power transmission and generator platform described in the previous chapters. Despite the lack of availability of the required multi-MW pumps or motors, it will be assumed

Parts of this chapter have been published in *IET Renewable Power Generation*, 8(4) and in *Journal of Computational and Nonlinear Dynamics*, 10(4) (Jarquin Laguna et al., 2014; Jarquin Laguna, 2015). The content is reproduced here with permission of the publishers and the co-authors. Note that minor changes have been introduced to make the text consistent with the other chapters of the thesis.

that these components exist and can perform with the same efficiency as available technology.

The reference turbine and the two hydraulic solutions are described in the following paragraphs. A simplified schematic of the overall conversion system of the three concepts is shown in Figure 4.1. The capital letters A, B and C are used as reference points for performance comparison in the next sections. Electrical efficiencies for the transformers and power cables were derived from existing literature (Parker and Anaya-Lara, 2013).

4.2.1. NREL REFERENCE TURBINE

This theoretical offshore wind turbine is used as baseline model. It is a generic three-bladed upwind rotor used for several research purposes in the wind energy field (Jonkman et al., 2009). The turbine comprises a gearbox with a flexible high-speed shaft and a variable speed generator with full-span pitchable blades. With 5 MW of electrical rated power, this turbine is fairly representative of the commercial offshore turbines in this class. A schematic with the main components of this turbine is shown in Figure 4.1(a). The schematic includes the electrical transformers and power cables used for the conditioning and transmission of electrical power within the farm.

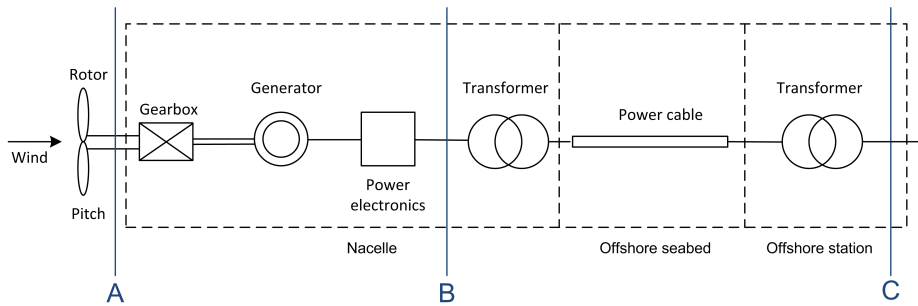
4.2.2. HYDRAULIC TURBINE WITH PASSIVE SPEED CONTROL (PSC)

The first hydraulic concept is a variable-speed, pitch controlled turbine with a passive torque control strategy. The passive-torque control allows the turbine to operate at (near) optimal aerodynamic performance below rated wind speed, see Section 3.4. Above rated wind speed, active pitch control is used to maintain the power output in a similar way as with conventional technology. Hence, fixed volumetric pumps and motors are used with a constant area nozzle. Furthermore, this concept integrates an oil-based closed circuit hydraulic transmission between the rotor and the water pump. The motivation for this concept is that it is regarded as a feasible solution by matching available technology and operating conditions.

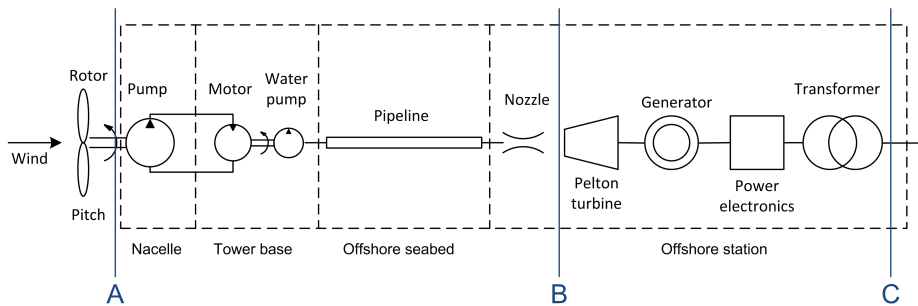
Using the rotor characteristics of the NREL turbine, a fixed nozzle area is chosen to optimize the power capture at a tip speed ratio of $\lambda = 7.55$. In this case the maximum tip speed of 80 m/s is reached at a wind speed of around 10.6 m/s which defines the rated wind speed using the passive control strategy. Thus, the rated power is limited to the values obtained at the reduced rated wind speed but with maximum aerodynamic performance below this value. This concept has been previously explored in (Diepeveen, 2013; Jarquin Laguna, 2015). A variable speed generator coupled to the Pelton turbine, allows to operate the whole wind farm efficiently and safely. A schematic with the main components of this turbine is shown in Figure 4.1(b).

4.2.3. HYDRAULIC TURBINE WITH ACTIVE SPEED CONTROL (ASC)

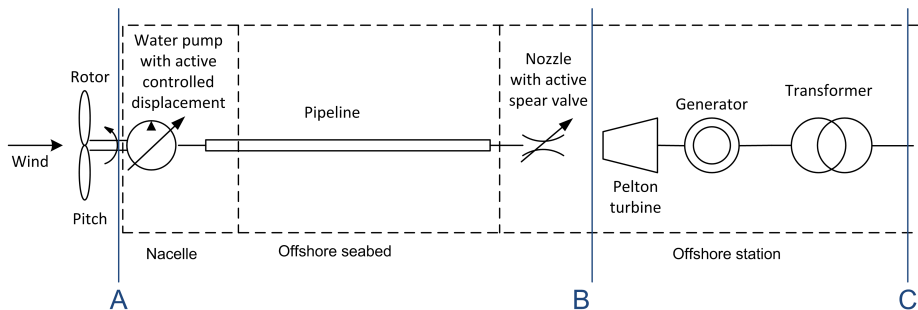
The second concept is also a variable-speed, pitch controlled turbine but it uses an active control strategy to regulate both the rotor speed and the hydraulic pressure in the system. A controlled pressure in the water line might be more desirable when extending towards wind farms, as it allows to connect more turbines to the hydraulic network. For this option, the same operational characteristics from the reference turbine are used.



(a) NREL reference turbine



(b) Hydraulic with PSC



(c) Hydraulic with ASC

Figure 4.1: Simplified schematic with the main components involved in the energy conversion for a reference offshore wind turbine and two proposed hydraulic concepts with passive and active speed control. The capital letters A, B and C are used as reference points for performance comparison.

The only difference is that the lower limit of the rotor speed is no longer limited by the generator, allowing to go as low as 4 rpm as derived from numerical computations. Together with a controllable spear valves at the nozzle, a fixed speed generator and Pelton turbine are included in the offshore station. Furthermore, the concept assumes the existence of a high efficient, low-speed and high-pressure water pump which is able to adjust its volumetric displacement. A similar concept of this turbine has also been discussed in (Buhagiar et al., 2015). The schematic of this concept is shown in Figure 4.1(c). The main design parameters of the three turbines described above are summarized in Table 4.1.

Table 4.1: Main design parameters for the reference rotor and the proposed hydraulic concepts with passive and active speed control respectively.

Design parameter	NREL (Jonkman et al., 2009) reference	Hydraulic PSC	Hydraulic ASC
Rotor diameter	126 m	126 m	126 m
Rated wind speed	11.4 m/s	10.6 m/s	11.4 m/s
Hub height	90 m	90 m	90 m
Design tip speed ratio λ	7.55	7.55	7.55
Max power coeff. C_p	0.485	0.485	0.485
Rated mech power	5.4MW	4.4 MW	5.4 MW
Rotor speed range	6.9-12.1 rpm	4-12.1 rpm	4-12.1 rpm
Drivetrain concept	Gearbox	Hydraulic	Hydraulic

4

4.3. MATHEMATICAL DESCRIPTION OF THE PHYSICAL SYSTEM

In this section, the mathematical models for the various subsystems are assembled into a global model. The dynamic interaction between the subsystems is shown in the block diagrams of Figures 4.2 and 4.4 for the passive and active concept respectively. The model corresponding to each block is described by the section or subsection whose number is given below the block's name.

4.3.1. AERODYNAMIC MODEL

The Blade Element Momentum (BEM) theory is used to obtain the aerodynamic characteristics of the rotor. Aeroelastic effects and unsteady aerodynamics are not accounted for as a quasi-static approach is sufficient to analyze the main dynamics of the proposed concept at a system level.

In order to account for more complex aerodynamic models, the power transmission and generator platform models presented in the next subsections can be implemented in advanced aeroelastic simulation packages through an external Dynamic Link Library file (DLL) file. Alternatively, the mathematical models presented here can be used in combination with other simulation packages used for design and certification of wind turbines, such as HAWC2 or GH Bladed (Larsen and Hansen, 2007; Bossanyi, 2010). The

implementation of such models through an external DLL file has been previously done for fluid power drivetrains in (Jarquin Laguna et al., 2014).

4.3.2. PITCH ACTUATOR MODEL

The pitch actuator is based on a pitch-servo model described by a proportional regulator with constant K_β . The demanded pitch β_{dem} was obtained from 3.6.1. The second order model includes a time constant t_β and an input delay δ from input u_β to the pitch rate $\dot{\beta}$; the delayed input is expressed as u_β^δ . The pitch actuator is implemented with pitch rate limits of $\pm 8^\circ/\text{s}$.

$$\ddot{\beta} = \frac{1}{t_{\beta}} \left(u_{\beta}^{\delta} - \dot{\beta} \right) \quad (4.1)$$

$$u_\beta = K_\beta (\beta_{dem} - \beta_{meas}) \quad (4.2)$$

4.3.3. STRUCTURAL MODEL

The motion of the top mass of the tower in the fore-aft direction z is described with a second order model:

$$m_{tm} \ddot{z} = F_{thrust} - B_{tower} \dot{z} - K_{tower} z \quad (4.3)$$

where K_{tower} and B_{tower} are the support structure stiffness and damping; F_{thrust} is the thrust force exerted by the rotor on the top mass of the tower m_{tm} , which includes the rotor and nacelle mass.

4.3.4. HYDRAULIC DRIVETRAIN MODEL

The primary function of the hydraulic drivetrain is to convert the mechanical power of the rotor shaft into hydraulic power for electricity generation. In the proposed hydraulic concept, the high-torque low-speed mechanical power from the rotor is converted into a high-pressure flow-rate of water just before it enters the hydraulic turbine. The hydraulic drivetrains for both the passive and active control options, are constructed by interconnecting different components like pumps, pipelines and actuators. Hence, the overall system model is obtained by assembling together the equations of the individual components presented in Chapter 2.

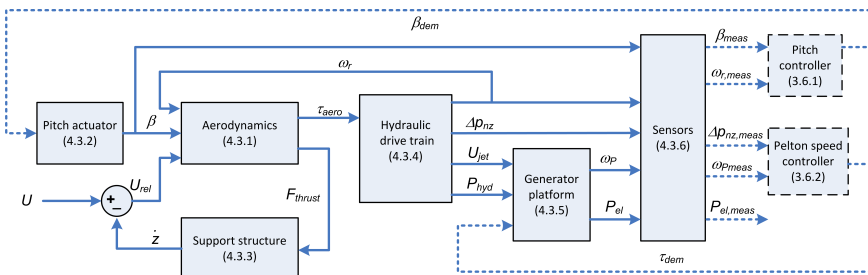


Figure 4.2: Subsystem block diagram of the hydraulic wind turbine with PSC.

Hydraulic with PSC. The hydraulic drivetrain of the PSC concept consists of an oil-based closed-loop circuit and a water-based open-loop with a fixed area nozzle as shown in Figure 4.1(b). The closed-loop circuit comprises a fixed displacement radial pump and a fixed displacement hydraulic motor; both components are interconnected through a high pressure pipeline. The rotational velocity of the low speed shaft with the rotor and pump assembly is described through a first order differential equation. This equation describes the change in angular momentum through the balance of torques acting on the shaft:

$$(J_r + J_p) \dot{\omega}_r = \tau_{aero} - \tau_p(\omega_r, \Delta p_p) - B_r \omega_r \quad (4.4)$$

The aerodynamic torque from the rotor τ_{aero} is opposed by the transmitted torque of the pump τ_p and a viscous friction torque expressed as a product of the coefficient B_r and rotational velocity of the rotor-pump assembly ω_r . The rotational mass moment of inertia of both the rotor J_r and the pump J_p are lumped together assuming they have a rigid connection. The reduced-order model of the pump is given by Equations 2.4 and 2.5; the oil line is described through the impedance model using Equation 2.63; the hydraulic motor model is given by Equations 2.6 and 2.7.

Similarly, for the high-speed shaft with the hydraulic motor and water pump, the rotational velocity of the assembly ω_m is also described through a first order differential equation model considering the inertias of both motor J_m and water pump J_{wp} including their respective transmitted torques τ_m and τ_{wp} .

$$(J_m + J_{wp}) \dot{\omega}_m = \tau_m(\omega_m, \Delta p_m) - \tau_{wp}(\omega_m, \Delta p_{wp}) - B_m \omega_m \quad (4.5)$$

Figure 4.3 shows the required equations and the input-output relation between the individual components of the drivetrain.

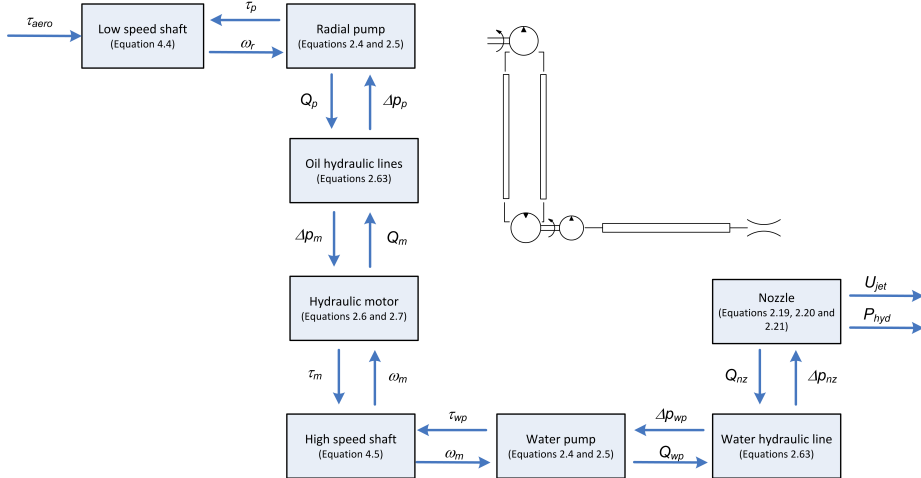


Figure 4.3: Subsystem block diagram of the drivetrain with PSC.

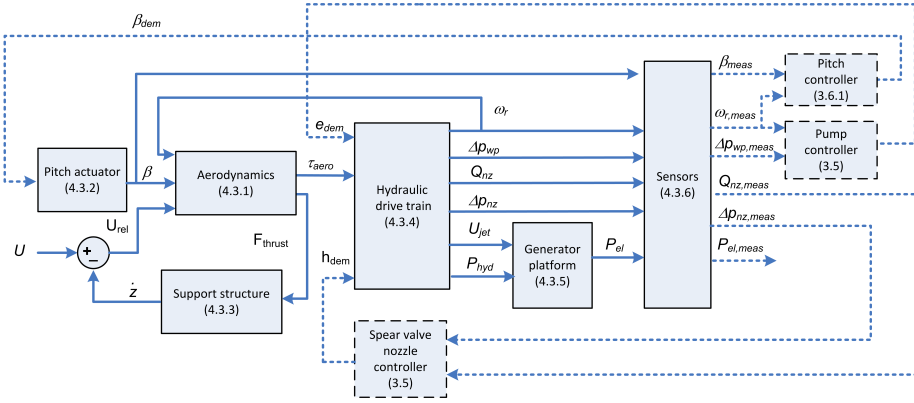


Figure 4.4: Subsystem block diagram of the hydraulic wind turbine with ASC.

Hydraulic with ASC. For the hydraulic drivetrain with ASC, only a water-based open-loop is considered with a variable area nozzle, see Figure 4.1(c). In this case a low-speed variable displacement water pump is directly coupled to the rotor shaft. A linear actuated spear valve is employed to modify the area of the nozzle at the downstream part of the water line. Similarly as in the PSC concept, the rotational velocity of the coupled rotor and water pump is described with the following equation:

$$(J_r + J_{wp}) \dot{\omega}_r = \tau_{aero} - \tau_{wp}(\omega_r, \Delta p_{wp}, e) - B_r \omega_r \quad (4.6)$$

In comparison with the drivetrain of the PSC subsystem, the ASC subsystem requires two more inputs. These inputs are related to the active control degrees of freedom, specifically the spear valve position demand h_{dem} , and the water pump volumetric displacement ratio e_{dem} . Equations 2.8, 2.9, 2.10 and 2.11 are used to describe the variable displacement water pump. The water line is again represented through the linear model from Equations 2.63. In addition to Equation 2.19 to model the nozzle, the nozzle area and spear valve position are incorporated through Equations 2.22 and 2.23 respectively. Figure 4.5 shows the required equations and the input-output relation between the individual components of the drivetrain.

4.3.5. GENERATOR PLATFORM MODEL

At the generator platform the conversion from hydraulic power into electrical power takes place using an impulse hydro turbine. The generator platform consists of the Pelton runner coupled to an electrical generator and power electronics.

Variable speed Pelton turbine - hydraulic PSC. In the case of the hydraulic PSC concept, a variable speed Pelton turbine is employed. Hence, to describe the rotational velocity of the Pelton runner ω_p , a first order differential equation is used. A rigid shaft is assumed between the Pelton runner and the generator, such that they have the same rotational speed.

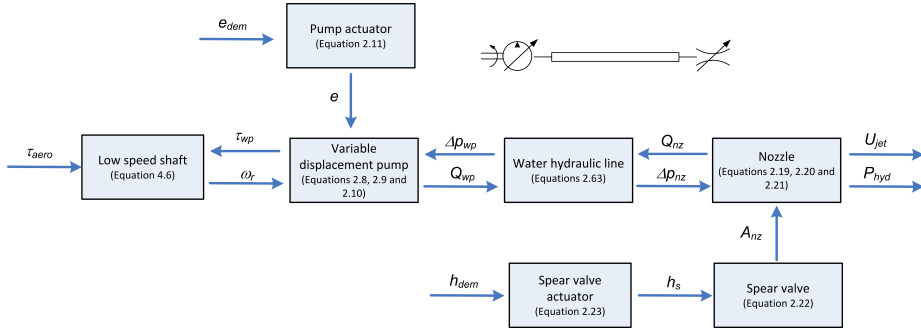


Figure 4.5: Subsystem block diagram of the drivetrain with ASC.

$$(J_{runner} + J_{gen}) \dot{\omega}_p = \tau_p + \tau_{gen} - B_p \omega_p \quad (4.7)$$

Here, B_p is a linear viscous friction coefficient; J_{runner} and J_{gen} are the mass moments of inertia of the runner and generator; τ_{gen} is an opposing generator torque to the torque produced by the Pelton runner τ_p . The Pelton torque is obtained according to the performance of the Pelton runner using Equations 2.14, 2.15 and 2.16.

The mechanical model of the variable speed generator is represented as a first order differential equation. The model includes the power electronics, which means that the generator speed is decoupled from the grid frequency. The system response is characterized through the generator time constant t_{gen} and a demand torque from the Pelton speed controller τ_{dem} .

4

$$\dot{t}_{gen} = \frac{1}{t_{gen}} (\tau_{dem} - \tau_{gen}) \quad (4.8)$$

The response of the electrical system is usually very fast, resulting in relatively small values of the generator constant. In this model the demand torque is used as a control variable to regulate the rotational speed of the Pelton turbine to a reference value. Finally the electrical power is obtained from Equation 2.17, where η_{el} accounts for the combined efficiency of the generator, power electronics and transformer.

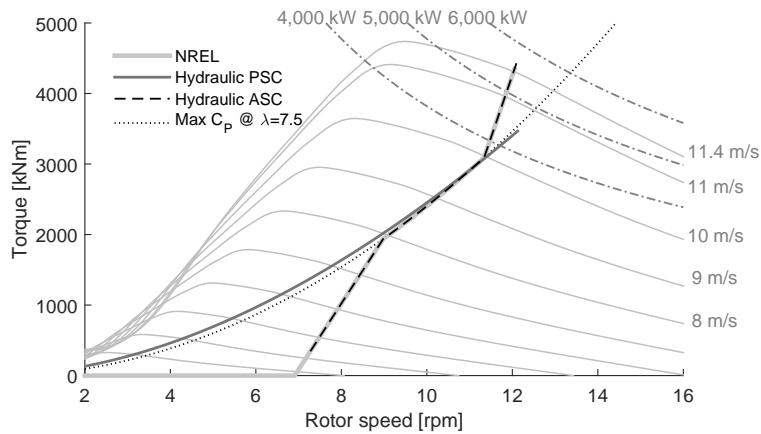
Constant speed Pelton turbine - hydraulic ASC. For the hydraulic ASC concept, the constant speed Pelton turbine is employed. Therefore, the generator rotational speed is determined by the grid frequency and Equation 4.7 can be omitted. The performance of the Pelton runner and electrical conversion is thus given only by Equations 2.14, 2.15 and 2.17. In this case, only the generator and transformer efficiencies are included in η_{el} .

4.3.6. SENSORS MODEL

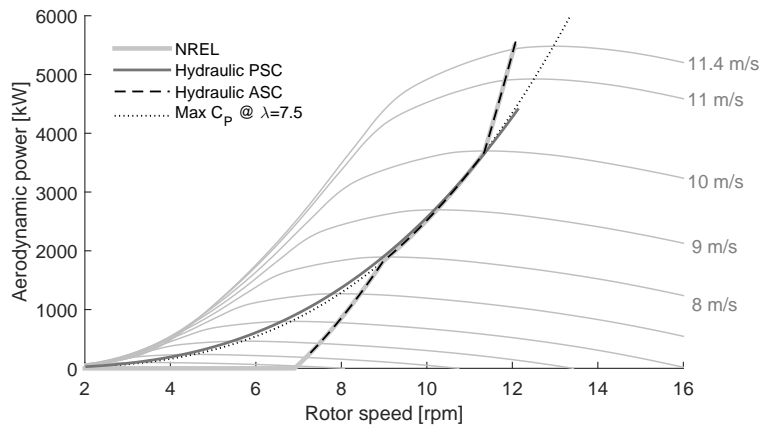
All the sensors are described through a first order discrete system. The measured output is delayed by a time constant and adjusted accordingly to the sensor resolution. The subscript $_{meas}$ is used to indicate the measured quantity.

4.4. STEADY-STATE PARAMETERS

From the drivetrain perspective, it is more common to compare the operational envelope of the variable speed turbines using the torque-speed curves as shown in Figure 4.6(a). In these curves the aerodynamic torque from the rotor is shown as a function of its rotational velocity for different operating wind speeds. In the same plot the transmitted torque from the electrical or hydraulic drivetrain is also shown as a function of its rotational speed. Hence, the intersection of both curves determines the equilibrium point and results in the steady-state values for each operating wind speed. The power-speed curves are directly obtained from the torque speed-curves resulting in a similar plot as shown in Figure 4.6(b).



(a) Torque-speed operating curves



(b) Power-speed operating curves

Figure 4.6: Operational envelopes for the different variable speed drivetrains.

The resulting steady-state operational parameters of the NREL reference turbine and the two hydraulic concepts are shown in Figure 4.7 for the operating wind speeds. The power curves consider the overall efficiency of the system, that is both the aerodynamic efficiency given through the C_P and the transmission efficiency up to point C from Figure 4.1. The numerical values for the parameters of the model are given in Appendix D.

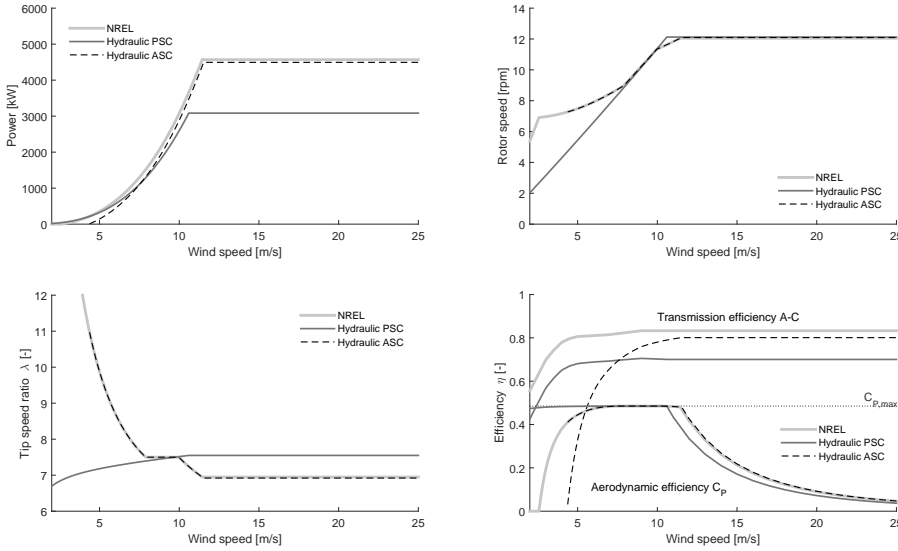


Figure 4.7: Power curves and steady-state rotor speed for the different concepts.

4.5. TIME-DOMAIN SIMULATIONS

In this section, results of the time-domain simulations of a single turbine are presented for the following operational conditions:

- Operational extreme gust, below rated.
- Turbulent wind speed, below rated.
- Turbulent wind speed, above rated.

4.5.1. RESPONSE TO AN EXTREME OPERATIONAL WIND GUST

In order to understand the dynamic response of the different concepts, it is useful to start by presenting the response to an operational wind gust in below rated conditions. The assumed time signature of the wind speed in the gust is shown in Figure 4.8.

The simulation results are shown in Figure 4.9, which presents the rotor speed, the low speed shaft torque and the transmitted power at point B from Figure 4.1. During the wind gust, all turbines experience the same maximum rotor speed, however the passive concept has a higher settling time during the decreasing gust and higher dynamic excursion with respect to the reference turbine. The higher overshoot observed during

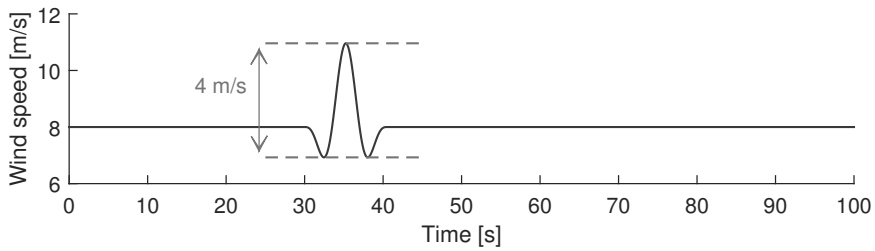


Figure 4.8: Wind gust of 4 m/s in 10.5s according to IEC standards, mean wind speed is 8 m/s.

deceleration might lead to undesired transient performance, as will be shown in the following subsections. In this passive control concept, the transmission torque and power experience very low fluctuations when compared to the reference. On the other hand, despite a lower power at the nozzle, the active control concept has a higher transmission torque. For this example, the assumption on steady aerodynamics has to be revised especially for the reference turbine which has the fastest response compared to the hydraulic concepts. In this operational condition example no pitch action is required.

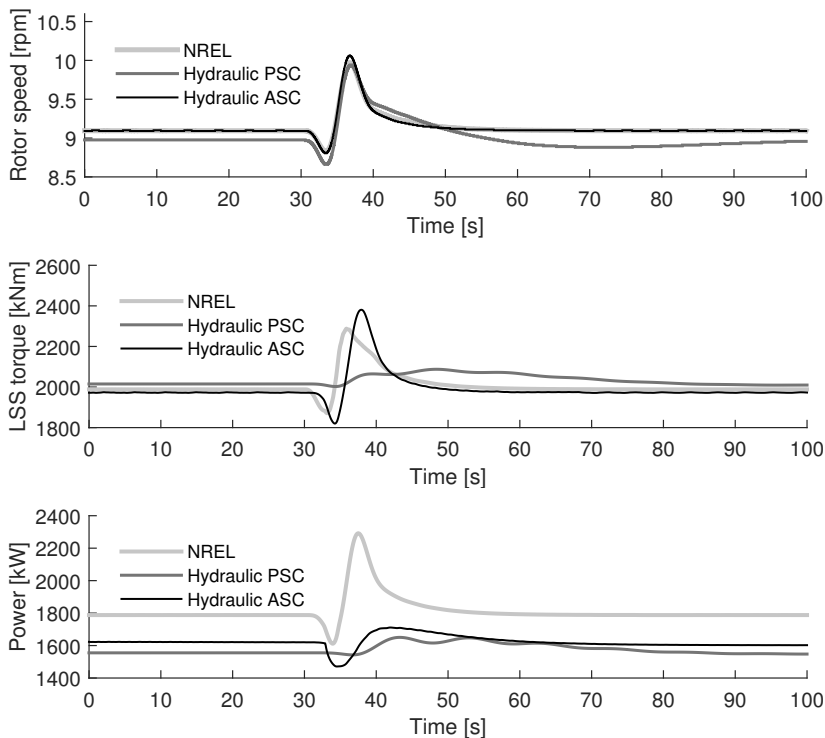


Figure 4.9: Transient response to a 4 m/s wind gust starting at $t = 30$ s.

4.5.2. BELOW RATED WIND SPEED CONDITIONS

In order to show the performance of the proposed model in below rated conditions, a wind speed signal of 8 m/s with a turbulence intensity (TI) of 17.67% is used based on the design conditions for a particular site offshore, see Figure 4.10. The 3D stochastic wind field was generated with the help of the commercial software GH Bladed with a von Karman spectrum for the turbulence and a seed of 765; the roughness length was adjusted to match the turbulence intensity (Bossanyi, 2010).

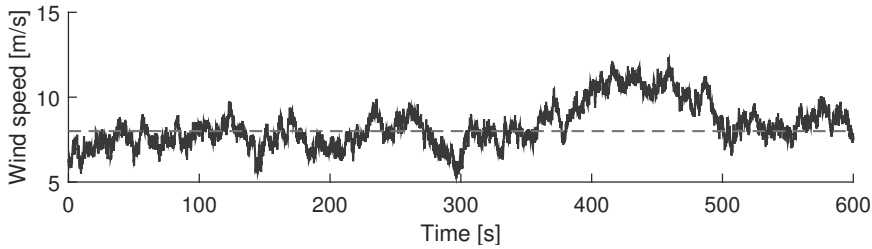


Figure 4.10: Hub height wind speed of 8 m/s with 17.67% TI.

The simulation results are shown in Figure 4.11, which presents the rotor speed, the pitch angle and the low speed shaft torque for the different concepts. The numerical results of the dynamic performance are summarized in Table 4.2. It is observed that the hydraulic concept with active control has a performance similar to the reference turbine in terms of both pitching action and rotor speed. For the passive concept, the rotor speed has a higher dynamic excursion than the reference; it shows a decelerating overshoot when a steep decrease of the wind speed occurs.

4

Regarding pitch action, there is only a brief moment in the wind time series where the conditions are above rated conditions around $t = 420$ s. The higher variation of the rotational speed of the hydraulic passive concept causes a higher pitch action required to keep the rotational speed at rated conditions. For this turbine, rated conditions occur already at 10.6 m/s which means that pitch action is required for a larger time in comparison with the other two concepts. The effect on the drivetrain transmission is shown

Table 4.2: Dynamic performance for below rated turbulent wind of 8m/s. The reference points A, B and C are shown in Figure 4.1.

	NREL reference			Hydraulic PSC			Hydraulic ASC		
	mean	std	std/mean	mean	std	std/mean	mean	std	std/mean
Mechanical power (point A) [MW]	2.27	1.05	46.3%	2.16	0.88	40.6%	2.25	1.06	47.0%
Transmitted power (point B) [MW]	2.14	0.99	46.2%	1.76	0.68	38.8%	1.95	1.07	55.0%
Electric power (point C) [MW]	1.90	0.88	46.2%	1.48	0.58	39.1%	1.71	0.94	55.1%
Drivetrain torque [kNm]	2195	719	32.8%	2152	522	24.2%	2169	729	33.6%
Rotor speed [rpm]	9.53	1.07	11.3%	9.30	1.61	17.3%	9.52	1.08	11.4%
Average power coefficient C_p		0.517			0.493			0.511	
Average efficiency η_{AB} [%]		94.4			81.4			87.0	
Average efficiency η_{BC} [%]		88.6			84.3			87.7	
Energy yield during simulation [kWh]		316.2			247.4			285.3	

by the transmitted torque at the low speed shaft, where the baseline exhibits larger oscillations and excursions than those of the fluid power transmission concept which show a much smoother and steady value. The oscillations in the reference turbine are due the stiff and slightly damped mechanical transmission.

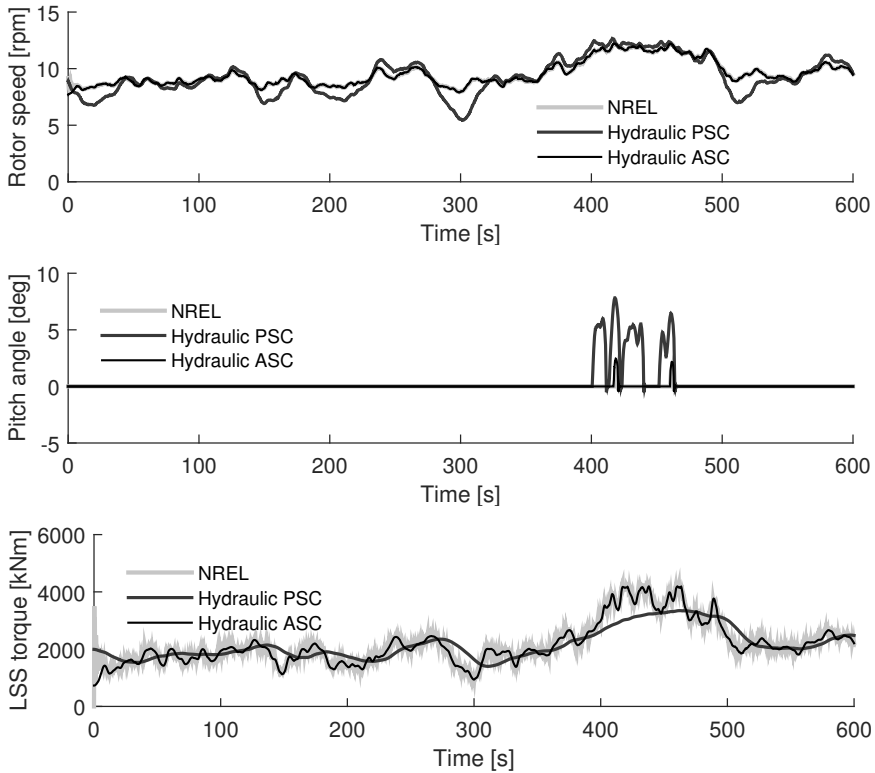


Figure 4.11: Transient response operation below rated wind speed.

At the generator platform, see Figure 4.12, the rotor speed of the Pelton turbine is modified proportional to the water jet velocity in order to keep the ratio with respect to the tangential velocity of the runner constant. As shown in the power graphs of Figure 4.13, the differences in aerodynamic performance are minor for the three concepts, with differences in the power coefficient between 0.51 and 0.49 for the active and passive concepts respectively. Nevertheless, both hydraulic concepts have a reduced transmission efficiency compared to the reference turbine. It is important to mention that the transmission efficiency of the reference turbine from point B to point C includes the individual efficiencies of the transformers and the power cable with values of 0.95 and 0.98 respectively.

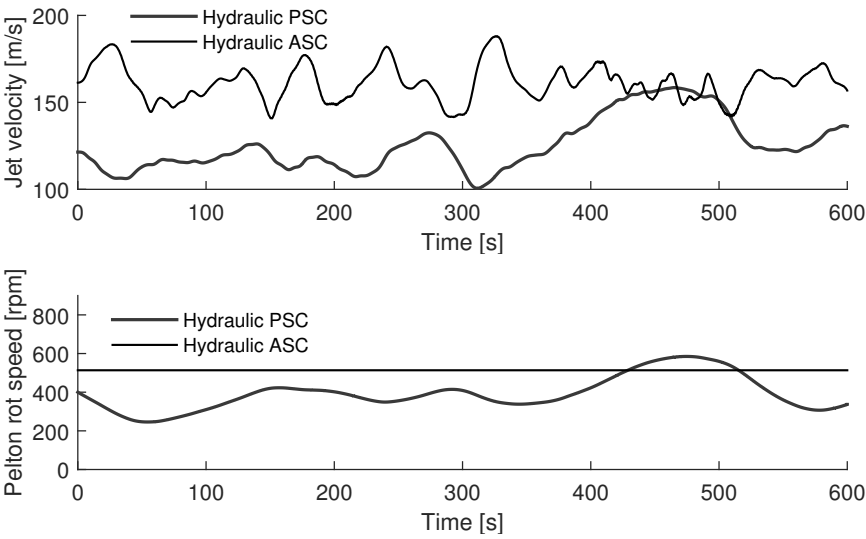


Figure 4.12: Generator platform operation below rated wind speed.

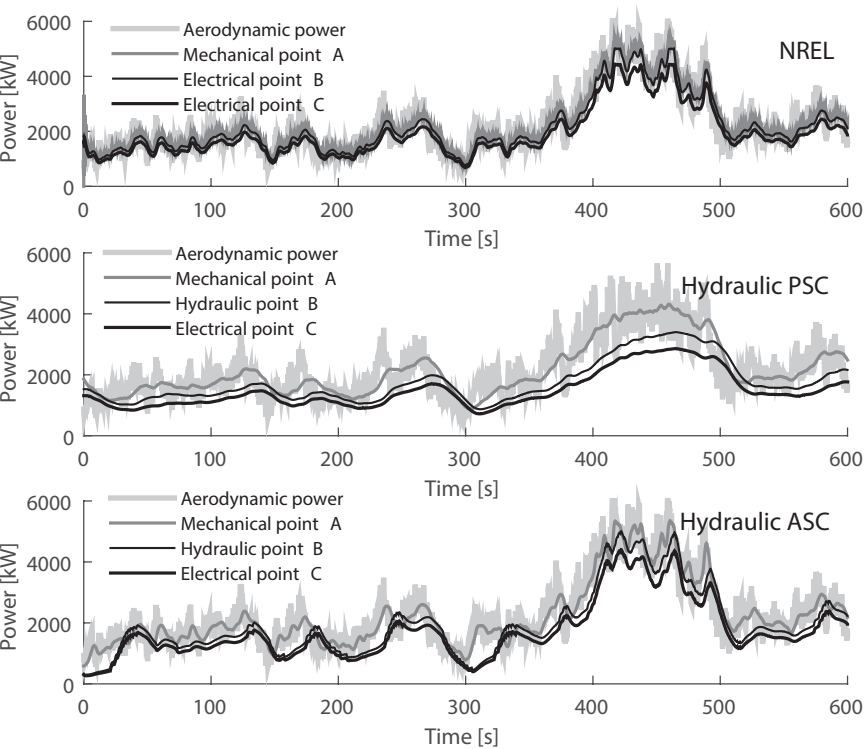


Figure 4.13: Performance comparison below rated wind speed.

4.5.3. ABOVE RATED WIND SPEED CONDITIONS

For above rated wind speed conditions, a turbulent wind speed signal of 15 m/s with turbulence intensity of 12% is used in the numerical model, see Figure 4.14.

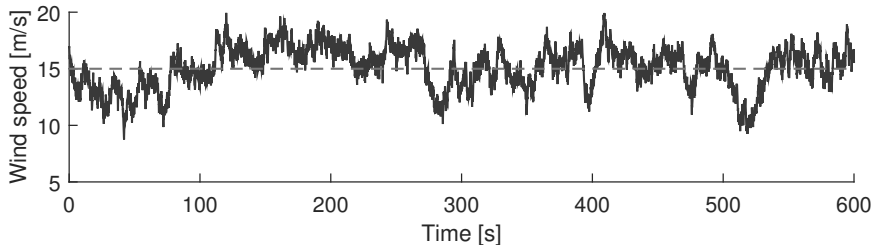


Figure 4.14: Hub height wind speed of 15 m/s with 12% TI.

The simulation results are shown in Figure 4.15, which presents the rotor speed, the pitch angle and the low speed shaft torque for the different concepts. The rotational speed of the rotor and pitching action show a similar response for the three turbines, with related

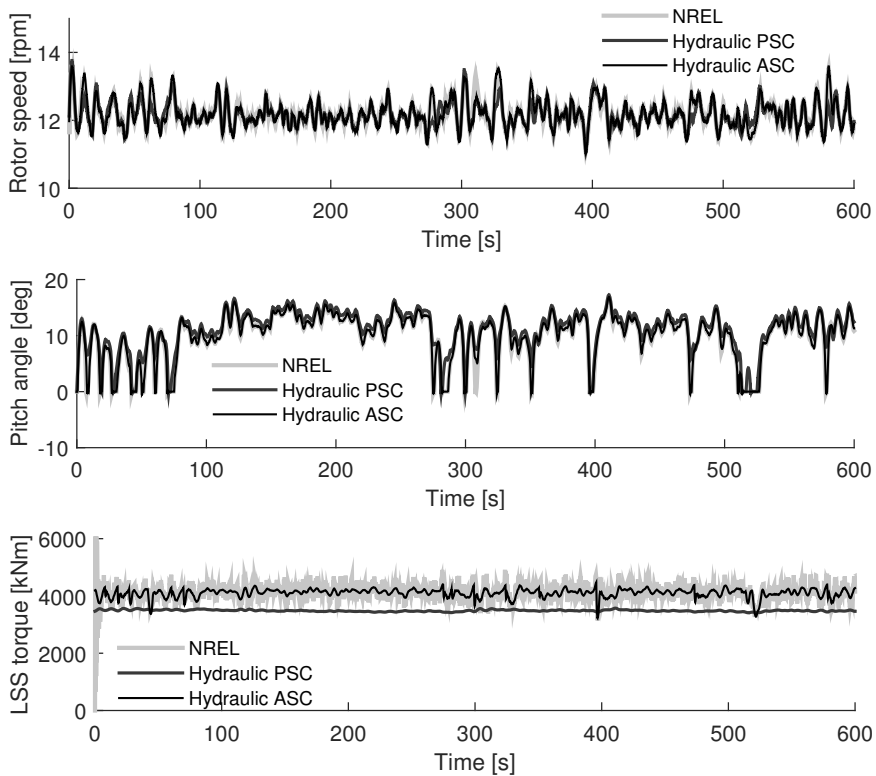


Figure 4.15: Transient response operation above rated wind speed.

fluctuations and excursions. These results are expected since the three turbines have the same control strategy and pitch controller for above rated wind speed conditions. In terms of the drivetrain torque, it is clear that the hydraulic transmission concepts show a more steady value and reduced fluctuations when compared to the reference turbine; as observed in the summarized results of Table 4.3.

Table 4.3: Dynamic performance for above rated turbulent wind of 15 m/s. The reference points A, B and C are shown in Figure 4.1.

	NREL reference			Hydraulic PSC			Hydraulic ASC		
	mean	std	std/mean	mean	std	std/mean	mean	std	std/mean
Mechanical power (point A) [MW]	5.26	0.34	6.5%	4.44	0.14	3.3%	5.23	0.19	3.67%
Transmitted power (point B) [MW]	4.97	0.14	2.9%	3.61	0.06	1.5%	4.87	0.13	2.6%
Electric power (point C) [MW]	4.40	0.13	2.9%	3.11	0.05	1.5%	4.29	0.11	2.6%
Drivetrain torque [kNm]	4128	281	6.8%	3486	29	0.8%	4101	148	3.6%
Rotor speed [rpm]	12.19	0.38	3.1%	12.16	0.35	2.9%	12.19	0.40	3.3%
Average power coefficient C_p	0.201			0.170			0.200		
Average efficiency η_{AB} [%]	94.4			81.3			93.1		
Average efficiency η_{BC} [%]	88.6			86.1			87.9		
Energy yield during simulation [kWh]	733.5			518.2			714.2		

Regarding the generator platform of the hydraulic concepts, both jet velocities and Pelton rotational speeds are kept to nominal values, ensuring a suitable performance for above rated conditions as can be observed in Figure 4.16. In contrast with below rated wind speeds, both hydraulic concepts perform in an adequate manner for above rated conditions. However, Figure 4.17 shows both hydraulic concepts, particularly the passive one, have lower efficiency in the power conversion than the reference.

4

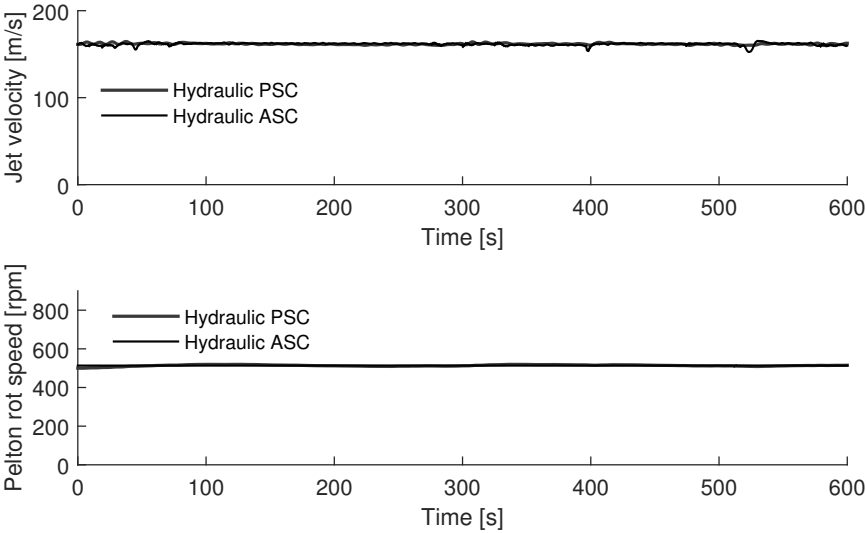


Figure 4.16: Generator platform operation above rated wind speed.

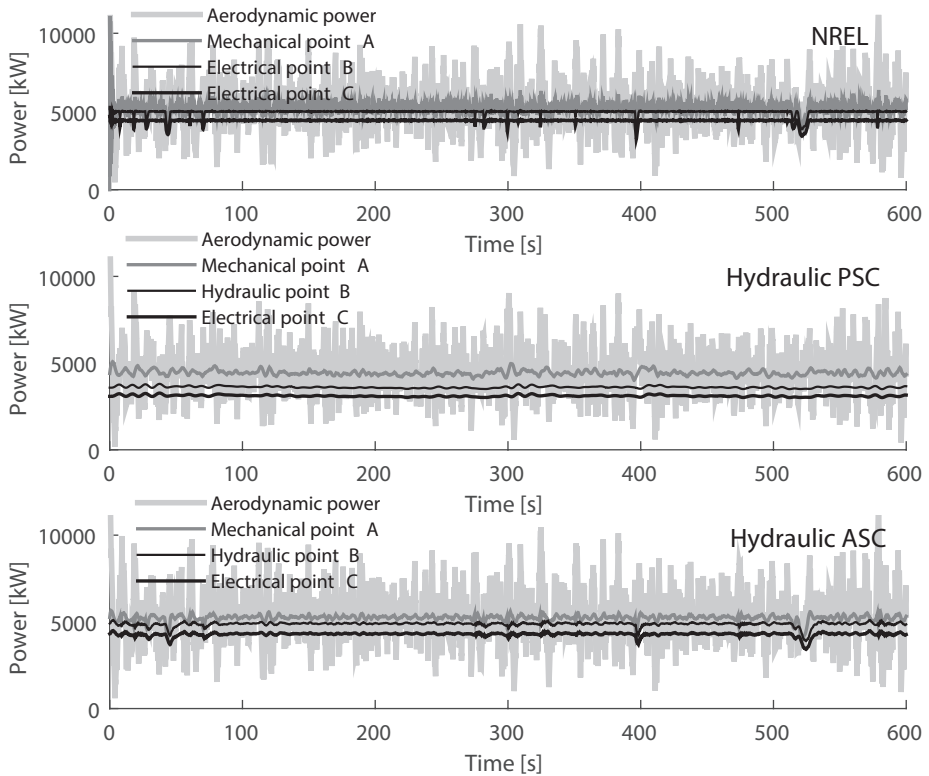


Figure 4.17: Performance comparison above rated wind speed.

4.6. CONCLUDING REMARKS

Simulations show that the operation below rated wind speed for a fluid power transmission with both passive and active control is feasible for a single turbine. A strongly damped response of the generated power and transmitted torque demonstrates a good dynamic performance for the hydraulic transmission with a passive system, while achieving slightly higher excursions for the variable rotor speed when compared to the reference turbine. For above rated conditions, both hydraulic concepts perform satisfactorily using the same pitch control strategy. However, they provide a lower energy capture than the reference. A reduced fluctuation of the drivetrain torque and power are also demonstrated for both hydraulic concepts.

The addition and simulation of more turbines to the hydraulic network is necessary to determine to which extent the benefits of a centralized wind farm compensate for the relatively lower efficiency using the proposed passive torque control.

5

HYDRAULIC NETWORK TRANSIENTS

5.1. INTRODUCTION

One of the key challenges in the quest for a centralized electricity generation is the use of hydraulic networks for collection and transport of the pressurised water from the individual wind turbines to the generator platform. This chapter presents an evaluation of the accuracy of a numerical time-domain model of a hydraulic network developed in the framework of this thesis. The numerical model should be able to accurately represent the transient response of the hydraulic network to enable the simulation of a more general wind power plant model. Thus, in order to evaluate the accuracy of the model, a semi-analytical approach is presented based on the impulse response method (IRM). This method has been extensively used for dynamic analyses in other areas such as vibrations of mechanical systems (Graff, 1991), however its use in hydraulic systems has not been completely exploited.

The chapter is organized as follows. In Section 5.2, a brief overview of the most common time-domain numerical models, to solve fluid transients in hydraulic networks, is presented. Then, in Section 5.3 a semi-analytical method is proposed. The analytical solution of a single line is extended to the solution of a more complex hydraulic network consisting of several hydraulic lines. To illustrate the application of the analytical method, a numerical example of a simple hydraulic network is treated in Section 5.4. Here, the time-domain results are compared with the ones obtained by using the modal method of analysis applied to the hydraulic network. Finally conclusions are presented in Section 5.5.

5.2. FLUID TRANSIENTS IN HYDRAULIC NETWORKS

Transient flow in hydraulic networks is a phenomenon that often occurs as a result of either accidental or normal operation of hydraulic systems. Its importance has been

This chapter has been published in *Heron*, 59(1) (Jarquin Laguna and Tsouvalas, 2014) and is reproduced here with permission of the co-author. Note that minor changes have been introduced to make the text consistent with the other chapters of the thesis.

well recognized due to abrupt changes in flow or pressure introduced by valve closures or component failures. Therefore, accurate and robust numerical models are necessary to analyze the traveling pressure waves as a result of such sudden changes. The most common approach to address this problem, has been the extension of the method of characteristics (MOC) towards more complex hydraulic networks, (Karney and McInnis, 1992; Wichowski, 2006). However, the MOC together with other discrete formulations such as finite differences (Pezzinga, 1999), require a spatial discretization of the lines in the network, which turns to be computationally demanding as discussed in (Wood et al., 2005).

As described earlier in Section 2.4 (and employed in Chapters 3 and 4), modal approximations of single pipelines are a convenient method to model the fluid transients. These approximations are suitable for time-domain models, especially when the pipelines are interconnected with other non-linear components such as variable displacement pumps or wind turbines. In addition, these models have also been used to construct hydraulic networks as a part of a complex fluid power system, i.e. through bond-graph models (Margolis and Yang, 1985; Yang et al., 2012). It is important to mention that when modal approximations are used to build networks, each line in the network should include enough number of modes to cover the frequency range of interest of both the overall system and input disturbance. Due to the different line geometries and interface conditions, the selection of the required number of modes for each line is not straightforward. Therefore, the modal method has the disadvantage of lacking a direct control on the accuracy of the results due to a propagation error introduced by the number of modes used for each line. Given that, a semi-analytical evaluation of the accuracy of the method is desirable.

5.3. PROPOSED SEMI-ANALYTICAL METHOD

5

In order to evaluate the accuracy of the hydraulic network model constructed from modal approximations, a semi-analytical method to analyze the entire network is presented. The latter method is based on a semi-analytical impulse response of the flow and includes the exact solution of a two-dimensional viscous problem in the frequency domain with various interface and boundary conditions. The inversion to the time-domain is accomplished by the use of the fast Fourier transform, followed by convolution of the impulse response applied function with the input signals.

For the analysis of a single pipeline element, this method has already been applied (Suo and Wylie, 1989; Kim, 2011). The work in this thesis presents a direct extension towards a solution for a hydraulic network system consisting of multiple lines including dissipative boundary conditions. The approach is remarkably simple in its application. It consists of a solution of a coupled system of linear algebraic equations and the use of the Fourier transform. The method is accurate and reliable for the solution of large networks, overcoming the disadvantages of several other approaches. An overview of the modal approximation method and the proposed approach is presented in Figure 5.1.

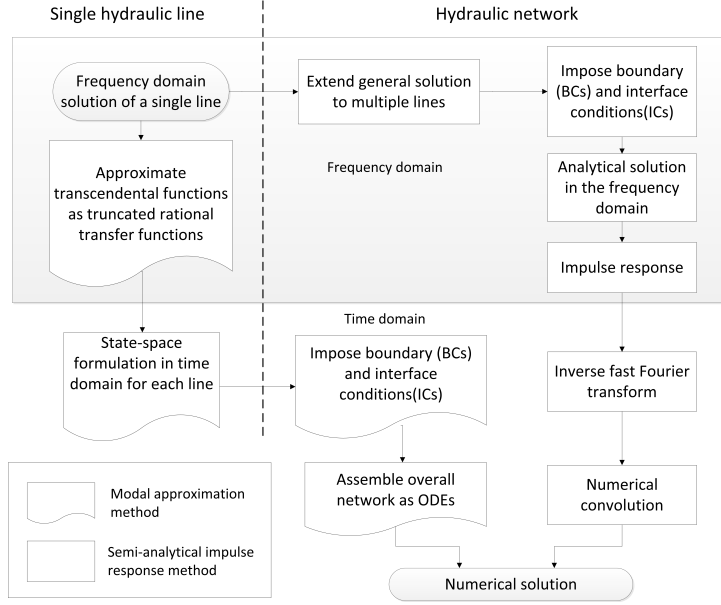


Figure 5.1: Overview of two different approaches used for the numerical analysis of hydraulic networks using continuous models.

5.3.1. NUMERICAL APPROACH AND CONSIDERATIONS

The solution for a complete hydraulic network consisting of multiple lines is an extension of the solution given by Equations 2.33 and 2.34. Using Equation 2.30, the general solution in the frequency domain for the flow and pressure of each of the lines of the network, denoted by the subscript i , is given by:

$$Q_i(x, \omega) = \left[A_i(\omega) \cos \frac{i\omega\beta_i}{c_o} x + B_i(\omega) \sin \frac{i\omega\beta_i}{c_o} x \right] \frac{\rho_o c_o}{Z_{0,i}} \frac{J_0 \left[i \left(\frac{i\omega r_{0,i}^2}{v_o} \right)^{\frac{1}{2}} \right]}{\beta_i^2} \quad (5.1)$$

$$P_i(x, \omega) = \left[A_i(\omega) \sin \frac{i\omega\beta_i}{c_o} x - B_i(\omega) \cos \frac{i\omega\beta_i}{c_o} x \right] \frac{\rho_o c_o}{\beta_i} J_0 \left[i \left(\frac{i\omega r_{0,i}^2}{v_o} \right)^{\frac{1}{2}} \right] \quad (5.2)$$

The difference between the above solution and that for a single pipeline is that the integration constants for the pressure and flow descriptions cannot be determined explicitly for each of the lines of the hydraulic network. Instead they are obtained numerically by solving a linear system of coupled algebraic equations compiled from the various boundary and interface conditions according to the particular configuration of the system. The system of equations with respect to the unknown coefficients can be written in the matrix as follows:

$$\mathbf{Ax} = \mathbf{b} \quad (5.3)$$

where \mathbf{A} is the global system matrix, whose elements are frequency dependent. The vector \mathbf{x} corresponds to the unknown integration constants for the network consisting of n lines:

$$\mathbf{x} = [A_1(\omega), B_1(\omega), A_2(\omega), B_2(\omega), \dots, A_n(\omega), B_n(\omega)]^T \quad (5.4)$$

The right-hand side vector \mathbf{b} corresponds to the external forcing terms at the boundary conditions or interfaces. Thus, the solution of a complex network is only limited by the computational considerations to solve a system of algebraic linear equations. The order of this system of equations is twice the number of lines in the hydraulic network, i.e. $2n$.

INTERFACE AND BOUNDARY CONDITIONS

The interface conditions correspond to the junction points or nodes in systems of branching pipes. At these particular locations, the continuity equation is used to relate the inflows and outflows of the discharges at each node or junction, see Equation 5.5. In addition, another set of equations is obtained through the general assumption of uniqueness of the pressure at each junction or node k according to Equation 5.6, where the superscripts l and r refer to the left and right side of the interface respectively.

$$\sum Q_{in}(x_k, \omega) - \sum Q_{out}(x_k, \omega) = 0 \quad (5.5)$$

$$P^l(x_k, \omega) = P^r(x_k, \omega) \quad (5.6)$$

The different boundary conditions at the terminations of the lines could include any linear static or dynamic hydraulic component. An example of a static boundary condition is a resistive component, which relates the volumetric flow with the pressure difference across the element at each moment in time through the hydraulic resistance R ; in the frequency domain this condition is given by

$$P_a(\omega) - P_b(\omega) - R Q_b(\omega) = 0 \quad (5.7)$$

5

A dynamic termination as a boundary condition is also possible, (i.e. a line termination with a large volume of fluid or an actuator). For this example the relation is given through a first order linear differential equation for the pressure p_b , where the hydraulic capacitance C_1 accounts for the fluid compressibility. The representation, in both time and frequency domain are given as:

$$C_1 \frac{dp_b(t)}{dt} - Q_b(t) = 0 \quad (5.8)$$

$$C_1 i\omega P_b(\omega) - Q_b(\omega) = 0 \quad (5.9)$$

The treatment of a non-linear boundary condition at one of the terminations is also possible through this method; in this case a simultaneous numerical solution of the non-linear boundary condition equation and the convolution integral at the boundary is required. An example is shown in (Suo and Wylie, 1989), for the particular case of a non-linear valve description.

5.3.2. IMPULSE RESPONSE METHOD FOR HYDRAULIC NETWORKS

The impulse response method makes use of the superposition property of linear systems; if an arbitrary but known input is decomposed into a series of impulses of different amplitudes, the response of the system is obtained by the superposition of the responses to each impulse. Thus, once the network response to an impulse is known in the time domain, its response to a general forcing function can be obtained through the convolution of the impulse response and the forcing function.

A known input at one of the boundaries of the hydraulic network can be given as either a pressure function $\Delta p(t)$ or flow function $\Delta Q(t)$. The pressure response of the system at a given location $p(x, t)$ is therefore provided by the convolution of the pressure response at the same location to a pressure impulse $r_p(x, t)$ and the desired pressure input function $\Delta p(t)$,

$$p(x, t) = \int_0^t r_p(x, t - \tau) \Delta p(\tau) d\tau \quad (5.10)$$

in which τ is a time variable used for the convolution. Or in the case of a flow input $\Delta Q(t)$ the convolution uses the pressure response to a flow impulse $r_Q(x, t)$ and the flow input function:

$$p(x, t) = \int_0^t r_{Qx}(t - \tau) \Delta Q(\tau) d\tau \quad (5.11)$$

Hence, in order to obtain the system response to an impulse, the complete hydraulic network is first analyzed in the frequency domain $r(x, \omega)$. Afterwards, the inverse Fourier transform of the pressure and/or flow is applied at the desired locations to obtain the time domain description $r_x(t)$.

$$r(x, t) = \frac{1}{2\pi} \int_{-\infty}^{\infty} r(x, \omega) e^{i\omega t} d\omega = \frac{1}{\pi} \text{Re} \left[\int_0^{\infty} r(x, \omega) e^{i\omega t} d\omega \right] \quad (5.12)$$

An efficient way to obtain such response from a numerical perspective, is to use the discrete fast Fourier transform (FFT). Although the FFT is based on a fixed discrete time step, the impulse response has only to be calculated once for the whole network. Once this response is available for the particular configuration, the numerical convolution is obtained in a separate step for any desired input without the necessity to solve the system once more. Furthermore the convolution can also be implemented for a variable step approach.

ASPECTS OF COMPUTATIONAL EFFICIENCY

For large hydraulic networks, the computational efficiency of the proposed impulse response method can be compared with other approaches such as the method of characteristics (MOC) and the modal method. A general overview is shown in Table 5.1.

Let us consider a network comprising of $n_{lines} = 100$. In the MOC, first of all an internal discretization is required; assuming that ten elements are used per line, a final grid of around 1,000 points is obtained. Every time step, a solution using finite differences is found for all the points in the grid. With the modal method no discretization is required, however a few modes are needed at least to model each line $n_{modesperline} = 4$. Assuming that four modes are used to describe accurately each line, a system of 800 ODEs is

Table 5.1: Overview of calculation requirements for hydraulic networks.

Approach	Calculation requirements per time step Δt
MOC	Solution required at all interior points of the grid; results are approximate.
Modal method	Solution to a system of linear ordinary differential equations $n_{lines}(2n_{modesperline})$; results are approximate.
IRM	Solution to a system of linear algebraic equations $2n_{lines} \times 2n_{lines}$; exact results in freq domain, accuracy in time domain depends on FFT required at the end of the method.

obtained. It is important to mention that the order of the final system might be considerably higher as some lines would require higher modes in order to obtain a minimum accuracy. Finally the IRM requires the solution of a linear system of equations of 200×200 per frequency, where the obtained solution is exact for each frequency. At the end of the method, an inverse FFT is required but the computational cost of this operation is low as this operation is independent of the number of lines in the network.

5.4. CASE STUDIES AND MODEL COMPARISON

In order to illustrate the proposed method and to compare the predictions with the modal approach proposed in the literature (Margolis and Yang, 1985), three cases are studied numerically based on the simple hydraulic network shown in Figure 5.2. The forcing input function $\Delta p(t)$ is a unit step pressure at the upstream side $x = 0$. The examples include different linear terminations and the input parameters for each case are summarized in Table 5.2. It is important to note that the dissipation coefficients of each line are relatively high $D_n \gg 0.0001$. D_n is a non-dimensional number which is given by Equation 2.40; a high value implies that the energy dissipation due to the shear friction at the wall of the line is important. Therefore the dissipative model with frequency-dependent friction will give a more accurate description of the transient behaviour than the linear friction model.

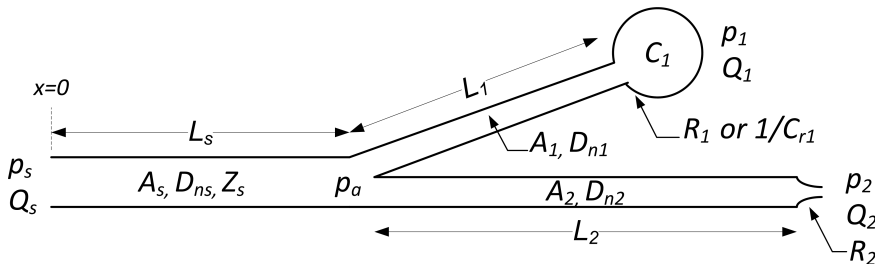


Figure 5.2: Schematic of the hydraulic network used for the numerical simulations.

Hydraulic network model based on modal approximations. With this approach, the hydraulic network is constructed by combining at least two single lines with different boundary conditions. These boundary conditions, at the upstream and downstream sides of each line, are related to the inputs and outputs of the hydraulic network. For the simple configuration given in Figure 5.2, the network is constructed from individual lines described through PQ-models. Figure 5.3 shows a schematic of such construction, where every pipeline model is represented with a linear state-space model.

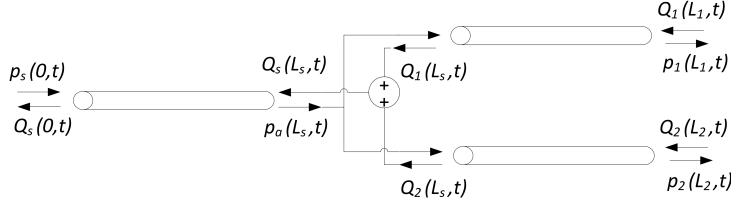


Figure 5.3: Schematic showing the model of the hydraulic network based on single line elements.

IRM approach. In general, in the frequency domain there exist two unknown integration constants for each line comprising the network. This means that for the particular configuration shown in Figure 5.2, six independent linear equations are required. The first equation corresponds to the boundary condition at the upstream side of the supply line where the required pressure impulse is applied at $x = 0$, see Equation 5.13. Three more equations are obtained from the interface conditions at the branching node a ; one for the continuity of flows, Equation 5.14; the other two for the assumption of a unique pressure at node a given by Equations 5.15 and 5.16. The supply line of the network is noted by the subscript s , while the two other branch lines are specified by the subscripts 1 and 2 respectively.

$$\text{at } x = 0 \quad P_s(0, \omega) = 1 \quad (5.13)$$

$$\text{at } x = L_s \quad Q_s(L_s, \omega) - Q_1(L_s, \omega) - Q_2(L_s, \omega) = 0 \quad (5.14)$$

$$P_s(L_s, \omega) - P_1(L_s, \omega) = 0 \quad (5.15)$$

$$P_s(L_s, \omega) - P_2(L_s, \omega) = 0 \quad (5.16)$$

Table 5.2: Numerical parameters for the different cases taken from (Margolis and Yang, 1985).

	D_{ns}	D_{n1}	D_{n2}	L_1/L_s	L_2/L_s	A_1/A_s	A_2/A_s	R_1/Z_s	R_2/Z_s	C_1/C_c^*
Case 1	0.1	0.1	0.1	1	1	1	1	∞	3	-
Case 2	0.01	0.01	0.1	1	5	1	0.5	∞	∞	-
Case 3	0.01	0.1	0.1	5	10	0.5	1	2	6	0.25

* with $C_c = \pi L_s r_s^2 / \rho c^2$

The fifth and sixth equations necessary to resolve the problem are derived from the boundary conditions at the terminations of the hydraulic lines 1 and 2, which are different for the three case studies and presented in the following subsections, see Equations 5.17 to 5.22. Once the integration constants are obtained for all the lines in the network, the average velocity and pressure can be evaluated at any desired location by Equations 5.1 and 5.2. The time domain response of the pressure impulse is obtained numerically through the discrete inverse FFT. For all cases, the number of samples used was $N = 2^{16}$, with a discrete step time of 0.0001s. The selected time step allows to follow the pressure wave propagation along the spatial coordinate with sufficient detail. Furthermore, it includes frequency components up to 5000 Hz which are sufficient to describe the step input considered in the examples. The final step is to convolute numerically the impulse response with a step function to obtain the desired step response of the system in the time domain. For the case of linear inputs, the convolution can be avoided by computing the solution directly in the frequency domain.

5.4.1. RESULTS AND DISCUSSION

The results for each case are compared with the results for the same network obtained using the modal method. The modal method is based on four modes for each of the lines in the hydraulic network as presented in (Margolis and Yang, 1985).

CASE 1

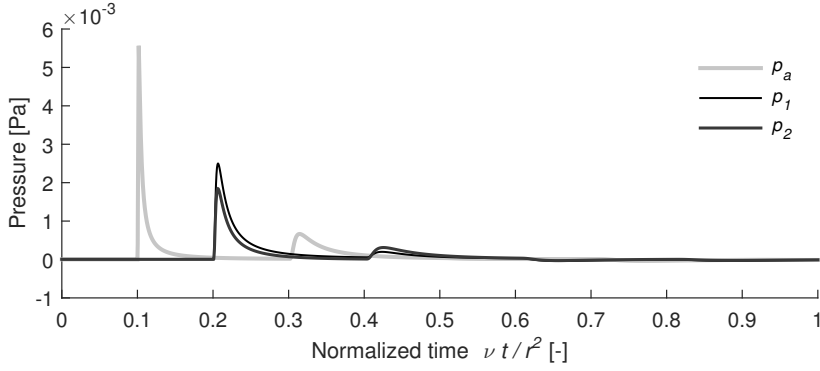
All the lines have the same geometric characteristics; one of the terminations of the pipeline is blocked while the other consists of a linear resistance element; the boundary conditions are shown in Equations 5.17 and 5.18:

$$\text{at } x = L_1 \quad Q_1(L_1, \omega) = 0 \quad (5.17)$$

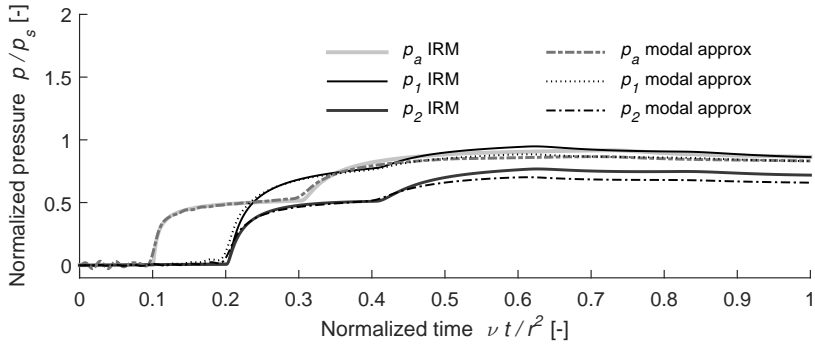
$$\text{at } x = L_2 \quad P_2(L_2, \omega) - R_2 Q_2(L_2, \omega) = 0 \quad (5.18)$$

5

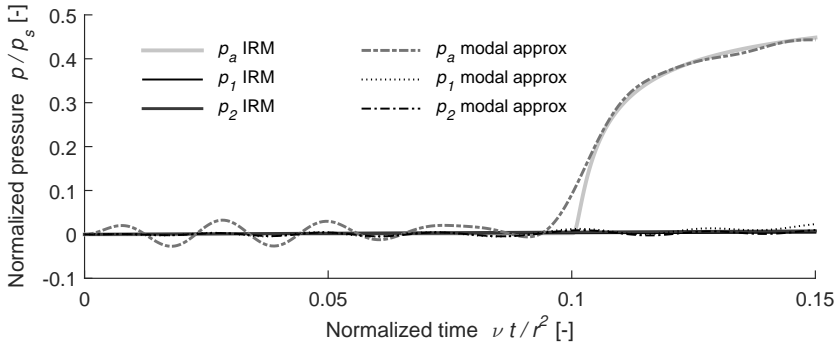
The pressure response to an impulse at the locations p_a, p_1, p_2 is shown in Figure 5.4(a); this response is numerically convoluted with a unit step input to obtain the results of the IRM. From the impulse response, the travel time of the wave fronts is clearly observed. Figure 5.4(b) shows the comparison of results with the modal method. The pressure transient shows a smooth response which is accurately described, with minor differences, by both methods. However, as observed in Figure 5.4(c), the modal method contains spurious oscillations at the initial moments in time, which are not present in the results of the IRM. The oscillations present in the modal method are introduced due to the finite number of modes used in each line. In the presented method such oscillations are absent since a sufficiently broad frequency band is accounted for.



(a) Impulse response used in the convolution of the IRM



(b) Step response comparison between the IRM and modal approximations



(c) Close-up of the step response comparison between the IRM and modal approximations

Figure 5.4: Time domain response comparison of case 1.

CASE 2

In this case, different geometries of the lines are used and both terminations are blocked; the respective boundary conditions are given in Equations 5.19 and 5.20.

$$\text{at } x = L_1 \quad Q_1(L_1, \omega) = 0 \quad (5.19)$$

$$\text{at } x = L_2 \quad Q_2(L_2, \omega) = 0 \quad (5.20)$$

As seen in Figure 5.5, when blocked terminations are used, the modal approximations are inadequate to provide an accurate response of the system. Spurious oscillations are again present at the initial moments of time for the reason explained previously. In addition, a higher dissipation of the transient response is observed in the modal approximations together with a phase difference.

The results provided by the IRM method also show sharp variations in the pressure response due to reflected wave fronts, however this effect is not captured correctly by the modal method.

CASE 3

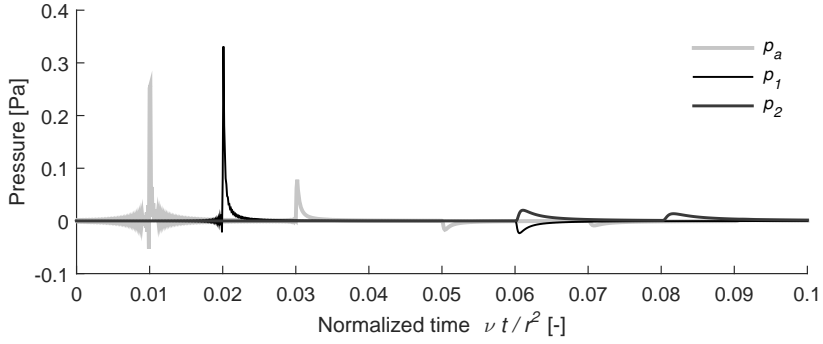
In the final case 3, different geometries are present with both dynamic and static terminations, such boundaries are given through Equations 5.21 and 5.22.

$$\text{at } x = L_1 \quad P_1(L_1, \omega) - \left(\frac{1}{C_1 i \omega} + R_1 \right) Q_1(L_1, \omega) = 0 \quad (5.21)$$

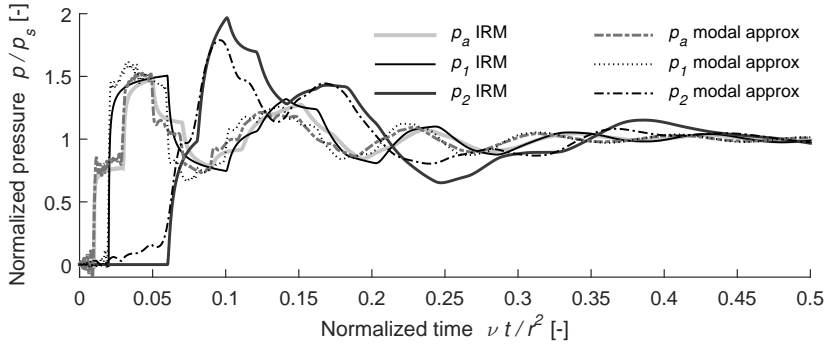
$$\text{at } x = L_2 \quad P_2(L_2, \omega) - R_2 Q_2(L_2, \omega) = 0 \quad (5.22)$$

In Figure 5.6 the results show a relatively smooth response for both methods. As can be seen, the pressure response p_a at the hydraulic branch using modal approximations, presents large oscillations especially after the first wave front surpasses the branch junction. The oscillations might be reduced by increasing the number of modes for this particular line. Hence, it is evident that even for a relatively simple network the modal method has not direct control in the required number of modes for each line.

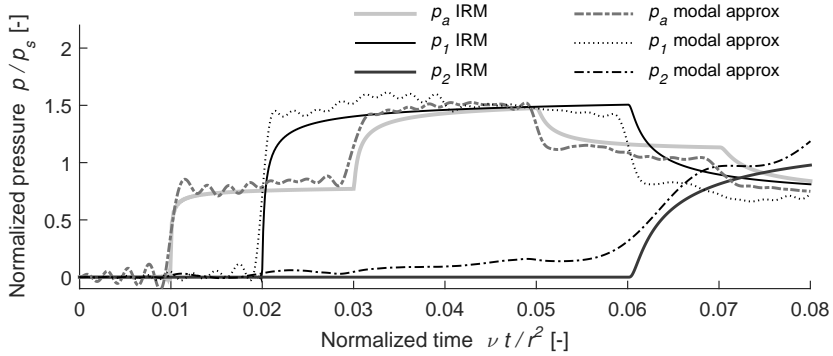
From the results presented in the previous cases, it is clear that sharp wave fronts and reflections cannot be approximated with a few number of modes. For larger networks with multiple number of lines, the inclusion of a large number of modes per line can be both computationally demanding and inexact. On the contrary, the adopted IRM method is based on an exact solution in the frequency domain, making this approach more accurate and reliable for the solution of larger networks, overcoming the disadvantages of several other approaches.



(a) Impulse response used in the convolution of the IRM

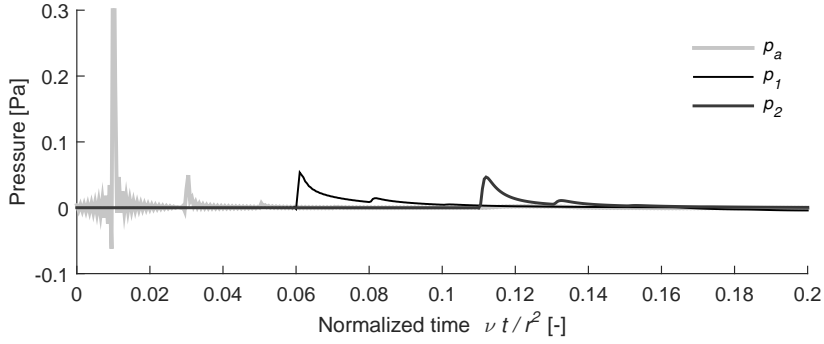


(b) Step response comparison between the IRM and modal approximations

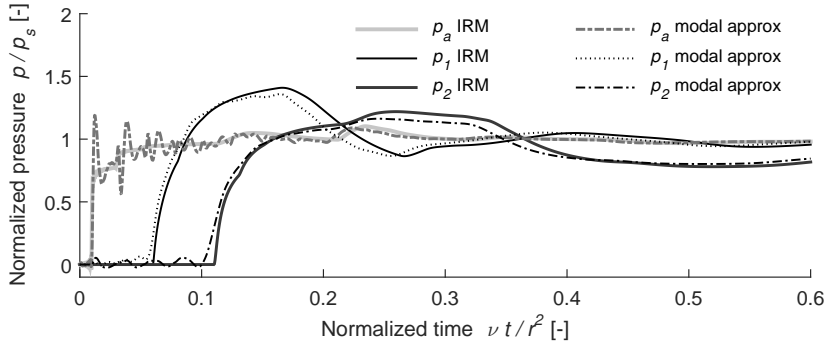


(c) Close-up of the step response comparison between the IRM and modal approximations

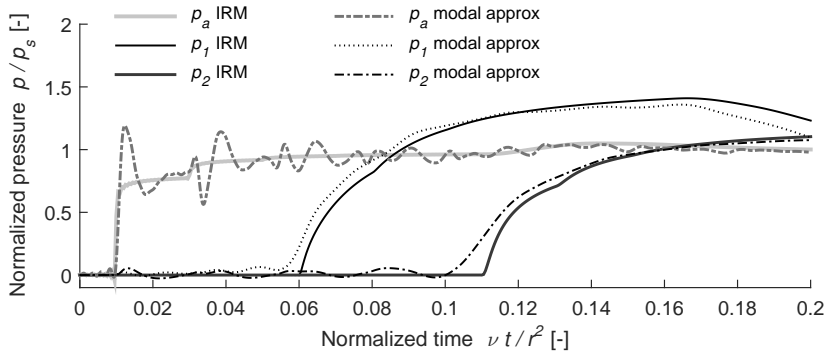
Figure 5.5: Time domain response comparison of case 2.



(a) Impulse response used in the convolution of the IRM



(b) Step response comparison between the IRM and modal approximations



(c) Close-up of the step response comparison between the IRM and modal approximations

Figure 5.6: Time domain response comparison of case 3.

5.5. CONCLUDING REMARKS

An application of a semi-analytical impulse response method to hydraulic networks was presented for transient laminar flow using a two-dimensional viscous compressible model. By solving analytically the complete network in the frequency domain, a unique impulse response of pressure and/or volumetric flow is obtained in the time-domain through the inverse FFT. A discrete numerical convolution with respect to time is then applied separately to obtain the response of the complete network to a chosen arbitrary input. Although the application of the method was shown for a simple hydraulic network, it can be easily extended to networks with large numbers of lines with various interface and boundary conditions.

The IRM does not require any spatial discretization and is only limited by the numerical considerations to solve a system of coupled linear algebraic equations and the fast Fourier transform. This means that for large networks, the increase in computational cost is only determined by the order of the global system matrix, which is linearly dependent on the number of lines forming the system. In addition, the presented results show that the adopted IRM method provides a more accurate description of the transient behaviour than the modal approximation of individual lines used for network modelling. For a large network, the modal method might provide inaccurate results, as the required number of modes for each line is not *a priori* known.

6

DYNAMICS AND PERFORMANCE OF AN OFFSHORE HYDRAULIC WIND POWER PLANT

6.1. INTRODUCTION

With the purpose to evaluate the performance of a complete hydraulic wind power plant, the components presented in previous chapters are joined into a single time-domain numerical model. The model for a single hydraulic wind turbine, introduced in Chapter 4, is extended to include more turbines for any given farm layout. The model is capable of accounting for the hydraulic network dynamics and wake turbine interaction. Hence, this model makes it possible to evaluate different hydraulic pipeline configurations and control strategies in order to achieve centralized electricity generation, while ensuring the proper operation of the individual turbines.

This chapter is organized as follows. In Section 6.2, a description of the model for the ambient wind field generation and aerodynamic interaction is presented. In addition, the time-domain model of the hydraulic network is introduced. Section 6.3 presents some intermediate results by analyzing a basic farm configuration consisting of only two turbines. Four different cases comprising different combinations of hydraulic network configurations and control strategies are used to assess the performance and stability. Finally, in Section 6.4, the model is extended to include five turbines and a generator platform. An active control strategy is used to ensure the dynamic stability of the operating turbines while producing electrical power in a centralized manner. For a particular case with turbulent wind conditions, the time-domain results of the individual turbines are presented and compared with those of a conventional wind farm under the same layout and environmental conditions.

Parts of this chapter have been published in *Journal of Physics: Conference Series*, 524(1); *Journal of Physics: Conference Series*, 753(1) (Jarquin Laguna, 2014, 2016) and under review in *Wind Energy Science*, 2016. Note that minor changes have been introduced to make the text consistent with the other chapters of the thesis.

6.2. EXTENDING THE MODEL TO MORE THAN ONE TURBINE

6.2.1. AMBIENT WIND FIELD

An existing open source toolbox is employed to incorporate the dynamic wind flow models and wake effects in the hydraulic wind power plant model for a given layout. The toolbox was developed as part of an European research project with the acronym *Aeolus* (The European Commission, 2012), for the study and research on ‘Distributed Control of Large-Scale Offshore Wind Farms’. Several studies have been carried out with the help of the aforementioned toolbox, mainly in the field of control systems, (Jelavić and Perić, 2009; Baotić, 2009; Borrelli et al., 2010; Pang and Grimble, 2010; Grimble and Majecki, 2010; Spudić et al., 2011; Knudsen et al., 2011; Soleimanzadeh and Wisniewski, 2011). The model implemented in the toolbox has the following characteristics:

- **Constant mean wind field.** The wind speed has a constant mean in the longitudinal direction and a zero lateral component.
- **Constant mean wind direction.** The wind speed direction is fixed with respect to the farm layout. For a change of mean wind direction, a model should be generated according to the rotated layout.
- **2D wind field.** The wind field does not account for wind shear or tower shadow effects. The wind field is generated at hub height plane
- **No yaw misalignment.** The flow is assumed perpendicular to the rotor plane of the turbines. In addition, the yaw degree of freedom of the turbines is not considered, therefore their yaw controller is not included.

In order to generate a wind field, two spectral matrices are used to describe the wind speed variations at different points within the wind farm domain according to (Veers, 1988). For non specific wind conditions, the wind field is generated according to recommendations from IEC 61400-3 regarding offshore wind turbines (International Electrotechnical Commission, 2009). A schematic overview of the ambient wind field generation is shown in Figure 6.1.

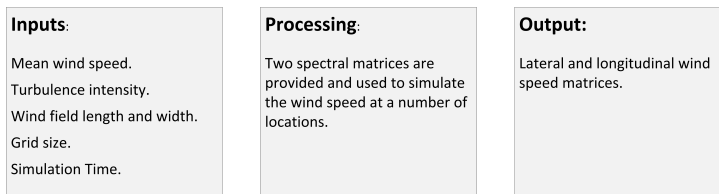


Figure 6.1: Ambient wind field generation inside Aeolus toolbox (Grunnet et al., 2010).

The Kaimal spectrum is used according to:

$$S_k(f) = \sigma_k^2 \frac{4 \frac{L_k}{U}}{\left(1 + 6f \frac{L_k}{U}\right)^{\frac{5}{3}}} \quad (6.1)$$

where f is the frequency in Hz, U is the mean wind speed at hub height, L is the velocity component integral scale parameter and k is the sub-index to denote the velocity component x or y . The variance σ_k , is determined by the turbulence intensity I according to:

$$\sigma_x = I \left(\frac{3}{4}U + 5.6 \right) \quad (6.2)$$

$$\sigma_y = 0.8 \sigma_x \quad (6.3)$$

The coherence between two points separated laterally by a distance l is given by

$$C_k(f) = e^{-c_k f \frac{l}{U}} \quad (6.4)$$

where c_k is the coherence parameter for each wind direction. The spectral and coherence parameters for hub heights above 60 m are given in Table 6.1 according to (Kristensen and Jensen, 1979).

Table 6.1: Spectral and coherence parameters for hub heights above 60m (Kristensen and Jensen, 1979).

	L_x	L_y	c_{xx}	c_{yy}
Parameter value	340.2	113.4	7.1	4.2

If Taylor's frozen turbulence hypothesis for inviscid flow is assumed, the longitudinal and lateral wind velocity fluctuations will travel with the average wind speed in the longitudinal direction (Davidson, 2004). The wind speeds at downwind grid points will be identical to the corresponding upwind points except for a time delay. This also means that the coherence between two points separated by a distance downwind will be equal to one. Although Taylor's frozen turbulence model is used very often to calculate rotor loads, this assumption is not realistic for wind speeds traveling through a wind farm. A more adequate description was proposed in (Sørensen et al., 2002), where the coherence between each turbine is needed according to the following equation,

$$c_{rc}(\alpha) = \sqrt{(c_{xx} \cos \alpha)^2 + (c_{yy} \cos \alpha)^2} \quad (6.5)$$

where α is an angle between wind direction and a line between turbine r and turbine c . The time delay t_{rc} from turbine r to turbine c is also needed and calculated as a function of the distance between turbines d_{rc} :

$$t_{rc} = \frac{d_{rc} \cos \alpha}{U} \quad (6.6)$$

Hence, the cross spectrum S_{rc} between turbines r and c is given as:

$$S_{rc}(f) = C_{rc}(f) \sqrt{S_{rr}(f) S_{cc}(f)} e^{-j2\pi f t_{rc}} \quad (6.7)$$

where C_{rc} is the coherence, and S_{rr} , S_{cc} are the autospectra at turbines r and c , respectively.

6.2.2. WAKE EFFECTS

When a wind turbine is in operation, the rotor blades exert forces on the wind flow which produce a flow structure downstream the rotor. This effect is commonly known as wind turbine wake and its properties have been studied extensively (Crespo et al., 1999; Vermeer et al., 2003; Sanderse et al., 2011). The following wake effects are considered in this work as shown in Figure 6.2:

- **Wake deficit.** It is a measure of the decrease in the wind speed caused by the extraction of energy from the flow by the turbine.
- **Wake expansion.** It describes the size of the cross-sectional area affected by the wake. As the flow decelerates under the influence of the blade forces, the stream tube of the wake will expand as an effect of the principle of conservation of mass.
- **Wake meandering.** It consists of large oscillating movements of the wake cross-sectional area in both lateral and vertical direction. The lateral position of this wake area is defined by a wake center.
- **Added turbulence intensity.** It describes the increased turbulence in the wind field. It is caused by the obstruction of the flow by the turbine and the resulting velocity gradients in the flow.

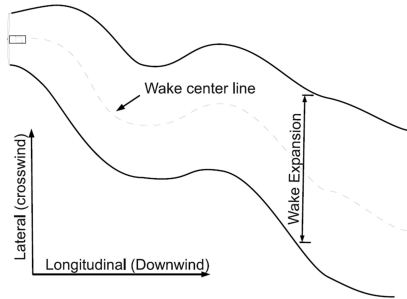


Figure 6.2: Wake meandering of a turbine, defined by its wake center and expansion (Grunnet et al., 2010).

Expressions for wake deficit, expansion and center are given in (Frandsen et al., 2006; Jensen, 1983). The three characteristics at a given point p downwind from a turbine at time t_1 , are defined by the wind field at the turbine and its coefficient of thrust at the time of tracer release, t_0 :

$$t_0 = t_1 - \frac{d}{U} \quad (6.8)$$

where d is the longitudinal distance between the upwind turbine and p .

WAKE DEFICIT AND EXPANSION

The wake expansion D , is defined in terms of the wake diameter at downwind distance d according to the following equation from (Frandsen et al., 2006):

$$D(d) = D_0 \left(\beta^{\frac{k}{2}} + \alpha \frac{d}{D_0} \right)^{\frac{1}{k}} \quad (6.9)$$

$$\beta = \frac{1 + \sqrt{1 - C_T}}{2\sqrt{1 - C_T}} \quad (6.10)$$

where C_T is the thrust coefficient, D_0 is the rotor diameter and α and k are model parameters with the values of 0.5 and 2 respectively. The wake deficit c behind a single turbine at distance d is given by the following equation from (Frandsen et al., 2006):

$$c = \frac{U(d)}{U_0} \approx 1 - \frac{C_T}{2} \frac{D_0^2}{D^2(d)} \quad (6.11)$$

WAKE CENTER

A good approximation of the meandering of the wake is to consider the wake center as a passive tracer which moves downwind with the mean wind speed (Larsen et al., 2008). Under this assumption, the wake meandering can be modelled by applying a low pass filter on the lateral velocity variations found at the center line of the wind turbine rotor (Larsen et al., 2008). The wake center at time t_k is a function of the center at time t_{k-1} and the average lateral wind speed, over the wake area:

$$W_i(d, t_{k-1}) = (x, y) | x = d \wedge y \in W_y \quad (6.12)$$

$$W_y = \left[w_i(d, t_{k-1}) - \frac{1}{2} D_i(d); w_i(d, t_{k-1}) + \frac{1}{2} D_i(d) \right] \quad (6.13)$$

$$w_i(d, t_k) = w_i(d, t_{k-1}) + \bar{v}_{y,i}(d, W_i(d, t_{k-1})) \quad (6.14)$$

where $w_i(d, t_k)$ is the wake center at time k , $W_i(d, t_{k-1})$ is the wake area distance d from the turbine at time t_{k-1} and $\bar{v}_{y,i}(d, W_i(d, t_{k-1}))$ is the average lateral wind speed over the wake area. For a row of turbines the deficit at turbine $n+1$ can be described as:

$$c_{n+1} = \frac{U_{n+1}}{U_0} = 1 - \left(\frac{D_n^2}{D_{n+1}^2} (1 - c_n) + \frac{C_{T_n}}{2} \frac{D_0^2}{D_{n+1}^2} c_n \right) \quad (6.15)$$

where c_{n+1} is the deficit at turbine $n+1$, D_n is the wake diameter at turbine $n+1$, c_n is the deficit at turbine n , C_{T_n} is the thrust coefficient of turbine n and D_0 is the diameter of the rotor.

ADDED TURBULENCE INTENSITY

The model of added turbulence intensity is included according to recommendations from IEC-61400-1 (International Electrotechnical Commission, 2005):

$$I_{add,j} = \frac{\sigma_{add,j}}{U_j} = \frac{1}{1.5 + 0.8 s_{i,j} \sqrt{C_{T,i}}} \quad (6.16)$$

where $\sigma_{add,j}$ is the added standard deviation in the wind field at the j th turbine which is in wake; U_j is the effective wind speed at the j th turbine; $s_{i,j}$ is the spacing in rotor diameters between the wake generating turbine and the wind turbine in wake; $C_{T,i}$ is the thrust coefficient of the wake generating turbine.

A snap shot of the ambient wind field and wake effects at a given simulation time, is shown in Figure 6.3 for a particular wind farm layout comprised of five turbines.

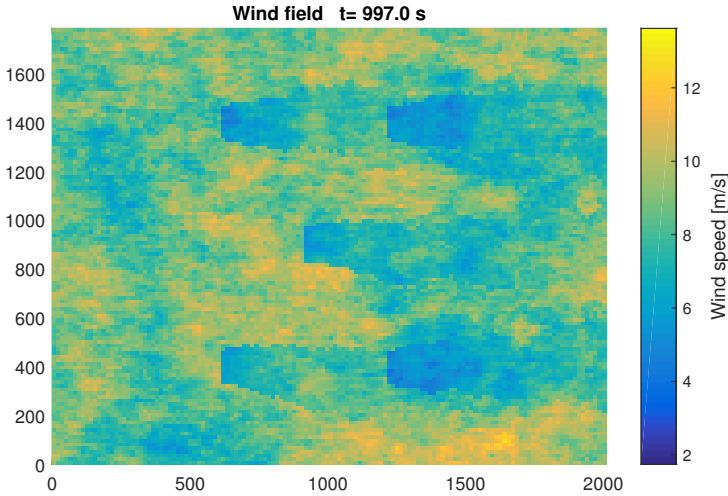


Figure 6.3: Snap shot of the wind field and wake effects.

6.2.3. INCORPORATING THE HYDRAULIC NETWORK

As previously mentioned in Chapter 5, a hydraulic network can be constructed from the individual single line models using modal approximations. In order to illustrate the construction of a particular configuration, the impedance model (Q-model) and the flow pressure model (QP-model) will be used in this section. These models were previously presented in Section 2.4. The Q-model uses the flow rates as given inputs and the pressures as outputs. The QP-model uses the upstream flow rate and downstream pressure as inputs, and the upstream pressure and downstream flow rate as outputs. The state-space representation of the QP-model is shown in Equation 6.17:

$$\text{QP-model} \left\{ \begin{array}{l} \dot{\mathbf{x}} = \mathbf{A}_{\text{QP}} \mathbf{x} + \mathbf{B}_{\text{QP}} \begin{bmatrix} Q_u \\ p_d \end{bmatrix} \\ \begin{bmatrix} Q_d \\ p_u \end{bmatrix} = \mathbf{C}_{\text{QP}} \mathbf{x} + \mathbf{D}_{\text{QP}} \begin{bmatrix} Q_u \\ p_d \end{bmatrix} \end{array} \right. \quad (6.17)$$

Using this description for individual line elements, it is possible to assemble the model for a whole hydraulic network. Consider the case where a number of m lines from individual turbines are in parallel with a common line at the end. Each of the parallel lines is modelled with a QP-model, where the input flow rate $Q_{p,i}$ of each turbine is given as an input at the upstream part of each parallel line. For the common line a Q-model is used where the upstream input flow rate $Q_{line,in}$ is the sum of the individual downstream flow rates Q_i , which are the output of each QP-model. This condition is a consequence of the flow continuity at the branching node, which relates the inflows and outflows of the flow rates. At this same location, it is assumed that the pressure at the branching node is unique. Hence, the upstream pressure of the common line is used as input for all the parallel lines. A schematic of the model showing the input-output causality for each element is shown in Figure 6.4.

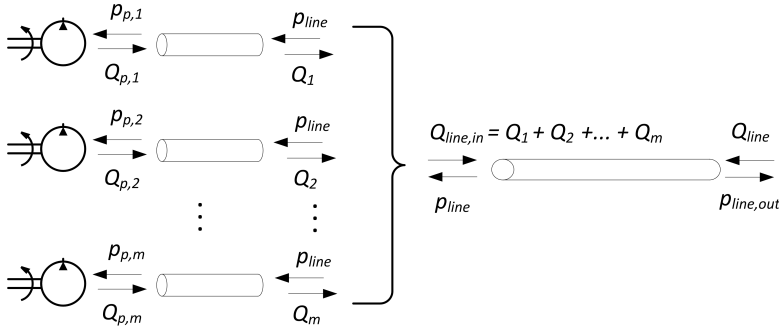


Figure 6.4: Schematic for parallel hydraulic lines connected to a common line.

The assembled model for the parallel pipelines interconnected with a common line is described by Equation 6.18. The numerical subscripts in vectors and matrices indicate column vectors; the superscripts between bracket indicate the pipeline element (i.e. $\mathbf{b}_1^{(\text{line})}$ is the first column of matrix \mathbf{B}_Q from the common line Q-model; $\mathbf{c}_2^{T(1)}$ indicates the second row vector of matrix \mathbf{C}_{QP} from the first parallel line with QP-model). The outputs of the assembled hydraulic network are given by Equation 6.19.

Other models for transient laminar flow can be used in this approach as long as they are represented with linear ordinary differential equations. In the case of a transient turbulent flow, different models in the form of non linear differential equations have been proposed and might also be used with the current approach, however their implementation into more complex hydraulic networks is beyond the scope of this thesis.

Assembly of hydraulic network model in the general state-space form:

$$\dot{\mathbf{x}} = \mathbf{Ax} + \mathbf{Bu}$$

$$\mathbf{y} = \mathbf{Cx} + \mathbf{Du}$$

$$\begin{bmatrix} \dot{\mathbf{x}}^{(1)} \\ \dot{\mathbf{x}}^{(2)} \\ \vdots \\ \dot{\mathbf{x}}^{(m)} \\ \dot{\mathbf{x}}^{(line)} \end{bmatrix} = \begin{bmatrix} \mathbf{A}_{QP}^{(1)} & 0 & \dots & 0 & \mathbf{b}_2^{(1)} \mathbf{c}_1^{T(line)} \\ 0 & \mathbf{A}_{QP}^{(2)} & \dots & 0 & \mathbf{b}_2^{(2)} \mathbf{c}_1^{T(line)} \\ \vdots & \vdots & \ddots & \vdots & \vdots \\ 0 & 0 & \dots & \mathbf{A}_{QP}^{(m)} & \mathbf{b}_2^{(m)} \mathbf{c}_1^{T(line)} \\ \mathbf{b}_1^{(line)} \mathbf{c}_1^{T(1)} & \mathbf{b}_1^{(line)} \mathbf{c}_1^{T(2)} & \dots & \mathbf{b}_1^{(line)} \mathbf{c}_1^{T(m)} & \mathbf{A}_Q^{(line)} + k \mathbf{b}_1^{(line)} \mathbf{c}_1^{T(line)} \end{bmatrix} \begin{bmatrix} \mathbf{x}^{(1)} \\ \mathbf{x}^{(2)} \\ \vdots \\ \mathbf{x}^{(m)} \\ \mathbf{x}^{(line)} \end{bmatrix} + \begin{bmatrix} \mathbf{b}_1^{(1)} & \mathbf{0} & \dots & \mathbf{0} & \mathbf{0} \\ \mathbf{0} & \mathbf{b}_1^{(2)} & \dots & \mathbf{0} & \mathbf{0} \\ \vdots & \vdots & \ddots & \vdots & \vdots \\ \mathbf{0} & \mathbf{0} & \dots & \mathbf{b}_1^{(m)} & \mathbf{0} \\ d_{11}^{(1)} \mathbf{b}_1^{(line)} & d_{11}^{(2)} \mathbf{b}_1^{(line)} & \dots & d_{11}^{(m)} \mathbf{b}_1^{(line)} & \mathbf{b}_2^{(line)} \end{bmatrix} \begin{bmatrix} Q_{p,1} \\ Q_{p,2} \\ \vdots \\ Q_{p,m} \\ Q_{line} \end{bmatrix} \quad (6.18)$$

$$\begin{bmatrix} Q_1 \\ p_{p,1} \\ Q_2 \\ p_{p,2} \\ \vdots \\ Q_m \\ p_{p,m} \\ p_{line} \\ p_{line,out} \\ Q_{line,in} \end{bmatrix} = \begin{bmatrix} \mathbf{c}_1^{T(1)} & \mathbf{0} & \dots & \mathbf{0} & d_{12}^{(1)} \mathbf{c}_1^{T(line)} \\ \mathbf{c}_2^{T(1)} & \mathbf{0} & \dots & \mathbf{0} & d_{22}^{(1)} \mathbf{c}_1^{T(line)} \\ \mathbf{0} & \mathbf{c}_1^{T(2)} & \dots & \mathbf{0} & d_{12}^{(2)} \mathbf{c}_1^{T(line)} \\ \mathbf{0} & \mathbf{c}_2^{T(2)} & \dots & \mathbf{0} & d_{22}^{(2)} \mathbf{c}_1^{T(line)} \\ \vdots & \vdots & \ddots & \vdots & \vdots \\ \mathbf{0} & \mathbf{0} & \dots & \mathbf{c}_1^{T(m)} & d_{12}^{(m)} \mathbf{c}_1^{T(line)} \\ \mathbf{0} & \mathbf{0} & \dots & \mathbf{c}_2^{T(m)} & d_{22}^{(m)} \mathbf{c}_1^{T(line)} \\ \mathbf{0} & \mathbf{0} & \dots & \mathbf{0} & \mathbf{c}_1^{T(line)} \\ \mathbf{0} & \mathbf{0} & \dots & \mathbf{0} & \mathbf{c}_2^{T(line)} \\ \mathbf{c}_1^{T(1)} & \mathbf{c}_1^{T(2)} & \dots & \mathbf{c}_1^{T(m)} & k \mathbf{c}_1^{T(line)} \end{bmatrix} \begin{bmatrix} \mathbf{x}^{(1)} \\ \mathbf{x}^{(2)} \\ \vdots \\ \mathbf{x}^{(m)} \\ \mathbf{x}^{(line)} \end{bmatrix} + \begin{bmatrix} d_{11}^{(1)} & \mathbf{0} & \dots & \mathbf{0} & \mathbf{0} \\ d_{21}^{(1)} & \mathbf{0} & \dots & \mathbf{0} & \mathbf{0} \\ \mathbf{0} & d_{11}^{(2)} & \dots & \mathbf{0} & \mathbf{0} \\ \mathbf{0} & d_{21}^{(2)} & \dots & \mathbf{0} & \mathbf{0} \\ \vdots & \vdots & \ddots & \vdots & \vdots \\ \mathbf{0} & \mathbf{0} & \dots & d_{11}^{(m)} & \mathbf{0} \\ \mathbf{0} & \mathbf{0} & \dots & d_{21}^{(m)} & \mathbf{0} \\ \mathbf{0} & \mathbf{0} & \dots & \mathbf{0} & \mathbf{0} \\ \mathbf{0} & \mathbf{0} & \dots & \mathbf{0} & \mathbf{0} \\ d_{11}^{(1)} & d_{11}^{(2)} & \dots & d_{11}^{(m)} & \mathbf{0} \end{bmatrix} \begin{bmatrix} Q_{p,1} \\ Q_{p,2} \\ \vdots \\ Q_{p,m} \\ Q_{line} \end{bmatrix} \quad (6.19)$$

$$\text{with} \quad k = d_{12}^{(1)} + d_{12}^{(2)} + \dots + d_{12}^{(m)} \quad (6.20)$$

The presented model of a hydraulic network is assembled with the rest of the algebraic and differential equations which describe the dynamics of the individual turbines. Following the same approach as in (Grunnet et al., 2010), the hydraulic transmission is incorporated instead of the mechanical gearbox; this same method was presented in (Jarquin Laguna, 2015). The volumetric flow rate from the motor-water pump assembly (high speed shaft) is used as an input to the hydraulic network, and the pressure at the water pumps is used as feedback to the turbine models. In this manner a complete model with the individual turbines coupled to the hydraulic network is obtained. The complete wind farm model is now described through a set of coupled algebraic and differential equations which can be solved numerically using a variable time step ODE solver via commercial software (MATLAB-Simulink®, 2014). Simple test cases of the overall model, using a constant wind speed input, were used to check the steady state conditions. Time domain simulations are performed to obtain the transient response to a stochastic wind input as described in the next sections.

6.3. SIMULATION OF TWO TURBINES

Before simulating the complete hydraulic wind power plant, some intermediate results are presented by analyzing first the simplest farm consisting of two turbines. The turbines are interconnected using two hydraulic network configurations. Time domain simulations of the reduced wind farm are used to evaluate the performance and rotor speed stability of both turbines under typical wind conditions. The individual turbines have the same characteristics as the ones evaluated in Chapter 4; the main parameters of a single turbine were given in Table 4.1.

In order to evaluate the performance and functionality of the control strategies, two turbines are placed inline with the mean wind speed direction as shown in Figure 6.5. A wind field with a mean wind speed of 9 m/s and 10% turbulence intensity is taken as the inflow condition. Simulations of the reduced wind farm behavior are performed during 1000s with zero initial conditions. Wake effects for the downwind turbine are determined by using the thrust coefficient C_T of the upwind turbine as described in Section 6.2.2.

6.3.1. CASE STUDIES DESCRIPTION

Four different cases are simulated for the same wind field. Each case includes two identical turbines and a specific combination of the hydraulic network and control strategy. Model 1 includes independent pipelines and nozzles for both turbines, see Figure 6.6(a). In this configuration, the turbines are uncoupled and are controlled passively. Because each turbine has an independent pipeline towards the offshore substation, this configuration might not be the most convenient from a practical and economical point of view. Furthermore, each central substation is limited to five or six turbines, which is the typical number of independent nozzles that a Pelton turbine is designed for. However, as this model is a direct extension of the model presented in Chapter 4, the results will be used as a reference. Model 2 presents a parallel configuration, in which the water pipelines from individual turbines are connected through a common line to a single nozzle, see Figure 6.6(b). A passive control strategy is employed in this configuration. Hence, the two turbines have a dynamic interaction through the flow in the hydraulic

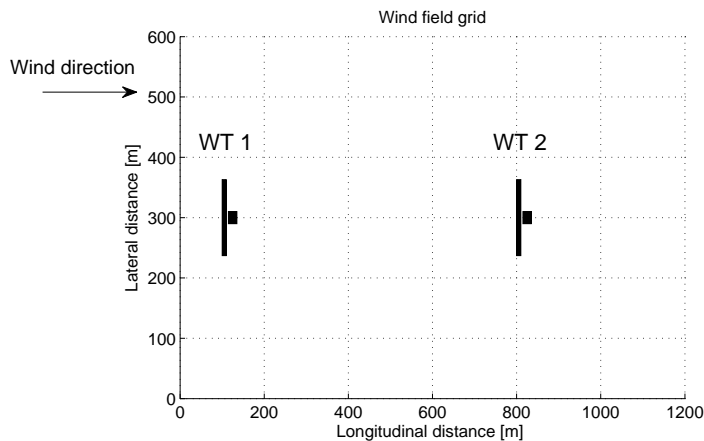
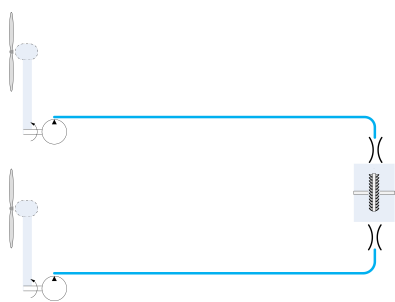


Figure 6.5: Wind field grid for two inline turbines; Mean wind speed of 9m/s with 10% TI.

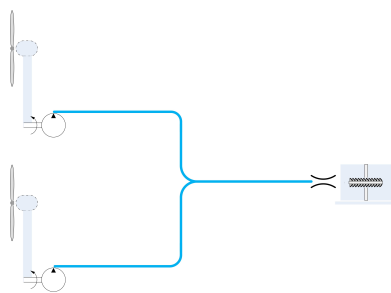
network. Model 3 uses the same configurations as the previous model but with an increased nozzle diameter, see Figure 6.6(c). By doing this, the passive control strategy is modified to work at a higher tip speed ratio and lower pressure. Finally, Model 4 includes parallel pipelines with an active control strategy to keep a constant pressure in the hydraulic network. A spear valve is used to modify the nozzle area, while the water pumps are controlled independently to maintain a variable speed functionality, see Figure 6.6(d). It is important to mention, that as an active control concept, the design of the controller has a direct influence in both the stability and performance of the system. The proposed controller is based on the control design from Section 3.5. An overview of the physical parameters used is shown in Table 6.2.

Table 6.2: Main physical properties of the hydraulic network.

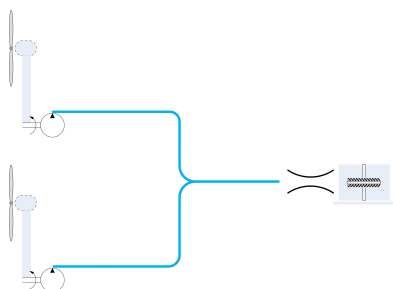
Network		Design parameter	Pipeline WT1	Pipeline WT2	Common pipeline	Main aspects for centralized generation
Model 1	Single	Line length [m]	1000	1000	-	× independent lines - no network
		Line diameter [m]	0.50	0.50	-	✓ nominal tip speed ratio
		Nozzle diameter [mm]	43.2	43.2	-	✓ dynamic stability
Model 2	Parallel	Line length [m]	500	500	500	✓ allows hydraulic network
		Line diameter [m]	0.50	0.50	0.7072	✓ nominal tip speed ratio
		Nozzle diameter [mm]	-	-	6.11	? dynamic stability unknown
Model 3	Parallel	Line length [m]	500	500	500	✓ allows hydraulic network
		Line diameter [m]	0.50	0.50	0.7072	! higher tip speed ratio
		Nozzle diameter [mm]	-	-	6.83	? dynamic stability unknown
Model 4	Parallel	Line length [m]	500	500	500	✓ allows hydraulic network
		Line diameter [m]	0.50	0.50	0.7072	✓ nominal tip speed ratio
		Nozzle diameter [mm]	-	-	variable	✓ dynamic stability



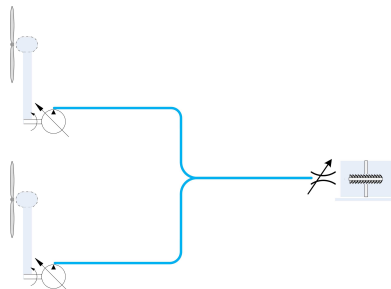
(a) Model 1: Network with independent pipelines and nozzles; passive control strategy.



(b) Model 2: Network with parallel pipelines with common line & nozzle; passive control strategy.



(c) Model 3: Network with parallel pipelines with common line & augmented nozzle; passive control strategy.



(d) Model 4: Network with parallel pipelines with common line; active control strategy to keep a constant pressure.

Figure 6.6: Schematic showing the different network configurations and control strategies for each model.

6.3.2. TIME-DOMAIN RESULTS

Figure 6.7 presents results for Model 1. In the upper graph a deficit can be noted in the effective wind speed at the second turbine WT 2; this is due to the wake from the first turbine WT 1. The reduced wind speed is seen by the second turbine after approximately 77.7 s, which is the time required for the wake from the first turbine to travel to the second turbine with the mean wind speed velocity. The passive control strategy works adequately for uncoupled turbines and their behavior only depends on the local effective wind speed. For short periods during which the rotor speed exceeds the maximum value, collective pitch action β is observed to maintain the turbine within operation limits as shown in the second and third graphs of Figure 6.7. A smooth pressure level and power output from each turbine is obtained while keeping the aerodynamic efficiency at its optimal value. The independent behavior of turbines also occurs in conventional wind farms which include individual generators and controllers per turbine.

In Model 2, the turbines are connected in parallel with a common line, which introduces coupling between the turbines. The pressure at the upstream side of the common line results in a similar torque feedback for both turbines. Since both turbines experience different effective wind speeds at a specific moment in time, the passive control strategy is severely limited. As shown in Figure 6.8, the passive control strategy is able to keep a relatively stable operation of both turbines only during the first 400 s. Afterwards, the torque unbalance in one of the turbines is high enough to increase the rotor speed of the first turbine while breaking the second turbine until it stops. During deceleration of the second turbine, its water pump also reduces the flow rate and the pressure in the common line is reduced. A lower pressure creates a higher torque unbalance in the first turbine to accelerate it even more and eventually reaches nominal rotor speed where pitch action is required. During the interaction, the transient flow rates and pressures result in an undesirable oscillatory power output. These results show the importance of having a hydraulic network which is coupled to the dynamics of single turbines, resulting in unstable operation with the passive control strategy.

In Model 3, an attempt to improve stability of the system while keeping a passive control strategy for a network with parallel lines with single nozzle is made. This is done by increasing the area of the nozzle, which effectively means that a higher tip speed ratio and lower pressure are imposed with the passive control strategy. Not only the optimal aerodynamic performance is sacrificed by operating at a high speed ratio, but also the rated wind speed and the rated mechanical power are decreased due to the constraint on maximum tip speed allowed. On the other hand, by operating at a higher tip speed ratio, higher stability of the system is achieved by allowing larger rotor speed excursions during transient behavior. Figure 6.9 shows clearly that stable operation is feasible. A higher rotor speed operation is observed, as expected for a higher tip speed ratio, and an increased pitch action is present compared to the previous models. By operating with a reduced aerodynamic performance, the deficit in wind speed at the second turbine has a lower effect than in the first model with independent lines. A smooth pressure and power output is also observed as with Model 1, but with transient oscillations during start-up for the first 200 s; for this pipeline configuration performance is compromised by rotor speed stability.

In Model 4 the active control allows to compensate for the hydraulic interaction effects. Figure 6.10 shows that each turbine is able to maintain its rotor speed well below the rated values, while keeping minimum pitch action compared with the previous cases. The aerodynamic efficiency of each turbine is kept close to its optimal value as reflected in the relatively constant power coefficients. A direct consequence is the increased power output from each turbine. However, this total power experiences higher fluctuations due to the required control actions to maintain a relatively constant pressure at the nozzle. The control actions for the variable displacement water pumps and the spear valve of the nozzle, are shown in Figure 6.11. From the results, it is observed that the high fluctuations of the pressure, are excited by the continuous change of the nozzle area, through the linear actuation of a spear valve.

6.3.3. PERFORMANCE COMPARISON

The performance of the different models is summarized in Table 6.3, where the averaged power and efficiency of the rotor are shown according to the same reference points as in Figures 4.1(b) and 4.1(c). The table shows that the configuration with an active control strategy appears to be most suitable in terms of both stability and performance.

Table 6.3: Performance overview of time domain results.

	Turbine	Averaged power [MW]		Efficiency [-]	
		Total mechanical point A	Transmitted point B	Power coeff C_P	A to B η_{AB}
Model 1	WT1	2.70	2.19	0.459	0.811
	WT2	2.18	1.78	0.465	0.813
Model 2	WT1	1.86	2.25	0.337	0.810
	WT2	0.93	2.25	0.178	0.811
Model 3	WT1	2.33	3.58	0.414	0.815
	WT2	2.06	3.58	0.442	0.818
Model 4	WT1	2.89	4.54	0.481	0.884
	WT2	2.25	4.54	0.483	0.884

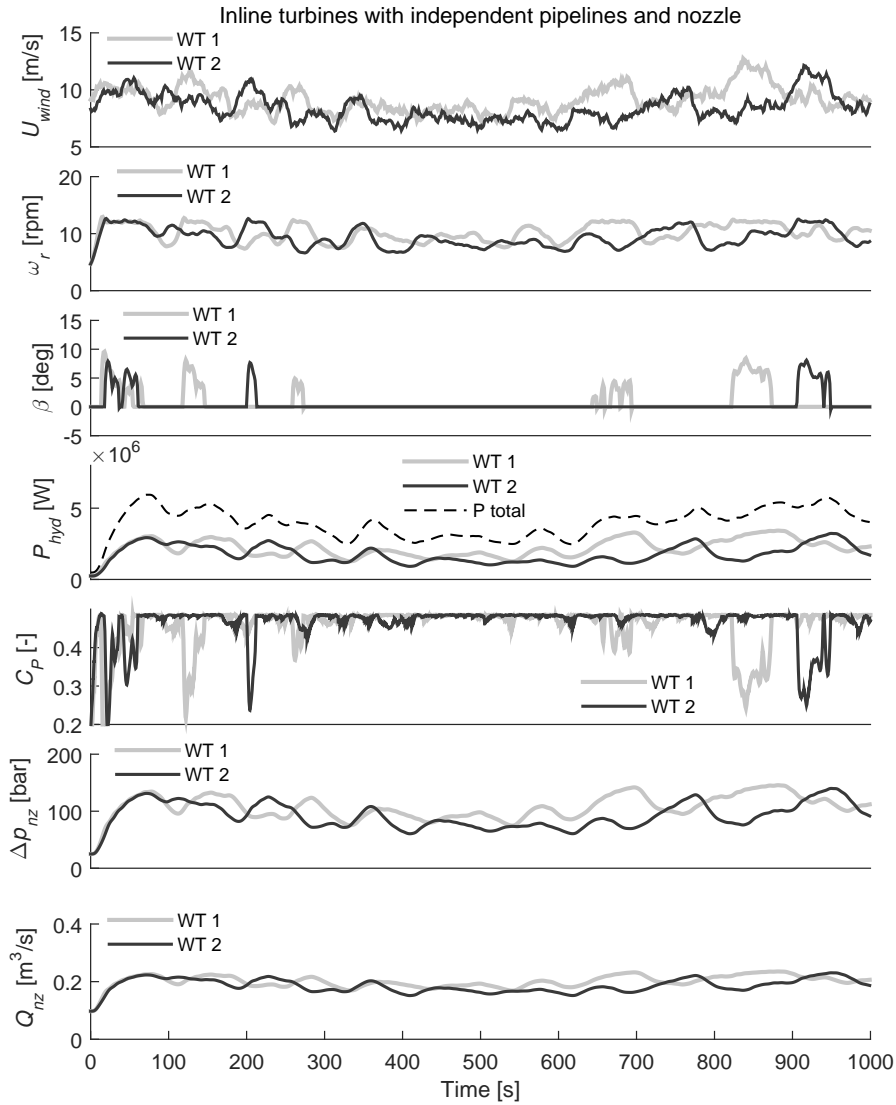


Figure 6.7: Model 1 wind farm simulation results, independent hydraulic network.

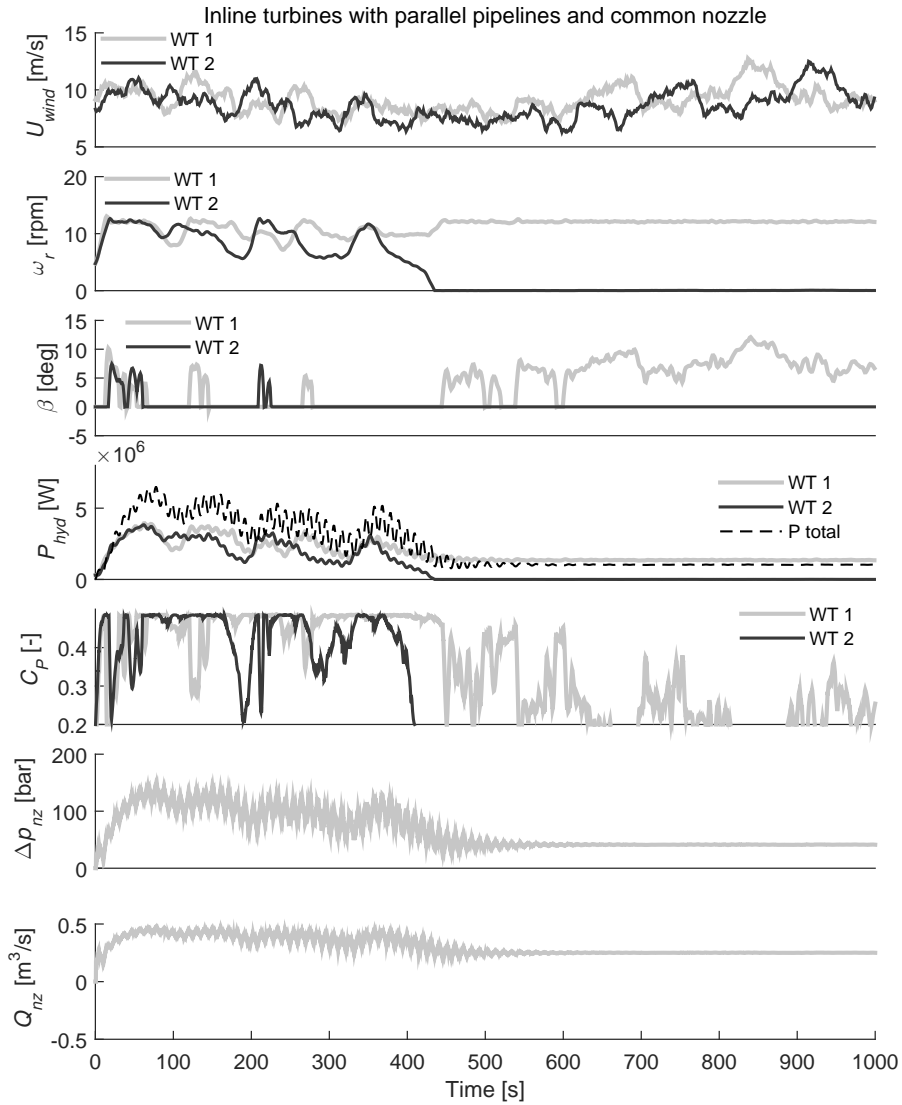


Figure 6.8: Model 2 wind farm simulation results, parallel pipelines.

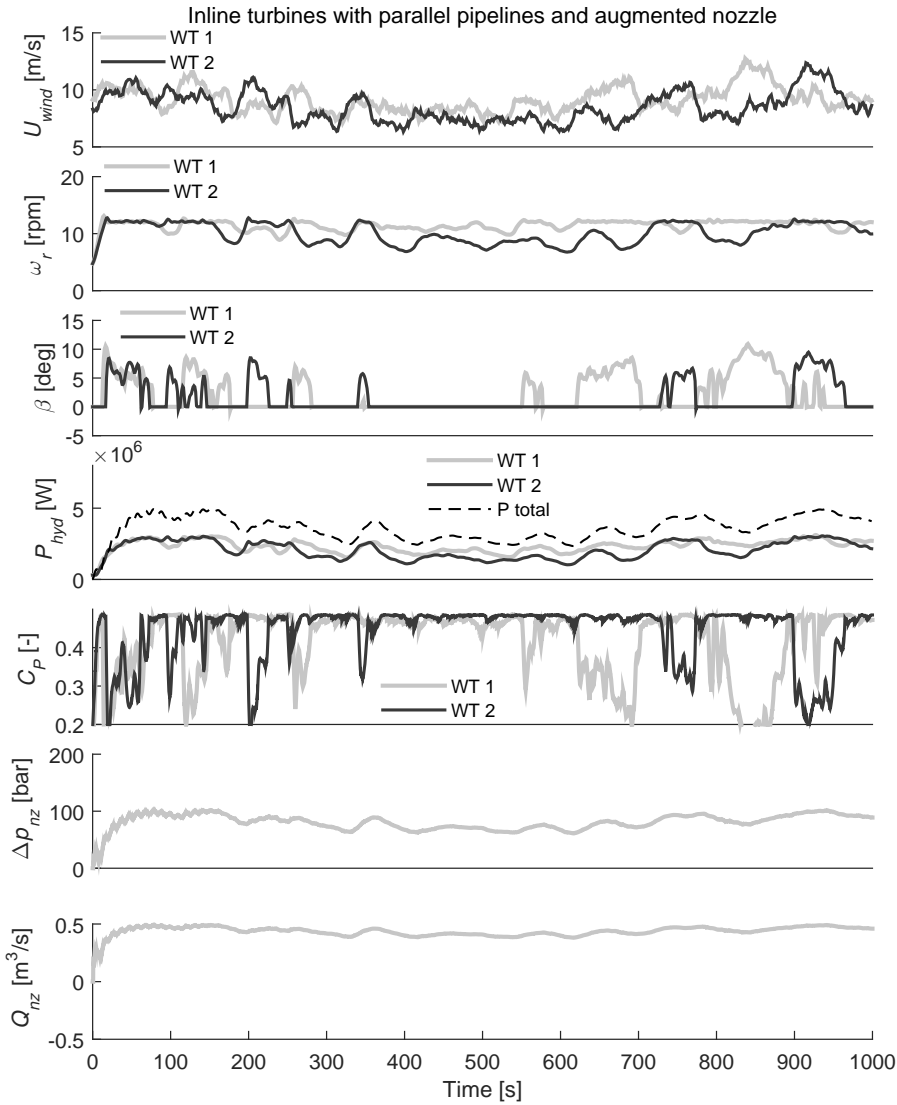


Figure 6.9: Model 3 wind farm simulation results, parallel pipelines with augmented nozzle.

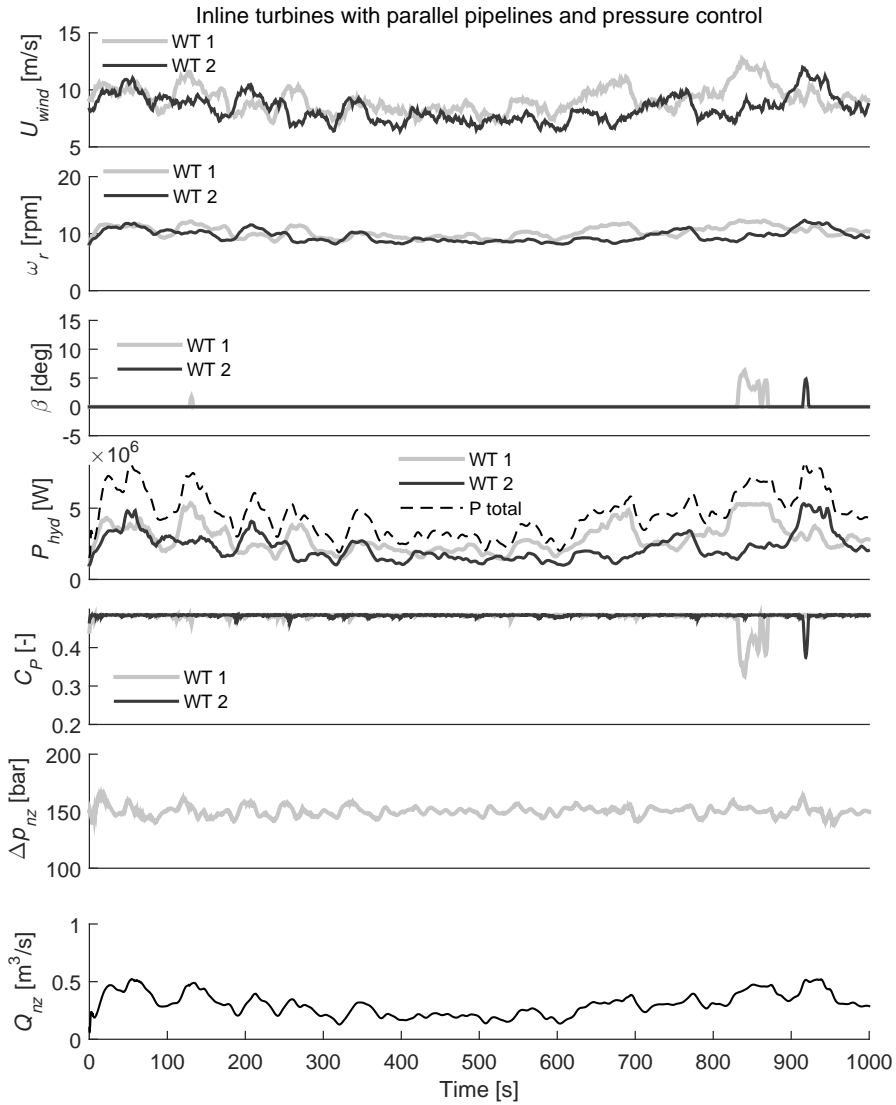


Figure 6.10: Model 4 wind farm simulation results, parallel pipelines with pressure control.

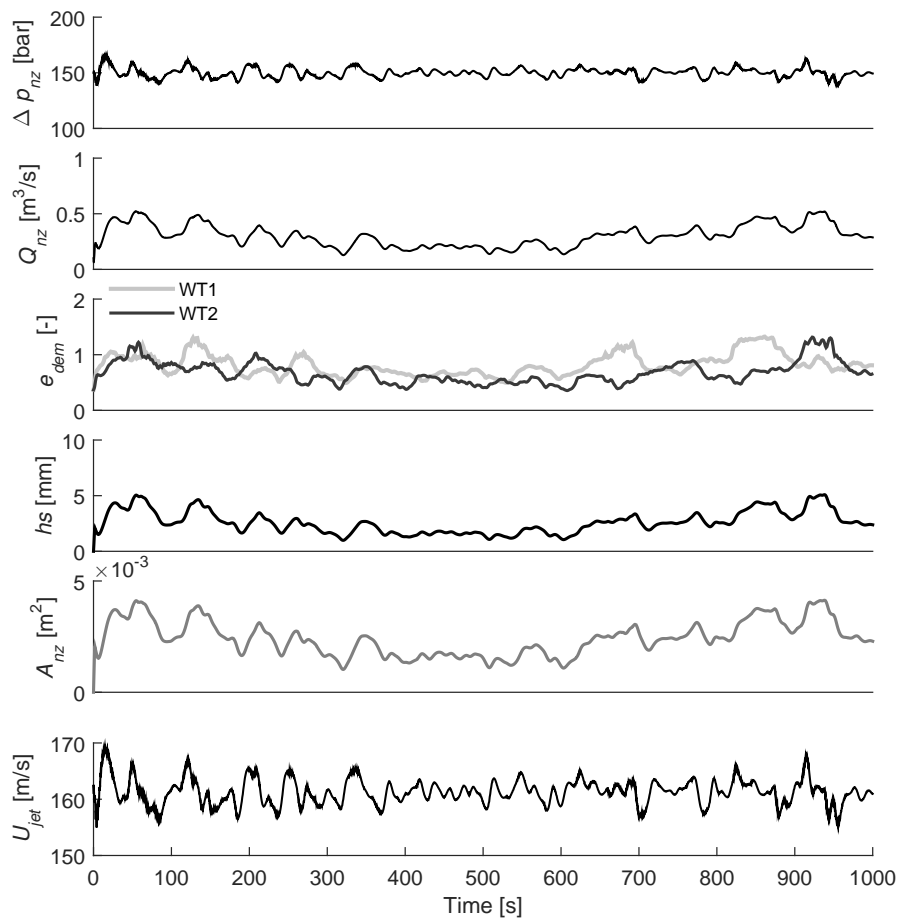


Figure 6.11: Model 4 wind farm simulation results, controller variables.

6.4. SIMULATION OF AN OFFSHORE WIND FARM

6.4.1. FARM LAYOUT AND ENVIRONMENTAL CONDITIONS

A hydraulic wind farm is now evaluated by incorporating more turbines. A small farm comprised of five turbines of 5 MW is used; the layout of the farm is shown in Figure 6.12. The turbines are interconnected through a hydraulic network consisting of five parallel lines and a common line, see Figure 6.4. A constant speed 25 MW Pelton turbine is used to generate electricity at an offshore platform located within 1 km distance from the individual turbines. An active control strategy is used to keep a constant pressure of 150 bars through a variable area nozzle, with the help of a linear actuated spear valve. Each turbine uses a variable displacement water pump to keep an independent variable-speed functionality. This configuration is an extension of the model schematized in Figure 4.1(c).

Two operating conditions corresponding to below and above rated wind speed are considered. For below rated wind speed conditions, a wind field with mean wind speed of 9 m/s and 10% turbulence intensity is used during 1000s. For above rated conditions, a mean wind speed of 15 m/s and 12% TI is employed. The results from the simulations will be compared with those of a reference wind farm that consists of conventional 5 MW NREL turbines (Jonkman et al., 2009), using the same wind farm layout and environmental conditions. In the reference wind farm the wind turbine generators produce electrical power directly, therefore electrical transformers and power cables are used for the conditioning and transmission of electrical power within the farm.

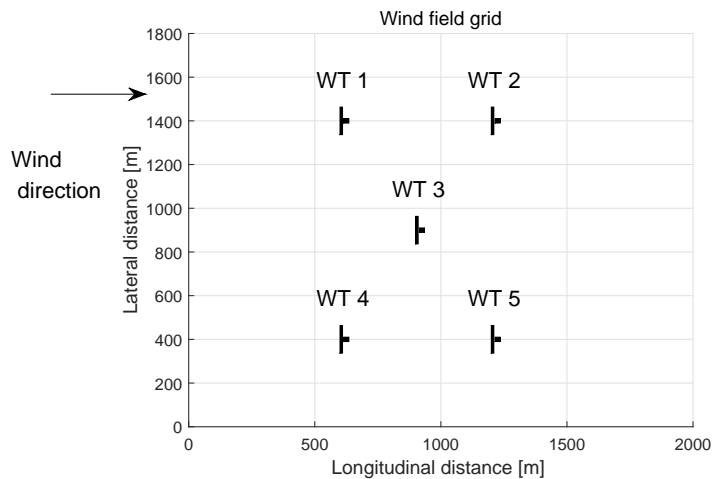


Figure 6.12: Layout of the proposed wind farm with five turbines of 5 MW each.

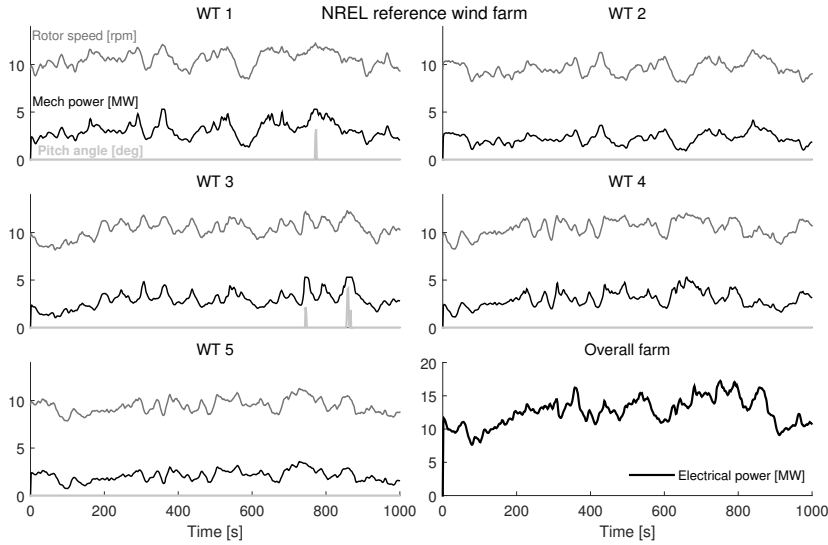
6.4.2. TIME-DOMAIN RESULTS

The results of the time domain simulations are presented in terms of the main operational parameters such as mechanical power, rotor speed and pitch angle for the five turbines. For below rated conditions Figures 6.13(a) and 6.13(b) show the transient response of the reference and the hydraulic wind farm, respectively. The results demonstrate that for the considered scenario and with the current control strategy, the hydraulic wind farm is able to generate electricity from the pressurized water flow to the central platform via a Pelton turbine.

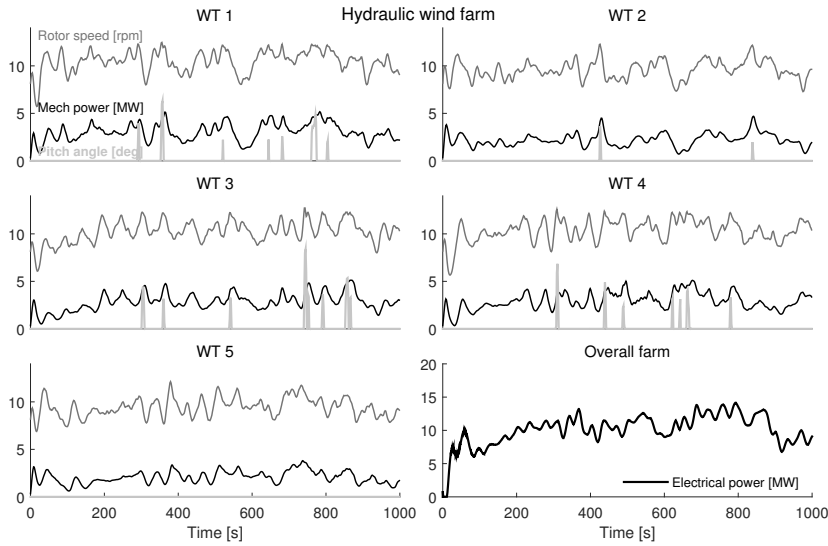
In terms of performance it is observed that the turbines in the hydraulic wind farm experience higher excursions of the rotor speed in comparison with the reference case; this effect is also reflected in the increased pitch action required for the same wind speed conditions. A possible explanation of the more pronounced changes of the rotor speed is that the resulting torque demand generated by the hydraulic system is slower than in the reference case due to the higher fluid inertia of the hydraulic network. From a reliability point of view, the increased pitch action might have an important consequence on the life time of the pitch system.

During the first 100s, the hydraulic wind farm shows high frequency fluctuations in the pressure and, consequently, in the total power output of the array. These higher fluctuations are due to the initial conditions of the pressure control settings in combination with the high fluid inertia in the hydraulic network. The changes in pressure and volumetric flow rate at the nozzle, have small influence on the efficiency of the Pelton turbine, which is maintained relatively constant and well above 90% during the whole simulation time, except for the first 100s of transient conditions.

For above rated conditions, the simulation results are shown in Figures 6.14(a) and 6.14(b). It is observed that both concepts are able to keep the rotor speed operating within a constant speed band while producing relatively constant power. Likewise, the pitch actuation is very similar in both wind farms, which is expected since the same pitch controller is used. Once more, the transient operation in the electrical power production is more pronounced in the case of the hydraulic wind farm because of the high hydraulic inertia of the hydraulic network. High frequency oscillations are observed in the electrical power as a consequence of the pressure waves travelling along the network.

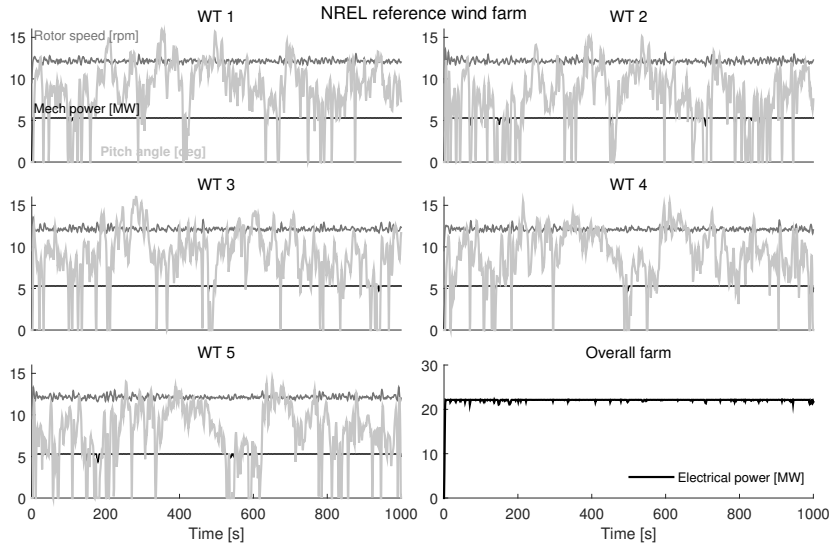


(a) Reference wind farm, below rated conditions.

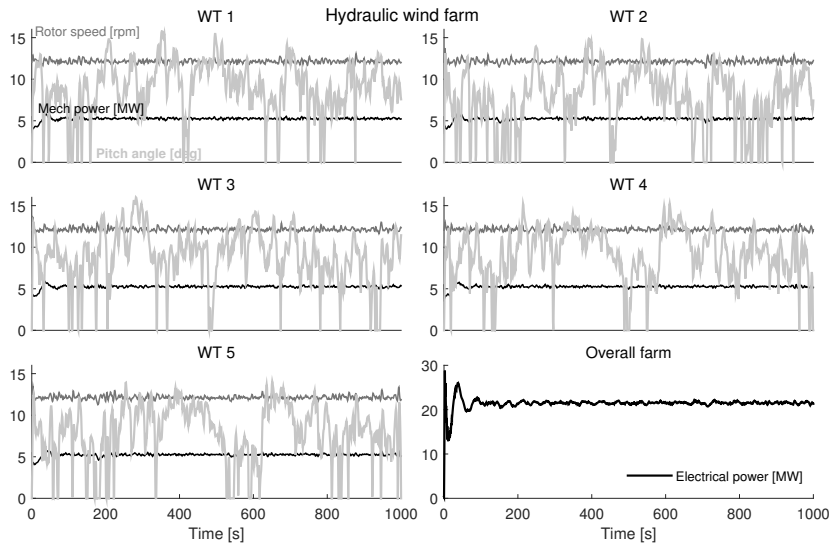


(b) Hydraulic wind farm, below rated conditions.

Figure 6.13: Time domain results for a wind farm comprising of five turbines subject to a wind field with mean speed of 9 m/s and 10% turbulence intensity.



(a) Reference wind farm, above rated conditions.



(b) Hydraulic wind farm, above rated conditions.

Figure 6.14: Time domain results for a wind farm comprising of 5 turbines subject to a wind field with a mean speed of 15 m/s and 12% turbulence intensity.

6.4.3. PERFORMANCE COMPARISON

The performance of both wind farms for the considered conditions is summarized in the bar charts of Figures 6.15 and 6.16, where the averaged values of the power transmission are displayed for the reference points A, B and C from Figure 4.1.

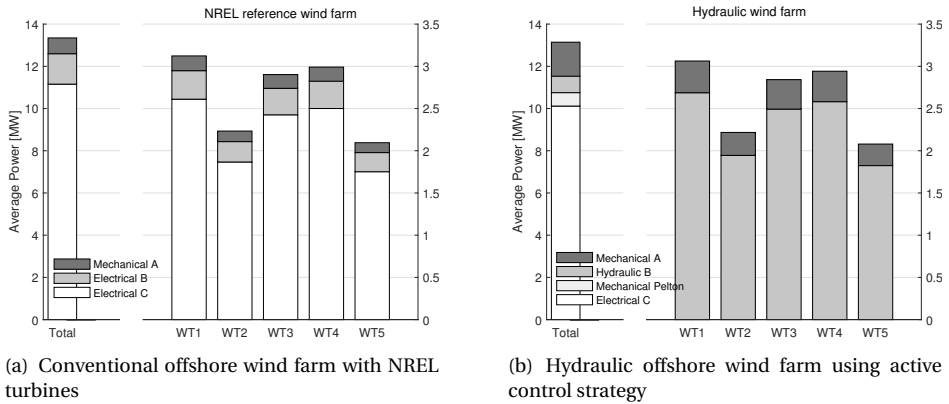


Figure 6.15: Averaged power performance for the reference and the hydraulic wind farm, below rated conditions.

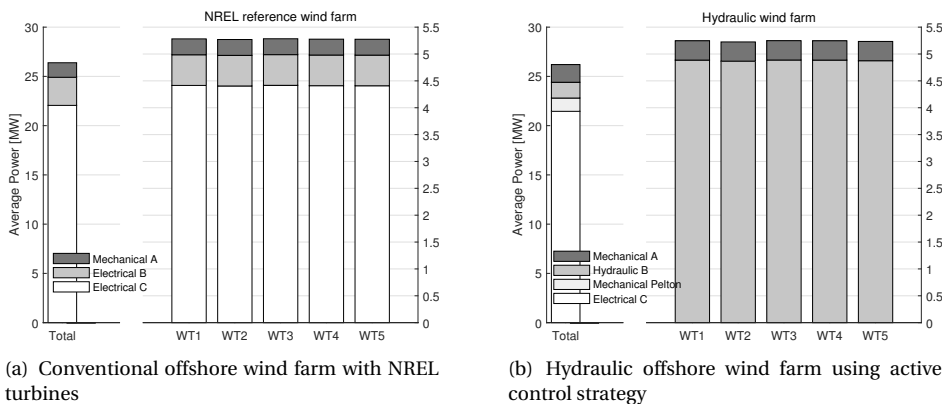


Figure 6.16: Averaged power performance for the reference and the hydraulic wind farm, above rated conditions.

The first observation based on the general results for both wind farms is the reduced power performance of turbines WT2 and WT5. The performance of these two turbines is directly affected by the generated wake from turbines WT1 and WT4. Under the current assumption that the wind direction is horizontal, as shown in Figure 6.12, turbines WT1, WT3 and WT4 are not affected by any other wake interaction.

The numerical values with the standard deviation together with the averaged efficiencies are presented in Tables 6.4 and 6.5. It is important to mention that for the hydraulic

Table 6.4: Performance overview of time domain results for below rated conditions.

Turbine	Averaged power [MW]						Efficiency [-]		
	Mechanical point A		Transmitted point B		Electrical point C		Power coefficient C_P	A to B η_{AB}	B to C η_{BC}
NREL reference wind farm									
	mean	std	mean	std	mean	std	mean	mean	mean
WT1	3.12	0.86	2.95	0.81	2.61	0.72	0.483	0.944	0.885
WT2	2.23	0.60	2.11	0.57	1.87	0.50	0.483	0.944	0.885
WT3	2.90	0.88	2.74	0.83	2.42	0.73	0.483	0.944	0.885
WT4	2.99	0.83	2.82	0.78	2.50	0.69	0.483	0.944	0.885
WT5	2.10	0.58	1.98	0.54	1.75	0.48	0.483	0.944	0.885
Total	13.3		12.6		11.1 1.90		-	-	-
Hydraulic wind farm with pressure control									
	mean	std	mean	std	mean	std	mean	mean	mean
WT1	3.06	0.92	-	-	-	-	0.479	-	-
WT2	2.22	0.69	-	-	-	-	0.482	-	-
WT3	2.84	0.90	-	-	-	-	0.479	-	-
WT4	2.94	0.89	-	-	-	-	0.480	-	-
WT5	2.08	0.65	-	-	-	-	0.482	-	-
Total	13.1		11.6	2.58	10.2	2.71	-	0.88	0.877

wind farm, the individual performance of the turbines at points B and C is not obtained. Instead, only the total hydraulic and electrical power at the mentioned locations is given. After including the performances of the main subsystems involved in the conversion and transmission of wind energy in a wind farm, the results show that the overall efficiency of a hydraulic wind farm is lower for a hydraulic concept compared to conventional technology. The total transmission efficiency which includes the complete collection, transmission and generation of electrical power of the wind farm is obtained using the average efficiencies from point A to point C.

For the presented operating conditions the transmission efficiency of the hydraulic wind farm is between 0.772–0.810 compared to 0.835 from the reference wind farm. The most important losses in the hydraulic concept are attributed to the variable displacement pumps and friction losses in the hydraulic network. Despite having a slower response due to high water inertia, the hydraulic concept also showed higher standard deviations in the generated electrical power due to pressure transients in the hydraulic network.

6.5. CONCLUDING REMARKS

The numerical model of a hydraulic wind power farm, which is used to generate electricity in a centralized manner, was presented. The model captures the most relevant physics of a wind farm including transient behaviour of the hydraulic network and Pelton turbine. In Chapter 4, it was shown that a single turbine is able to operate with a pas-

Table 6.5: Performance overview of time domain results for above rated conditions.

Turbine	Averaged power [MW]						Efficiency [-]		
	Mechanical point A		Transmitted point B		Electrical point C		Power coefficient C_P	A to B η_{AB}	B to C η_{BC}
NREL reference wind farm									
	mean	std	mean	std	mean	std	mean	mean	mean
WT1	5.28	0.22	4.99	0.21	4.41	0.18	0.249	0.944	0.885
WT2	5.27	0.23	4.97	0.22	4.40	0.19	0.284	0.944	0.885
WT3	5.28	0.22	4.99	0.21	4.42	0.18	0.251	0.944	0.885
WT4	5.28	0.23	4.98	0.22	4.41	0.19	0.244	0.944	0.885
WT5	5.27	0.23	4.98	0.22	4.41	0.19	0.277	0.944	0.885
Total	26.4		24.9		22.1 0.92		-	-	-
Hydraulic wind farm with pressure control									
	mean	std	mean	std	mean	std	mean	mean	mean
WT1	5.24	0.18	-	-	-	-	0.247	-	-
WT2	5.22	0.19	-	-	-	-	0.282	-	-
WT3	5.25	0.18	-	-	-	-	0.250	-	-
WT4	5.25	0.18	-	-	-	-	0.243	-	-
WT5	5.23	0.19	-	-	-	-	0.274	-	-
Total	26.2		24.4	1.40	21.4	1.44	-	0.931	0.87

sive control strategy while keeping a stable variable-speed operation. However, when two turbines are incorporated in a farm, the same passive control strategy has strong limitations in terms of performance and stability when these two turbines are coupled through a hydraulic network. An increased stability of the rotor speed for both turbines is possible by operating at a higher tip speed ratio, but the performance of the wind farm is then compromised. For individual turbines with independent lines and nozzles this is not the case. However, based on the design principles for centralized electricity generation, it is preferred to have a combination of parallel and common pipelines.

From a wind farm perspective, an active control strategy is more suitable to maintain the individual turbines performance. Based on a constant pressure control strategy, the simulation of a hypothetical hydraulic wind farm consisting of five turbines was presented for a stochastic turbulent wind, including wake effects. For the presented case study, the results indicate that the individual wind turbines are able to operate within operational limits with the current active control concept. In terms of performance, the simulations show that the hydraulic collection and transmission has a lower efficiency when compared with a reference wind farm that employs conventional technology. The main energy losses are associated with the variable displacement water pumps and friction losses in the hydraulic network.

7

CONCLUSIONS

This dissertation addresses the idea of using pressurized water as a mean to centralize electricity generation in an offshore wind farm. In the proposed concept the conventional geared or direct-drive power drivetrain is replaced by a positive displacement pump. In this manner the rotor nacelle assemblies are dedicated to pressurize water into a hydraulic network. The high pressure water flow is then collected from the wind turbines of the farm and redirected into a central offshore platform where the electricity is generated through a Pelton turbine.

In order to enable the performance evaluation of the proposed centralized generation scheme, a numerical tool is developed and implemented for the simulation of the proposed hydraulic wind farm under operating conditions. In this process, a time-domain approach is employed to analyze the overall system in order to deal with the presence of non-linearities in the mathematical modelling. The set of time-domain sub-models has been presented for the main hydraulic components in Chapter 2.

With respect to the control aspects, the variable rotor speed functionality of the individual turbines, aimed to keep maximum aerodynamic performance for below rated wind speed conditions, is realized by using hydraulic components as a replacement for the conventional torque-controller used in modern wind turbines. Using fluid power technology, two control strategies are analyzed in Chapter 3 using feedback control tools in both the frequency and time domain for a 5 MW turbine. The passive speed control (PSC) is based on the proper dimensioning of the hydraulic components to match the optimal tip speed ratio of the rotor while having a variable pressure in the hydraulic lines. For below rated wind speeds, the PSC is able to maintain the operation of the turbine close to optimal aerodynamic performance without any measurements or manipulation of the turbine settings. In addition, the PSC shows to be inherently stable for a single turbine by using a constant area nozzle.

A different approach is also studied, in which the variable speed functionality is realized through active speed control (ASC). With this strategy the transmitted torque from the drivetrain is manipulated by adjusting continuously the volumetric displacement of the water pump. In combination with an adjustable spear valve at the nozzle side, a constant

pressure across the hydraulic drives is realized in what is known as ‘secondary control’ in hydraulic control systems. Special attention has to be paid to the controller design to avoid undesired pressure waves in the hydraulic lines as a result of sudden control actions. A combination of a PI control in series with a low-pass filter and notches is proposed for the pressure controller to account for this effect. Since the performance and design of the controllers is limited to the framework of linear control theory, there are high expectations that other non-linear control methods can improve the dynamic performance of the system.

Before looking at a complete hydraulic wind farm, the dynamics and performance of a single hydraulic wind turbine are presented in Chapter 4. Two different wind turbines with hydraulic transmissions are analyzed based on the PSC and ASC strategies of Chapter 3 for different wind speed conditions. The design parameters of the hydraulic concepts are obtained using as a basis the same rotor as the NREL 5 MW offshore wind turbine reference. The simulation results indicate that the operation in below and above rated wind speed conditions is possible for a single turbine with both PSC and ASC strategies. Despite a lower transmission efficiency when compared to the reference turbine, the hydraulic transmission with PSC has a strongly damped response of the generated electrical power and transmitted torque to the rotor.

From a design point of view, the PSC is limited in two different ways. The first one is the choice of rated wind speed and consequently rated power. The design rated wind speed is limited by the combination of the optimal tip speed ratio and the maximum tangential velocity of the blades. In the considered examples of Chapter 4, the rotor of the NREL turbine with an optimal tip speed ratio, $\lambda = 7.55$ and maximum tangential velocity of 80 m/s, resulted in a rated wind speed of 10.4 m/s with only 4.4 MW compared to the original 5.4 MW for rated wind speed of 11.4 m/s. It is possible to design the PSC for a lower tip speed ratio in order to reach the original rated wind speed. However a lower tip speed ratio implies a compromise in both aerodynamic performance and rotor speed stability. A dedicated design of the rotor which includes the PSC into consideration could result in an alternative solution that has yet to be evaluated. Furthermore, the reliability of the system is not compromised due to the passive nature of the control strategy.

The following step towards a wind farm with centralized electricity generation is to include more than one turbine in the energy conversion process. To this end, the use of a hydraulic network consisting of hydraulic lines from each turbine into a central offshore platform is required. The development and implementation of the flow dynamics in the hydraulic network through a continuous time-domain model is presented in Chapter 5. The hydraulic network model is assembled from individual models of single hydraulic lines with different boundary conditions. For each line, an approximation of the solution in the frequency domain of a two-dimensional viscous compressible laminar flow is employed. These ‘modal approximations’ replace the transcendental transfer functions with a finite summation of low-order rational polynomials, which can be directly translated into the time domain as a set of linear ordinary differential equations. For different boundary conditions, a linear time-invariant system is formulated in the state-space form. The main disadvantage of using the method of modal approximations is the lack of direct control of the accuracy of the results due to a propagation error introduced

by a limited number of modes used for each line. In general, these approximations are not able to capture the sharp or steep pressure variations in the wave fronts. In order to assess the suitability of the hydraulic network model, a semi-analytical approach based on the impulse response method is proposed to study accurately the entire hydraulic network with linear boundary conditions. The proposed method is only limited by the numerical considerations to solve a system of coupled linear algebraic equations and the fast Fourier transform.

The assumption in the hydraulic models of laminar flow through the pipelines is certainly not realistic. Friction losses due to turbulent flow have a direct impact on the performance of the system and need to be taken into account. While accurate modelling of transient turbulent flow is currently an on going research topic, it is expected that the turbulent flows will result in higher energy dissipation which is translated as higher damping in the fluid pressure oscillations. From this perspective, the models for laminar flow give a more conservative response in terms of fluid transients.

Finally, the turbines, the hydraulic network and the central offshore platform are integrated into a wind farm model in Chapter 6. The ambient wind field conditions and wake interaction are considered from existing models used in the field of distributed control for large-scale offshore wind farms. For the modelling of each rotor-nacelle assembly, the aerodynamic loading is simplified to an axial thrust force acting at the top of the support structure and an aerodynamic torque acting on the hydraulic drivetrain. In the simulations both loads are obtained through the steady-state performance coefficients, while aeroelastic and unsteady effects are not accounted for. Although this assumption is not realistic, in terms of quantifying the energy conversion at a wind farm level the accuracy is not significantly compromised by these simplified models. Furthermore, the computational cost is greatly reduced, especially when several turbines need to be included in the farm model. Since the modelling of the turbulent wind field is limited to a 2D approach where wind shear and tower shadow effects are not included, the overall wind farm models are consistent in the level of simplification. It is possible to further develop the current model to include a more realistic aerodynamic description with more complex simulation codes.

The simulation results indicate that by incorporating more than one turbine into the hydraulic network, the PSC strategy is limited by the use of independent lines and nozzles for each turbine. From a centralized generation point of view, it is more suitable to use a combination of parallel and common pipelines rather than independent pipelines in the hydraulic network. Under this scheme, at the central platform, a Pelton turbine is limited to cope with a finite number of wind turbines, which is determined by the maximum number of nozzles allowed by the conventional Pelton runner designs. A more appropriate solution is possible with the ASC strategy in which a constant pressure system allows to incorporate more than one turbine to the hydraulic network. Hence, a relatively small hydraulic wind power plant with ASC and constant pressure is simulated for five turbines coupled to the same hydraulic network. It is important to mention that as more turbines are incorporated in the hydraulic network, the overall hydraulic inertia of the system is increased. Thus, the hydraulic wind farm has a slower response when compared to the reference wind farm with conventional technology.

The wind farm numerical model demonstrates that, on the basis of physical principles it is possible to generate electricity in a centralized manner by dedicating the individual turbines inside a wind farm to pressurize water into a hydraulic network and then use the pressurized flow in a Pelton turbine. The performance of the hydraulic wind farm is obtained from time-domain simulations, which indicate that both PSC and ASC concepts have overall energy conversion efficiencies between 68–70% and 77–81%, respectively. The numerical model accounts for the different stages related to the energy conversion process, namely the aerodynamic performance, hydraulic collection, transmission and generation of electricity. The obtained performance is lower than that of a conventional wind farm with electrical power conditioning, with an overall conversion efficiency between 82–84%.

Future prospects of the hydraulic concept include the development and integration of an energy storage system using hydraulic accumulators. It is expected that these hydraulic devices will minimize the electrical power fluctuations despite the turbulent wind conditions. Further development of the proposed hydraulic concept requires validation of the numerical model and comparison between simulation results and experiments. The integration of wind energy and fluid power technology can also contribute to existing applications in which the production of electrical power is not the primary goal. Some examples of such applications include seawater desalination, pumped hydro-storage and thermal energy production for both heating and cooling.

BIBLIOGRAPHY

- Albers, P. *Motion control in offshore and dredging*. Springer Science, 2010.
- Al'tshul', A. and Margolin, M. S. Effect of vortices on the discharge coefficient for flow of a liquid through an orifice. *Hydrotechnical Construction*, 2(6):507–510, 1968.
- Angehlm, R. Safety Engineering for the 423MW-Pelton runners at Bieudron. In *20th IAHR Symposium*. VATECH HYDRO, August 2000.
- Artemis Intelligent Power. www.artemisip.com, accessed: December 2016.
- Ayalew, B. and Kulakowski, B. T. Modal approximation of distributed dynamics for a hydraulic transmission line with pressure input-flow rate output causality. *J. Dyn. Syst. Meas. Control*, vol. 127:p.503–507, 2005.
- Baotić, M. Polytopic computations in constrained optimal control. *Automatika: Journal for Control, Measurement, Electronics, Computing & Communications*, 50(3-4):p.119–134, 2009.
- Bianchi, F., Battista, H., and Mantz, R. Article title. In Editor, A., editor, *Wind Turbine Control Systems: Principles, Modelling and Gain Scheduling Design*, volume 1 of *Advances in Industrial Control*, Chapter 1, pages 1–3. Springer London, 1st edition, May 1997.
- Borrelli, F., Baotić, M., Pekar, J., and Stewart, G. On the computation of linear model predictive control laws. *Automatica*, 46(6):p.1035–1041, 2010.
- Bosch-Rexroth. Hydraulic Control Technology for Wind Turbine Generators. www.boschrexroth.com/ics Bosch-Rexroth brochure, accessed: January 2015.
- Bossanyi, E. The design of closed loop controllers for wind turbines. *Wind Energy*, 3(3):p.149–163, 2000.
- Bossanyi, E. and Witcher, D. Controller for 5 MW reference turbine. Technical report 11593/BR/04, Integrated Wind Turbine Design - UpWind, Bristol, England, July 2009.
- Bossanyi, E. Bladed User Manual. Technical report, Garrad Hassan and Partners Ltd, Bristol, England, 2010.
- Brown, F. The transient response of fluid lines. *J. Basic Eng*, vol. 84:p.547–553, 1962.
- Buhagiar, D., Sant, T., and Bugeja, M. K. Control of an open-loop hydraulic offshore wind turbine using a variable-area orifice. In *Proceedings of the International Conference on Offshore Mechanics and Arctic Engineering - OMAE*, volume 9, 2015.

- Buhagiar, D., Sant, T., and Bugeja, M. A comparison of two pressure control concepts for hydraulic offshore wind turbines. *Journal of Dynamic Systems, Measurement, and Control*, 2016.
- Burton, T., Jenkins, N., Sharpe, D., and Bossanyi, E. *Wind Energy Handbook, Second Edition*, chapter 8. The controller. *Wind Energy Handbook, Second Edition*. John Wiley & Sons, Ltd., 2011.
- Chen, Z., Guerrero, J., and Blaabjerg, F. A review of the state of the art of power electronics for wind turbines. *IEEE Transactions on Power Electronics*, 24(8):pp. 1859–1875, August 2009.
- Crespo, A., Hernandez, J., and Frandsen, S. Survey of modelling methods for wind turbine wakes and wind farms. *Wind Energy*, 2(1):p.1–24, 1999.
- Cundiff, J. S. *Fluid power circuits and controls: fundamentals and applications*, volume 21. CRC Press, 2001.
- Davidson, P. A. *Turbulence*. Oxford University Press, 2004.
- Deldar, M., Izadian, A., Vaezi, M., and Anwar, S. Modeling of a hydraulic wind power transfer utilizing a proportional valve. *IEEE Transactions on Industry Applications*, 51(2):p.1837–1844, 2015.
- Det Norske Veritas and Germanischer Lloyd. Offshore Wind: A Manifesto for Cost Reduction. DNV GL manifesto for offshore wind cost reduction, 2015.
- Diepeveen, N. *On the Application of Fluid Power Transmission in Offshore Wind Turbines*. PhD thesis, Technical University of Delft, August 2013.
- Diepeveen, N. and Jarquin Laguna, A. Wind tunnel experiments to prove a hydraulic passive torque control concept for variable speed wind turbines. In *Journal of Physics: Conference Series*, volume 555(1), page 012028. the European Academy of Wind Energy, IOP Publishing, 2014. The Science of Making Torque from Wind 2012.
- Dixon, S. and Hall, C. *Fluid mechanics and thermodynamics of turbomachinery*. Butterworth-Heinemann, 7th edition, 2014.
- Doble, W. A. The tangential water-wheel. *Transactions of the American Institute of Mining Engineers, California Meeting* 29, pages 852–894, 1899.
- DOT. B.V. <http://www.dotpower.nl/>, contacted: November 2016.
- D'Souza, A. and Oldenburger, R. Dynamic response of fluid lines. *J. Basic Eng*, vol. 86: p.589–598, 1964.
- Fleming, P., Ning, A., Gebraad, P. M. O., and Dykes, K. Wind plant system engineering through optimization of layout and yaw control. *Wind Energy*, 19(2):p.29–344, 2016.

- Frandsen, S., Barthelmie, R., Pryor, S., Rathmann, O., Larsen, S., and Højstrup, J. Analytical modelling of wind speed deficit in large offshore wind farms. *Wind Energy*, 9: p.39–53, 2006.
- Ghidaoui, M. S., Zhao, M., McInnis, D. A., and Axworthy, D. H. A review of water hammer theory and practice. *Applied Mechanics Reviews*, 58(1-6):p. 49–75, 2005.
- Goodson, R. and Leonard, R. A survey of modeling techniques for fluid line transients. *J. Basic Eng*, vol. 94:p.474–482, 1972.
- Graff, F. *Wave motion in elastic solids*. Dover, 1991.
- Grimble, M. and Majecki, P. Polynomial approach to non-linear predictive generalised minimum variance control. *IET control theory & applications*, 4(3):p.411–424, 2010.
- Grunnet, J., Soltani, M., Knudsen, T., Kragelund, M., and Bak, T. Aeolus toolbox for dynamics wind farm model, simulation and control. In *The European Wind Energy Conference & Exhibition, EWEK 2010*, 2010.
- Hägglunds Drive Systems. www.hagglunds.com, accessed: January 2014.
- Höhn, B. Future Transmissions for Wind Turbines. *Applied Mechanics and Materials*, vol. 86:p.18–25, 2011.
- Hsue, C. and Hullender, D. Modal approximations for the fluid dynamics of hydraulic and pneumatic transmission lines. In *Transmission Line Dynamics, ASME Special Publication*, pages p.51–77, 1983.
- Hydrautrans. www.hydrautrans.com, accessed: September 2014.
- Innes-Wimsatt, C., E. Qin and Loth, E. Economic benefits of hydraulic-electric hybrid wind turbines. *International Journal of Environmental Studies*, 71(6):p.812–827, 2014.
- International Electrotechnical Commission. Wind turbines-part 1: Design requirements. *IEC 61400*, 1, 2005.
- International Electrotechnical Commission. Wind turbines-part 3: Design requirements for offshore wind turbines. *IEC 61400*, 3, 2009.
- Jarquín Laguna, A. Fluid power network for centralized electricity generation in offshore wind farms. In *Journal of Physics: Conference Series*, volume 524(1), page 012075. the European Academy of Wind Energy, IOP Publishing, 2014. The Science of Making Torque from Wind 2014.
- Jarquín Laguna, A. Modeling and analysis of an offshore wind turbine with fluid power transmission for centralized electricity generation. *Journal of Computational and Nonlinear Dynamics: Special issue wind turbine modelling*, 10(4):pp.11–24, 2015.
- Jarquín Laguna, A. Simulation of an offshore wind farm using fluid power for centralized electricity generation. In *Journal of Physics: Conference Series*, volume 753(10), page 102004. the European Academy of Wind Energy, IOP Publishing, 2016. The Science of Making Torque from Wind 2016.

- Jarquín Laguna, A. and Tsouvalas, A. Transient laminar flow in hydraulic networks based on a semi-analytical impulse response method. *HERON: Special issue dynamics of structures*, 59(1):pp.37–55, 2014.
- Jarquín Laguna, A., Diepeveen, N., and Van Wingerden, J. Analysis of dynamics of fluid power drive-trains for variable speed wind turbines: Parameter study. *IET Renewable Power Generation*, 8(4):pp.398–410, 2014.
- Jelavić, M. and Perić, N. Wind turbine control for highly turbulent winds. *Automatika: Journal for Control, Measurement, Electronics, Computing & Communications*, 50, 2009.
- Jensen, J., Furuseth, A., Chang, P., and Thomsen, K. Technological Advances in Hydraulic Drive Trains for Wind Turbines. In *Proceedings of the European Wind Energy Association*. EWEA, April 2012.
- Jensen, N. A note on wind generator interaction. Technical report, Risø National Laboratory, 1983.
- JERICO. Hydraulic Wind Energy Conversion. Technical report, Jacobs Energy Research, July 1981.
- Jonkman, J., Butterfield, S., Musial, W., and Scott, G. Definition of a 5MW Reference Wind Turbine for Offshore System Development. Technical report NREL/TP-500-38060, National Renewable Energy Laboratory, Golden, Colorado, February 2009.
- Karney, B. W. and McInnis, D. Efficient calculation of transient flow in simple pipe networks. *J. Hyd. Eng.*, vol. 118(7):p.1014–1030, 1992.
- Keck, H., Vulllioud, G., and Joye, P. Commissioning and Operation Experience with the Worlds Largest Pelton Turbines Bieudron. Technical report, VATECH hydro, 2000.
- Kim, S. Holistic unsteady-friction model for laminar transient flow in pipeline systems. *J. Hyd. Eng.*, vol. 137(12):p.1649–1658, 2011.
- Knudsen, T., Bak, T., and Soltani, M. Prediction models for wind speed at turbine locations in a wind farm. *Wind Energy*, 14(7):p.877–894, 2011.
- Kristensen, L. and Jensen, N. O. Lateral coherence in isotropic turbulence and in the natural wind. *Boundary-Layer Meteorology*, 17:p.353–373, 1979.
- Larsen, G. C., Madsen, H. A., Thomsen, K., and Larsen, T. J. Wake meandering: A pragmatic approach. *Wind Energy*, 11:p.377–395, 2008.
- Larsen, T. and Hansen, A. How to HAWC2, the users manual. Technical Report Riso-R-1597(en), Risoe National Laboratory, Technical University of Denmark, Denmark, 2007.
- Lim, G., Chua, P., and He, Y. Modern water hydraulics—the new energy-transmission technology in fluid power. *Applied Energy*, 76(1):p. 239–246, 2003.

- Liserre, M., Cardenas, R., Molinas, M., and Rodriguez, J. Overview of multi-mw wind turbines and wind parks. *IEEE Transactions on Industrial Electronics*, 4(58):p.1081–1095, 2011.
- Mäkinen, J., Piche, R., and Ellman, A. Fluid transmission line modeling using a variable method. *J. Dyn. Syst. Meas. Control*, vol. 122:p.153–162, 2000.
- Makinen, J., Pertola, P., and Marjamaki, H. Modeling Coupled Hydraulic-Driven Multi-body Systems using Finite Element Method. In *The 1st Joint International Conference on Multibody System Dynamics*. Lappeenranta University of Technology, May 2010.
- Margolis, D. and Yang, W. Bond graph models for fluid networks using modal approximation. *J. Dyn. Syst. Meas. Control*, vol. 107:p.169–175, 1985.
- MATLAB-Simulink®. *version 8.4.0 (R2014b)*. The MathWorks Inc., Natick, Massachusetts, 2014.
- Merritt, H. *Hydraulic control systems*. John Wiley & Sons, 1967.
- Mitsubishi-Heavy-Industries. Sea Angel, the future of offshore wind. www.mhps.com/products/seaangel, accessed: December 2015.
- Murrenhoff, H. Systematic approach to the control of hydrostatic drives. *Proceedings of the Institution of Mechanical Engineers. Part I: Journal of Systems and Control Engineering*, 213(5):333–347, 1999.
- Murrenhoff, H. and Linden, D. *Umdruck zur Vorlesung Grundlagen der Fluidtechnik*. Shaker, 1997.
- Ogata, K. *Modern control engineering*. Prentice Hall PTR, 2001.
- Pang, Y. and Grimble, M. J. Ngmv control of delayed piecewise affine systems. *IEEE Transactions on Automatic Control*, 55(12):p.2817–2821, 2010.
- Parker, M. and Anaya-Lara, O. Cost and losses associated with offshore wind farm collection networks which centralise the turbine power electronic converters. *IET Renewable Power Generation*, 7(4):p.390–400, July 2013.
- Payne, G., Kiprakis, A., Ehsan, M., Rampen, W., Chick, J., and Wallace, A. Efficiency and dynamic performance of digital displacement™ hydraulic transmission in tidal current energy converters. *Proceedings of the Institution of Mechanical Engineers, Part A: Journal of Power and Energy*, vol. 221(2):p.207–218, 2007.
- Pezzinga, G. Quasi-2d model for unsteady flow in pipe networks. *J. Hyd. Eng.*, vol. 125(7):p.676–685, 1999.
- Piché, R. and Ellman, A. A fluid transmission line model for use with ode simulators. In *The Eighth Bath International Fluid Power Workshop*, 1995.

- Rybak, S. Description of the 3MW SWT-3 Wind Turbine at San Gorgonio Pass, California. Technical report, The Bendix Corporation Energy, Environment and Technology Office, 1981.
- Salter, S. Hydraulics for wind. In *European Wind Energy Conference*, pages p.534–541. EWEC, October 1984.
- Sanderse, B., van der Pijl, S., and Koren, B. Review of computational fluid dynamics for wind turbine wake aerodynamics. *Wind Energy*, 14(7):p.799–819, 2011.
- Schaap, M. Seawater Driven Piling Hammer. In *Proceedings of the Dutch Fluid Power Conference in Ede*, September 2012.
- Scheid, F. *Schaum's outline of theory and problems of numerical analysis*. McGraw-Hill, 1988.
- Schmitz, J., Vatheuer, N., and Murrenhoff, H. Development of a Hydrostatic Transmission for Wind Turbines. *Proceedings of the International Fluid Power Conference 2010*, vol. 3:p.479–488, 2010.
- Schmitz, J., Vatheuer, N., and Murrenhoff, H. Hydrostatic drive train in Wind Energy Plants. In *Proceedings of the European Wind Energy Association*. EWEA, 2011.
- Schmitz, J., Diepeveen, N., Vatheuer, N., and Murrenhoff, H. Dynamic transmission response of a hydrostatic transmission measured on a test bench. In *Proceedings of the European Wind Energy Association*. EWEA, 2012.
- Segeren, M. and Diepeveen, N. Influence of the rotor nacelle assembly mass on the design of monopile foundations. *Heron*, vol. 59(1):p.17–36, 2014.
- Silva, P., Giuffrida, A., Fergnani, N., Macchi, E., Cantù, M., Suffredini, M., R. and Schiavetti, and Gigliucci, G. Performance prediction of a multi-mw wind turbine adopting an advanced hydrostatic transmission. *Energy*, 64:p. 450–461, 2014.
- Skaare, B., Hörnsten, B., and Nielsen, F. Energy Considerations for Wind Turbines with Hydraulic Transmission Systems. In *Proceedings of EWEA Offshore Conference*, Amsterdam, Netherlands. EWEA, December 2011.
- Skaare, B., Hörnsten, B., and Nielsen, F. Modeling, Simulation and Control of a Wind Turbine with a Hydraulic Transmission Systems. *Wind Energy*, October 2012.
- Soleimanzadeh, M. and Wisniewski, R. Controller design for a wind farm, considering both power and load aspects. *Mechatronics*, 21(4):p.720–727, 2011.
- Soumelidis, M., Johnston, D., K.A., E., and Tilley, D. A comparative study of modelling techniques for laminar flow transients in hydraulic pipelines. In *Proceedings JFPS conference*, 2005.
- Spudić, V., Jelavić, M., and Baotić, M. Wind turbine power references in coordinated control of wind farms. *Automatika–Journal for Control, Measurement, Electronics, Computing and Communications*, 52(2), 2011.

- Sørensen, P., Hansen, A. D., André, P., and Rosas, C. Wind models for simulation of power fluctuations from wind farms. *Journal of Wind Engineering and Industrial Aerodynamics*, 90:p.1381–1402, 2002.
- Stecki, J. and Davis, D. Fluid transmission lines-distributed parameter models, part 1: A review of the state of the art. *Proc. Inst. Mech. Eng., Part A*, vol. 200:p.215–228, 1986.
- Suo, L. and Wylie, E. Impulse response method for frequency-dependent pipeline transients. *ASME Trans. J. Fluids Eng.*, vol. 111:p.478–483, 1989.
- Taylor, J. The Artemis Digital Displacement Transmission; a Lightweight, Network-Supporting Power-Train for Sea-Angel. *EWEA Annual Event Conference Proceedings*, April 2012.
- Thake, J. *The Micro-hydro Pelton Turbine Manual*. Practical Action Publishing, 2000.
- The European Commission. Aeolus, distributed control of large scale offshore wind farms. <http://www.ict-aeolus.eu/>, January 2012. European research project under the IST framework programme 7.
- Tijsseling, A. Fluid-structure interaction in liquid-filled pipe systems: A review. *J. Fluids Struct.*, vol. 10:p.109–146, 1995.
- Trikha, A. An efficient method for simulating frequency-dependent friction in transient liquid flow. *ASME Trans. J. Fluids Eng.*, vol. 97:p.97–105, 1975.
- Trostmann, E. *Water hydraulics control technology*. CRC Press, 1995.
- van Kuik, G. A. M., Peinke, J., Nijssen, R., Lekou, D., Mann, J., Sørensen, J. N., Ferreira, C., van Wingerden, J. W., Schlipf, D., Gebraad, P., Polinder, H., Abrahamsen, A., van Bussel, G. J. W., Sørensen, J. D., Tavner, P., Bottasso, C. L., Muskulus, M., Matha, D., Lindeboom, H. J., Degraer, S., Kramer, O., Lehnhoff, S., Sonnenschein, M., Sørensen, P. E., Künneke, R. W., Morthorst, P. E., and Skytte, K. Long-term research challenges in wind energy – a research agenda by the european academy of wind energy. *Wind Energy Science*, 1(1):p.1–39, 2016.
- Van Schothorst, G. *Modeling of Long-Stroke Hydraulic Servo-Systems for Flight Simulator Motion Control and System Design*. PhD thesis, Technical University of Delft, September 1997.
- van Zuijlen, E., Zaaier, M., and Meijer, B. TKI Wind op Zee - Roadmap 2015 - 2020. <http://www.tki-windopzee.nl/page/tki-wind-op-zee>, 2014.
- Vardy, A. and Brown, J. Transient, turbulent, smooth pipe friction. *J. Hydraul. Res.*, vol. 33:p.435–456, 1995.
- Vardy, A., Hwang, K., and Brown, J. A weighting model of transient turbulent pipe friction. *J. Hydraul. Res.*, vol. 31:p.533–548, 1993.
- Veers, P. S. Three-dimensional wind simulation. Technical Report SAND88-0152 UC-261, Sandia National Laboratories, 1988.

- Vermeer, L., J.N., S., and Crespo, A. Wind turbine wake aerodynamics. *Progress in Aerospace Sciences*, 39(6-7):p.467–510, 2003.
- Watton, J. and Tadmori, M. A comparison of techniques for the analysis of transmission line dynamics in electrohydraulic control systems. *Appl. Math. Modelling*, vol. 12:p.457–466, 1988.
- Whittaker, T., Collier, D., Folley, M., Osterried, M., Henry, A., and Crowley, M. The development of oyster—a shallow water surging wave energy converter. In *Proceedings of the 7th European Wave and Tidal Energy Conference, Porto, Portugal*, pages 11–14, 2007.
- Wichowski, R. Hydraulic transients analysis in pipe networks by the method of characteristics (moc). *Archives of Hydro-Engineering and Environmental Mechanics*, vol. 53 (3):p.267–291, 2006.
- WindEurope. European Wind Energy Association. The European offshore wind industry - key trends and statistics 2016, January 2017a.
- WindEurope. European Wind Energy Association. Wind in power: 2016 European statistics, January 2017b.
- Wood, D., Lingireddy, S., Boulos, P., Karney, B., and McPherson, D. Numerical methods for modeling transient flow in distribution systems. *Journal American Water Works Association*, vol. 97(7):p.104–115, 2005.
- Wylie, E., Streeter, V., and Suo, L. Analysis of oscillatory flow in systems. In *Fluid Transients in Systems*. Prentice-Hall, 1993a.
- Wylie, E., Streeter, V., and Suo, L. Basic differential equations for transient flow. In *Fluid Transients in Systems*. Prentice-Hall, 1993b.
- Yang, L., Hals, J., and Moan, T. Comparative study of bond graph models of hydraulic transmission lines with transient flow dynamics. *J. Dyn. Syst. Meas. Control*, vol. 134 (3):p.031005, 2012.
- Yang, W. C. and Tobler, W. E. Dissipative modal approximation of fluid transmission lines using linear friction model. *J. Dyn. Syst. Meas. Control*, vol. 113:p.152–162, 1991.
- Zhang, Z. Flow interactions in Pelton turbines and the hydraulic efficiency of the turbine system. *Proceedings of the Institution of Mechanical Engineers, Part A: Journal of Power and Energy*, 221(3):343–357, May 2007.
- Zielke, W. Frequency-dependent friction in transient pipe flow. *J. Basic Eng.*, vol. 90: p.109–115, 1968.



NAVIER STOKES EQUATIONS

A.1. GENERAL VECTOR FORM

In the most general form, the Navier-Stokes equations are given by:

The continuity equation or conservation of mass

$$\frac{D\rho}{Dt} + \rho \nabla \cdot \mathbf{u} = 0 \qquad \frac{\partial \rho}{\partial t} + \nabla \cdot (\rho \mathbf{u}) = 0 \quad (\text{A.1})$$

The motion equation or conservation of momentum

$$\rho \frac{D\mathbf{u}}{Dt} = \rho \left[\frac{\partial \mathbf{u}}{\partial t} + \mathbf{u} \cdot (\nabla \mathbf{u}) \right] = -\nabla p + \nabla \cdot \mathbf{T} + \mathbf{f} \quad (\text{A.2})$$

The state-equation for liquids is given by:

$$\frac{d\rho}{\rho} = \frac{dp}{K} \quad (\text{A.3})$$

In the equation of motion, \mathbf{f} represents the body forces and \mathbf{T} is the so-called viscous stress tensor, which is a material property. For a Newtonian fluid, the viscous stress tensor is linearly proportional to the rate of strain (velocity gradient). The linear constitutive equation used for fluid can be written as:

$$\mathbf{T} = \mu \left[\nabla \mathbf{u} + (\nabla \mathbf{u})^T - \frac{2}{3} (\nabla \cdot \mathbf{u}) \right] + \xi (\nabla \cdot \mathbf{u}) \quad (\text{A.4})$$

When the Stokes relation is assumed (zero Bulk viscosity $\xi = 0$), the hydrostatic pressure is equal to the thermodynamic pressure. Furthermore, considering a constant dynamic viscosity coefficient μ_o the motion equation or conservation of momentum becomes:

$$\rho \left[\frac{\partial \mathbf{u}}{\partial t} + \mathbf{u} \cdot (\nabla \mathbf{u}) \right] = -\nabla p + \mu_o \nabla^2 \mathbf{u} + \frac{1}{3} \mu_o \nabla (\nabla \cdot \mathbf{u}) + \mathbf{f} \quad (\text{A.5})$$

In addition to these, the coefficients used in the fundamental equations may be expressed also as functions of pressure and temperature.

A.2. CYLINDRICAL COORDINATES

The previous equations may be written in different coordinate systems. For a general fluid in cylindrical coordinates, the explicit form of the equations reads:

$$\text{mass : } \frac{\partial \rho}{\partial t} + \frac{\partial}{\partial x}(\rho u_x) + \frac{1}{r} \frac{\partial}{\partial r}(\rho r u_r) + \frac{1}{r} \frac{\partial}{\partial \theta}(\rho u_\theta) = 0 \quad (\text{A.6})$$

$$\begin{aligned} x\text{-momentum : } & \rho \left(\frac{\partial u_x}{\partial t} + u_x \frac{\partial u_x}{\partial x} + u_r \frac{\partial u_x}{\partial r} + \frac{u_\theta}{r} \frac{\partial u_x}{\partial \theta} \right) = \\ & - \frac{\partial p}{\partial x} + \left(\frac{\partial \tau_{xx}}{\partial x} + \frac{1}{r} \frac{\partial}{\partial r}(r \tau_{xr}) + \frac{1}{r} \frac{\partial \tau_{x\theta}}{\partial \theta} \right) + f_x \end{aligned} \quad (\text{A.7})$$

$$\begin{aligned} r\text{-momentum : } & \rho \left(\frac{\partial u_r}{\partial t} + u_x \frac{\partial u_r}{\partial x} + u_r \frac{\partial u_r}{\partial r} + \frac{u_\theta}{r} \frac{\partial u_r}{\partial \theta} - \frac{u_\theta^2}{r} \right) = \\ & - \frac{\partial p}{\partial r} + \left(\frac{\partial \tau_{rx}}{\partial x} + \frac{1}{r} \frac{\partial}{\partial r}(r \tau_{rr}) + \frac{1}{r} \frac{\partial \tau_{r\theta}}{\partial \theta} - \frac{\tau_{\theta\theta}}{r} \right) + f_r \end{aligned} \quad (\text{A.8})$$

$$\begin{aligned} \theta\text{-momentum : } & \rho \left(\frac{\partial u_\theta}{\partial t} + u_x \frac{\partial u_\theta}{\partial x} + u_r \frac{\partial u_\theta}{\partial r} + \frac{u_\theta}{r} \frac{\partial u_\theta}{\partial \theta} + \frac{u_r u_\theta}{r} \right) = \\ & - \frac{1}{r} \frac{\partial p}{\partial \theta} + \left(\frac{\partial \tau_{\theta x}}{\partial x} + \frac{1}{r^2} \frac{\partial}{\partial r}(r^2 \tau_{r\theta}) + \frac{1}{r} \frac{\partial \tau_{\theta\theta}}{\partial \theta} \right) + f_\theta \end{aligned} \quad (\text{A.9})$$

Shear stress constitutive equation:

$$\tau_{xx} = \mu \left[2 \frac{\partial u_x}{\partial x} - \frac{2}{3} (\nabla \cdot \mathbf{u}) \right] + \xi (\nabla \cdot \mathbf{u}) \quad (\text{A.10})$$

$$\tau_{rr} = \mu \left[2 \frac{\partial u_r}{\partial r} - \frac{2}{3} (\nabla \cdot \mathbf{u}) \right] + \xi (\nabla \cdot \mathbf{u}) \quad (\text{A.11})$$

$$\tau_{\theta\theta} = \mu \left[2 \left(\frac{1}{r} \frac{\partial u_\theta}{\partial \theta} + \frac{u_r}{r} \right) - \frac{2}{3} (\nabla \cdot \mathbf{u}) \right] + \xi (\nabla \cdot \mathbf{u}) \quad (\text{A.12})$$

$$\tau_{xr} = \tau_{rx} = \mu \left[\frac{\partial u_x}{\partial r} + \frac{\partial u_r}{\partial x} \right] \quad (\text{A.13})$$

$$\tau_{x\theta} = \tau_{\theta x} = \mu \left[\frac{1}{r} \frac{\partial u_x}{\partial \theta} + \frac{\partial u_\theta}{\partial x} \right] \quad (\text{A.14})$$

$$\tau_{r\theta} = \tau_{\theta r} = \mu \left[r \frac{\partial}{\partial r} \left(\frac{u_\theta}{r} \right) + \frac{1}{r} \frac{\partial u_r}{\partial \theta} \right] \quad (\text{A.15})$$

The cylindrical coordinate system expansion of the divergence of the velocity vector $\nabla \cdot \mathbf{u}$ is given as:

$$\nabla \cdot \mathbf{u} = \frac{\partial u_x}{\partial x} + \frac{1}{r} \frac{\partial}{\partial r}(r u_r) + \frac{1}{r} \frac{\partial u_\theta}{\partial \theta} \quad (\text{A.16})$$

A.3. CYLINDRICAL COORDINATES, CONSTANT VISCOSITY

When a constant dynamic viscosity coefficient is considered, Equation A.5 is reduced to the following equations:

$$\begin{aligned}
x\text{-momentum:} \quad & \rho \left(\frac{Du_x}{Dt} \right) = \rho \left[\frac{\partial u_x}{\partial t} + u_x \frac{\partial u_x}{\partial x} + u_r \frac{\partial u_x}{\partial r} + \frac{u_\theta}{r} \frac{\partial u_x}{\partial \theta} \right] \\
& = -\frac{\partial p}{\partial x} + \mu_o \left[\frac{\partial^2 u_x}{\partial x^2} + \frac{1}{r} \frac{\partial}{\partial r} \left(r \frac{\partial u_x}{\partial r} \right) + \frac{1}{r^2} \frac{\partial^2 u_x}{\partial \theta^2} \right] \\
& \quad + \frac{\mu_o}{3} \frac{\partial}{\partial x} \left[\frac{\partial u_x}{\partial x} + \frac{1}{r} \frac{\partial(r u_r)}{\partial r} + \frac{1}{r} \frac{\partial u_\theta}{\partial \theta} \right] + f_x
\end{aligned} \tag{A.17}$$

$$\begin{aligned}
r\text{-momentum:} \quad & \rho \left(\frac{Du_r}{Dt} - \frac{u_\theta^2}{r} \right) = \rho \left[\frac{\partial u_r}{\partial t} + u_x \frac{\partial u_r}{\partial x} + u_r \frac{\partial u_r}{\partial r} + \frac{u_\theta}{r} \frac{\partial u_r}{\partial \theta} - \frac{u_\theta^2}{r} \right] \\
& = -\frac{\partial p}{\partial r} + \mu_o \left[\frac{\partial^2 u_r}{\partial x^2} + \frac{1}{r} \frac{\partial}{\partial r} \left(r \frac{\partial u_r}{\partial r} \right) + \frac{1}{r^2} \frac{\partial^2 u_r}{\partial \theta^2} - \frac{u_r}{r^2} - \frac{2}{r^2} \frac{\partial u_\theta}{\partial \theta} \right] \\
& \quad + \frac{\mu_o}{3} \frac{\partial}{\partial r} \left[\frac{\partial u_x}{\partial x} + \frac{1}{r} \frac{\partial(r u_r)}{\partial r} + \frac{1}{r} \frac{\partial u_\theta}{\partial \theta} \right] + f_r
\end{aligned} \tag{A.18}$$

$$\begin{aligned}
\theta\text{-momentum:} \quad & \rho \left(\frac{Du_\theta}{Dt} + \frac{u_r u_\theta}{r} \right) = \rho \left[\frac{\partial u_\theta}{\partial t} + u_x \frac{\partial u_\theta}{\partial x} + u_r \frac{\partial u_\theta}{\partial r} + \frac{u_\theta}{r} \frac{\partial u_\theta}{\partial \theta} + \frac{u_r u_\theta}{r} \right] \\
& = -\frac{1}{r} \frac{\partial p}{\partial \theta} + \mu_o \left[\frac{\partial^2 u_\theta}{\partial x^2} + \frac{1}{r} \frac{\partial}{\partial r} \left(r \frac{\partial u_\theta}{\partial r} \right) + \frac{1}{r^2} \frac{\partial^2 u_\theta}{\partial \theta^2} - \frac{u_\theta}{r^2} + \frac{2}{r^2} \frac{\partial u_r}{\partial \theta} \right] \\
& \quad + \frac{\mu_o}{3} \frac{1}{r} \frac{\partial}{\partial \theta} \left[\frac{\partial u_x}{\partial x} + \frac{1}{r} \frac{\partial(r u_r)}{\partial r} + \frac{1}{r} \frac{\partial u_\theta}{\partial \theta} \right] + f_\theta
\end{aligned} \tag{A.19}$$

A.3.1. AXISYMMETRIC CONDITION

For the axisymmetric condition, the equations for a constant dynamic viscosity reduce to:

$$\text{mass:} \quad \frac{\partial \rho}{\partial t} + \rho \frac{\partial u_r}{\partial r} + \rho \frac{u_r}{r} + \rho \frac{\partial u_x}{\partial x} + u_r \frac{\partial \rho}{\partial r} + u_x \frac{\partial \rho}{\partial x} = 0 \tag{A.20}$$

$$\begin{aligned}
x\text{-momentum:} \quad & \rho \left(\frac{Du_x}{Dt} \right) = \rho \left[\frac{\partial u_x}{\partial t} + u_x \frac{\partial u_x}{\partial x} + u_r \frac{\partial u_x}{\partial r} \right] \\
& = -\frac{\partial p}{\partial x} + \mu \left[\frac{4}{3} \frac{\partial^2 u_x}{\partial x^2} + \frac{\partial^2 u_x}{\partial r^2} + \frac{1}{r} \frac{\partial u_x}{\partial r} + \frac{1}{3} \frac{\partial}{\partial x} \left(\frac{\partial u_r}{\partial r} + \frac{u_r}{r} \right) \right]
\end{aligned} \tag{A.21}$$

$$\begin{aligned}
r\text{-momentum:} \quad & \rho \left(\frac{Du_r}{Dt} \right) = \rho \left[\frac{\partial u_r}{\partial t} + u_x \frac{\partial u_r}{\partial x} + u_r \frac{\partial u_r}{\partial r} \right] \\
& = -\frac{\partial p}{\partial r} + \mu \left[\frac{4}{3} \frac{\partial^2 u_r}{\partial r^2} + \frac{4}{3} \frac{1}{r} \frac{\partial u_r}{\partial r} - \frac{4}{3} \frac{u_r}{r^2} + \frac{\partial}{\partial x} \left(\frac{1}{3} \frac{\partial u_x}{\partial r} + \frac{\partial u_r}{\partial x} \right) \right]
\end{aligned} \tag{A.22}$$

B

ON THE LIMITATIONS OF THE PIPELINE MODEL

B.1. ASSUMPTION ON EFFECTIVE ACOUSTIC SPEED

The isentropic speed of sound in the fluid is only valid for a line with rigid walls. In reality the effects of the conduit elasticity have a direct influence on the acoustic wave speed. This effect can be simplistically accounted for using the following equation:

$$\frac{1}{c_o^2} = \frac{d\rho}{dp} + \frac{\rho}{A} \frac{dA}{dp}$$

The variation of the area with respect to the pressure depends not only on the material and the geometrical properties of the pipe, but also on the pipe restraint conditions for movement, some of these effects are presented in (Wylie et al., 1993b; Ghidaoui et al., 2005). Furthermore the movement and inertia of the pipe also have an influence on the effective acoustic speed (Tijsseling, 1995).

B.2. ASSUMPTION REGARDING UNIFORM PRESSURE DISTRIBUTION

When a uniform pressure over the cross section is assumed, the equation of motion in the radial direction can be neglected. This is only true when the plane wave attenuation effects are neglected and the radius of the conduit is much smaller than the wavelength of the propagating disturbance. Furthermore, a few limitations are imposed on the frequency components ω for which this approximation is valid (Brown, 1962),

$$\frac{\omega v_o}{c_o^2} \ll 1 \quad \text{and} \quad \frac{\omega r_o}{c_o} \ll 1$$

$$\frac{v_o}{r_o c_o} \ll 1$$

B.3. CONDITIONS FOR NON-LINEAR CONVECTIVE TERMS TO BE NEGLECTED

In order to justify this assumption, the order of magnitude of the different terms involved is considered (D'Souza and Oldenburger, 1964). Let L be the characteristic length along the axis of the pipe, U the characteristic velocity, and c_o the speed of sound in the fluid.

$$u \frac{\partial u}{\partial x} \approx \frac{U^2}{L} \quad \text{and} \quad \frac{\partial u}{\partial t} \approx \frac{U}{L/c_o}$$

Hence,

$$\frac{u \frac{\partial u}{\partial x}}{\frac{\partial u}{\partial t}} \approx \frac{\frac{U^2}{L}}{\frac{U}{L/c_o}} \approx \frac{U}{c_o}$$

This means that when $U \ll c_o$, the term $u_x \frac{\partial u_x}{\partial x}$ and similarly $u_r \frac{\partial u_x}{\partial r}$ may be neglected when compared with $\frac{\partial u_x}{\partial t}$.

B

B.4. OTHER VISCOUS TERMS NEGLECTED

Following the same approach, the viscous term $\frac{4}{3} \frac{\partial^2 u_x}{\partial x^2}$ which appears at the right hand side of Equation A.21 may also be neglected. Let u_x be of order U , x of order L and r of order ϵL where $\epsilon \ll 1$.

$$\frac{4}{3} \frac{\partial^2 u_x}{\partial x^2} \approx \frac{4}{3} \frac{U}{L^2}$$

$$\frac{\partial^2 u_x}{\partial r^2} \approx \frac{U}{\epsilon^2 L^2} \quad \text{and} \quad \frac{1}{r} \frac{\partial u_x}{\partial r} \approx \frac{U}{\epsilon^2 L^2}$$

Hence,

$$\frac{\partial^2 u_x}{\partial r^2} \gg \frac{4}{3} \frac{\partial^2 u_x}{\partial x^2} \quad \text{and} \quad \frac{1}{r} \frac{\partial u_x}{\partial r} \gg \frac{4}{3} \frac{\partial^2 u_x}{\partial x^2}$$

The other viscous terms from Equation A.21, $\frac{1}{3} \frac{\partial}{\partial x} \left(\frac{\partial u_r}{\partial r} + \frac{u_r}{r} \right)$ vanish as they become zero when integrated along the cross section with respect to r , from $r = 0$ to $r = r_o$.

$$\frac{1}{3} \frac{\partial}{\partial x} \int_0^{r_o} 2\pi r \left(\frac{\partial u_r}{\partial r} + \frac{u_r}{r} \right) dr = 0$$

C

STATE-SPACE REPRESENTATION OF PIPELINE DYNAMICS

The following continuous time models are based on the work by (Mäkinen et al., 2000) and reproduced from (Makinen et al., 2010).

C.1. ADMITTANCE MODEL

The linear dynamic Equation 2.43, with pressures as input and flow rates as output, is rewritten in the state-space form as,

$$\dot{\mathbf{x}} = \mathbf{Ax} + \mathbf{Bu} \quad (\text{C.1})$$

$$\mathbf{y} = \mathbf{Cx} \quad (\text{C.2})$$

Here, \mathbf{x} is the state vector, \mathbf{u} is the input vector and \mathbf{y} is the output vector. For a hydraulic line with pressures as inputs these vectors are defined as:

$$\mathbf{x} = \begin{pmatrix} q_0 \\ r_1 \\ q_1 \\ \vdots \\ r_n \\ q_n \end{pmatrix}, \quad \mathbf{u} = \begin{pmatrix} \Delta p_p \\ \Delta p_m \end{pmatrix}, \quad \mathbf{y} = \begin{pmatrix} Q_{in} \\ Q_{out} \end{pmatrix} \quad (\text{C.3})$$

The matrices \mathbf{A} , \mathbf{B} and \mathbf{C} are defined as:

$$\mathbf{A} = \text{diag} \left(-\frac{8D_n}{T}, \mathbf{A}_1, \mathbf{A}_2, \dots, \mathbf{A}_n \right), \quad \mathbf{A}_i = \begin{pmatrix} 0 & 1 \\ -\frac{\omega_i}{T^2} & -\frac{\epsilon_i}{T} \end{pmatrix} \quad (\text{C.4})$$

$$\mathbf{B} = \begin{pmatrix} \mathbf{B}_0 \\ \mathbf{B}_1 \\ \vdots \\ \mathbf{B}_n \end{pmatrix}_{(2n+1) \times 2} \quad \left\{ \begin{array}{l} \mathbf{B}_0 = \frac{1}{Z_0 T} \begin{pmatrix} 1 & -1 \end{pmatrix} \\ \mathbf{B}_{2i-1} = \frac{2\sigma_{2i-1}}{Z_0 T} \begin{pmatrix} 0 & 0 \\ 1 & 1 \end{pmatrix} \\ \mathbf{B}_{2i} = \frac{2\sigma_{2i}}{Z_0 T} \begin{pmatrix} 0 & 0 \\ 1 & -1 \end{pmatrix} \end{array} \right. \quad (\text{C.5})$$

$$\mathbf{C} = \begin{pmatrix} 1 & 0 & 1 & 0 & 1 & 0 & 1 & \dots \\ 1 & 0 & -1 & 0 & -1 & 0 & -1 & \dots \end{pmatrix}_{2 \times (2n+1)} \quad (\text{C.6})$$

C.2. Q-P MODEL

Q-p model assumes upstream flow rate and downstream pressure as input and downstream flow rate and upstream pressure as output. The linear dynamic Equation 2.45 is rewritten in the state-space form according to:

$$\begin{pmatrix} \dot{Q}_2 \\ \dot{\mathbf{x}} \end{pmatrix} = \begin{pmatrix} e_0 & \mathbf{e}^T \mathbf{C} \\ 0 & \mathbf{A} \end{pmatrix} \cdot \begin{pmatrix} Q_2 \\ \mathbf{x} \end{pmatrix} + \begin{pmatrix} 0 & \mathbf{e}^T \mathbf{d} \\ \mathbf{b}_1 & \mathbf{b}_2 \end{pmatrix} \cdot \begin{pmatrix} Q_1 \\ \Delta p_2 \end{pmatrix} \quad (\text{C.7})$$

$$\begin{pmatrix} Q_2 \\ \Delta p_1 \end{pmatrix} = \begin{pmatrix} -1 & 0 \\ 0 & \mathbf{f}^T \mathbf{C} \end{pmatrix} \cdot \begin{pmatrix} Q_2 \\ \mathbf{x} \end{pmatrix} + \begin{pmatrix} 0 & 0 \\ 0 & 1 + \mathbf{f}^T \mathbf{d} \end{pmatrix} \cdot \begin{pmatrix} Q_1 \\ \Delta p_2 \end{pmatrix} \quad (\text{C.8})$$

Here, \mathbf{x} is the state vector and \mathbf{u} is the input vector and \mathbf{y} is the output vector. For the hydraulic line with pressures as inputs these vectors are defined as:

$$\mathbf{x} = \begin{pmatrix} x_0 \\ x_1 \\ \vdots \\ x_{2n} \end{pmatrix}, \quad \mathbf{u} = \begin{pmatrix} Q_1 \\ \Delta p_2 \end{pmatrix}, \quad \mathbf{y} = \begin{pmatrix} Q_2 \\ \Delta p_1 \end{pmatrix} \quad (\text{C.9})$$

The matrices \mathbf{A} , \mathbf{B} and \mathbf{C} are defined as:

$$\mathbf{A} = \text{diag} \left(0, \mathbf{A}_1, \mathbf{A}_2, \dots, \mathbf{A}_n \right), \quad \left\{ \begin{array}{l} \mathbf{A}_{(2i,1)} = (-1)^{i+1} \frac{Z_0}{T} \\ \mathbf{A}_i = \begin{pmatrix} -\frac{\epsilon_i}{T} & -\frac{\omega_i}{T^2} \\ 1 & 0 \end{pmatrix} \end{array} \right. \quad (\text{C.10})$$

$$\mathbf{B} = \begin{pmatrix} \mathbf{B}_0 \\ \mathbf{B}_1 \\ \vdots \\ \mathbf{B}_n \end{pmatrix} \quad \left\{ \begin{array}{l} \mathbf{B}_0 = \begin{pmatrix} 1 & 0 \end{pmatrix} \\ \mathbf{B}_i = -\frac{2}{(2i-1)\pi} \begin{pmatrix} 0 & 1 \\ 0 & 0 \end{pmatrix} \end{array} \right. \quad (\text{C.11})$$

$$\mathbf{C} = \begin{pmatrix} \mathbf{c} & \mathbf{C}^* \end{pmatrix} \begin{cases} (\mathbf{c})_i = (-1)^{i+1} \frac{2\sigma_i Z_0}{T} \\ (\mathbf{C}^*)_{i,2i} = \frac{2\sigma_i(8b_1 D_n - \epsilon_i)}{T} \\ (\mathbf{C}^*)_{i,2i+1} = -\frac{2\sigma_i \omega_i^2}{T^2} \\ (\mathbf{C}^*)_{k,l} = 0, \text{ when } k \neq 2l \text{ or } k \neq 2l+1 \end{cases} \quad (\text{C.12})$$

The following vectors \mathbf{e} , \mathbf{d} , \mathbf{f} and e_0 are defined as:

$$(\mathbf{d})_i = -\frac{4\sigma_i}{(2i-1)\pi} \quad (\text{C.13})$$

$$e_0 = -\frac{8b_2 D_n}{T}, \quad (\mathbf{e})_i = -\frac{(2i-1)\pi}{2TZ_0} \quad (\text{C.14})$$

$$(\mathbf{f})_i = (-1)^{i+1} \quad (\text{C.15})$$

With the modal natural frequency ω_i and the modal damping coefficient ϵ_i :

$$\omega_i = \alpha_i - \frac{1}{2}\sqrt{2\alpha_i D_n} + \frac{1}{2n} \quad (\text{C.16})$$

$$\omega_i = \alpha_i - \frac{1}{4}\sqrt{\alpha_i \epsilon} + \frac{1}{2} \quad (\text{C.17})$$

$$\epsilon_i = \sqrt{2\alpha_i D_n} + D_n, \quad i = 1, 2, 3, \dots, n \quad (\text{C.18})$$

The attenuation factors with Riemann windowing read

$$\sigma_i = \frac{\sin \beta_i}{\beta_i} \quad (\text{C.19})$$

$$\alpha_i = \frac{(2i-1)\pi}{2}, \quad \beta_i = \frac{(2i-1)\pi}{2n+1} \quad (\text{C.20})$$

$$b_1 = \left(2 \sum_{i=1}^n \frac{\sigma_i}{\omega_i^2} \right)^{-1}, \quad b_2 = \pi b_1 \sum_{i=1}^n (-1)^{i+1} (2i-1) \frac{\sigma_i}{\omega_i^2} \quad (\text{C.21})$$

C.3. BLOCKED LINE EXAMPLE

The following graph presents a blocked line example to show the comparison between results of the method of characteristics, the modal approximation and the modal approximation with attenuation factors or filtering.

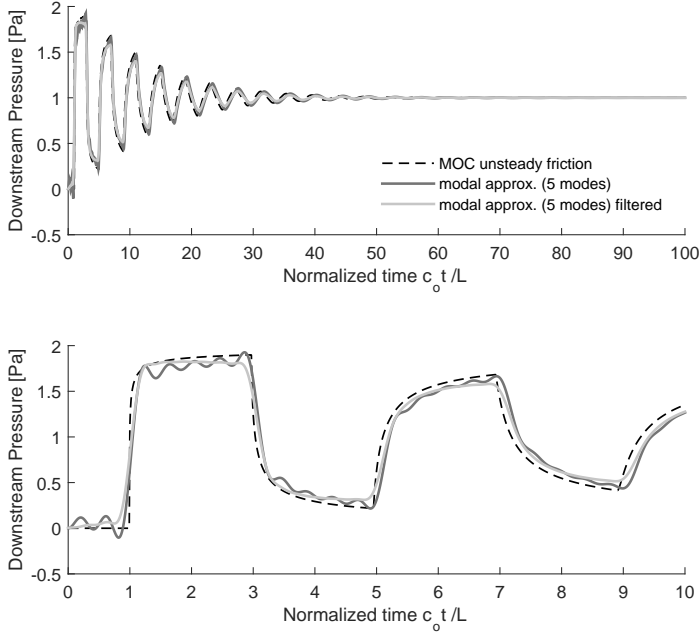


Figure C.1: Comparison of the pressure response of a blocked line to a step pressure, $D_n = 0.01$.

D

MODEL PARAMETERS FOR TIME-DOMAIN SIMULATIONS

The parameter values used for the time domain simulations of the hydraulic concepts are given by the following Table.

Parameter	Symbol	Unit	Value	Parameter	Symbol	Unit	Value
Pump mass moment of inertia	J_p	[kgm ²]	3680	Motor mass moment of inertia	J_m	[kgm ²]	50
Water pump mass moment of inertia	J_{wp}	[kgm ²]	51	Pelton runner mass moment of inertia	J_{runner}	[kgm ²]	80
Generator mass moment of inertia	J_{gen}	[kgm ²]	50	Pump volumetric displacement	\bar{V}_p	[L/rev]	626
Motor volumetric displacement	\bar{V}_m	[L/rev]	4.9	Water pump volumetric displacement	\bar{V}_{wp}	[L/rev]	10.2
Nom. press. of pump & motor	p_{nom}	[Pa]	350e5	Nom. press. of water pump	$p_{wp,nom}$	[Pa]	250e5
Nom. volumetric eff of pump	$\eta_{vol,p}$	[-]	0.98	Nom. volumetric eff of motor	$\eta_{vol,m}$	[-]	0.98
Nom. volumetric eff of water pump	$\eta_{vol,wp}$	[-]	0.90	Pump nom. speed	n_p	[rpm]	12
Motor nom. speed	n_m	[rpm]	1500	Water pump nom. speed	n_{wp}	[rpm]	1500
Pump laminar leakage coeff.	$C_{s,p}$	[m ³ /s/Pa]	7.1e-11	Motor laminar leakage coeff.	$C_{s,m}$	[m ³ /s/Pa]	7.0e-11
Water pump laminar leakage coeff.	$C_{s,wp}$	[m ³ /s/Pa]	1.0e-9	Pump dry friction coeff.	$C_{f,p}$	[-]	0.02
Motor dry friction coeff.	$C_{f,m}$	[-]	0.02	Water pump dry friction coeff.	$C_{f,wp}$	[-]	0.02
Pump viscous damping coeff.	B_p	[Nms]	50e3	Motor viscous damping coeff.	B_m	[Nms]	2.5
Water pump viscous damping coeff.	B_{wp}	[Nms]	1.0	Rotor shaft viscous damping coeff.	B_r	[Nms]	0
Motor shaft viscous damping coeff.	B_{shaft}	[Nms]	1.0	Generator shaft viscous damping coeff.	B_{gen}	[Nms]	0.0
Pitch servo constant	K_β	[deg/s]	10.0	Pitch time constant	t_β	[s]	0.05
Pitch time delay	δ	[s]	0.05	Oil pipe line internal diameter	D_{oc}	[m]	0.25
Water pipe line internal diameter	D_{wc}	[m]	0.50	High pressure oil line length	L_{oc}	[m]	100
Water line length	L_{wc}	[m]	1000	Nozzle discharge coeff.	C_d	[-]	0.95
Nozzle vena contracta	C_v	[-]	0.99	Pelton pith circle diameter	D_{PCD}	[m]	3.0
Pelton buckets friction factor	ξ	[-]	0.9	Jet relative angle	γ	[deg]	165
Density of mineral oil	ρ_{oil}	[kg/m ³]	917	Density of seawater	ρ_{sw}	[kg/m ³]	1020
Kinematic viscosity of oil	ν_{oil}	[m ² /s]	40e-6	Kinematic viscosity of seawater	ν_{sw}	[m ² /s]	1e-6
Effective bulk modulus of oil	E_{oil}	[Pa]	1.0e9	Effective bulk modulus of seawater	E_{sw}	[Pa]	2.0e9

SAMENVATTING

Offshore-windenergie is een competitieve energiebron in de toekomstige Europese energiemix aan het worden. De groei van wind op zee is duidelijk zichtbaar in de grote windparken die worden gepland en gebouwd in de Noordzee, waarmee al vermogens op GW-niveau worden behaald. In de huidige toepassing wordt de geproduceerde elektriciteit per wind turbine in een windpark naar een centraal offshore-platform geleid en daar geconditioneerd, voordat het door kabels over de zeebodem naar de kust wordt getransporteerd. Zo gezien kan een offshore-windpark worden beschouwd als één energiecentrale die elektriciteit produceert door middel van honderden multi-MW-generatoren. De motivatie achter deze dissertatie volgt daarom het idee van elektriciteitsproductie op een gecentraliseerde wijze in een windpark, waarvoor slechts enkele hoge-capaciteitsgeneratoren benodigd zijn.

Het gepresenteerde werk in deze dissertatie verkent een nieuwe manier van generatie, bijeenbrenging en transmissie van windenergie binnen een windpark, waar geen tussentijdse elektrische omzetting plaatsvindt, totdat de energie het centrale offshore-platform heeft bereikt. Een gecentraliseerde vorm van energiegeneratie is beschouwd, waarbij gebruik gemaakt wordt van watertechnologie. In het voorgestelde concept is de conventionele versnellingskast of de directe aandrijving vervangen door een verdringingspomp, waardoor vanuit de rotor-gondelassenblage water onder druk in een hydraulisch netwerk gebracht wordt. Het water wordt onder hogedruk vanaf de wind turbines van het windpark bijeengebracht en doorgeleid naar het centrale offshore-platform, waar vervolgens elektriciteit wordt gegenereerd door een Peltonturbine.

Voor het beschrijven van de energie-omzetting, alsmede het voornaamste dynamische gedrag van de voorgestelde hydraulische windkrachtcentrale, is een numeriek model ontwikkeld. Het model vat de relevante fysica van de dynamische interactie tussen de verschillende turbines, gekoppeld met een algemeen hydraulisch netwerk en een regelaar. Gereduceerde-orde modellen voor de verschillende componenten worden gepresenteerd in de vorm van gekoppelde algebraïsche vergelijkingen en gewone differentiaalvergelijkingen voor hun toepassing in tijdsdomeinsimulaties. Bijzondere aandacht wordt gegeven aan het modeleren van hydraulische netwerken, waar een semi-analytische aanpak wordt gepresenteerd voor transiënte laminaire stromingen, gebruikmakend van een tweedimensionaal viskeus compressiemodel. Het model biedt de mogelijkheid om sterke variaties in de voortgaande drukgolven te analyseren, welke resultaten van abrupte veranderingen in de stroming of druk geïntroduceerd door ventielsluitingen of componentfalen. Daarnaast kan met het model de geschiktheid van andere methoden, zoals modale benaderingen, gebruikt voor het representeren van kortdurende aspecten van het hydraulische netwerk, worden beoordeeld.

Vanuit het regelsysteem gezien dient als gevolg van het verwijderen van de individuele generatoren en de vermogenselektronica uit de turbines de hydraulische aandrijving de regelacties te vervangen om hetzelfde of ten minste een vergelijkbare variabele-

snelheidsfunctionaliteit van moderne windturbines te bereiken. Zowel passieve als actieve regelstrategieën worden voorgesteld, gebruikmakend van hydraulische componenten voor een enkele variabele-snelheidswindturbine. Lineaire regelanalyse-instrumenten worden gebruikt om de prestatie van de voorgestelde regelaars te evalueren. De passieve controlestrategie toont aan inherent stabiel te zijn door gebruik te maken van een spuitmond met een constant oppervlak voor windsnelheden lager dan de optimale windsnelheid. De toepassing van deze strategie vergt het geschikt dimensioneren van de hydraulische componenten gebruikt om de optimale snellopendheid te bereiken, terwijl de druk in het hydraulische netwerk variabel is. De passieve strategie is simpel en robuust, maar is beperkt tot een enkele turbine. Aangezien meerdere turbines tot hetzelfde hydraulische netwerk behoren zou een constante-druksysteem de voorkeur verdienen. Een actieve regelstrategie is ook geanalyseerd om een variabele-snelheidsrotor te verkrijgen, terwijl de druk in het hydraulische netwerk constant gehouden wordt. De constante-drukregelaar is bereikt door het oppervlak van de spuitmond aan te passen door een lineaire actuator. Een combinatie van een PI-regelaar in serie met een laagdoorlaatfilter en inkepingen is toegepast om de invloed van de pijplijndynamica op de drukresponsie te reduceren. Hiernaast is een pomp met variabel debiet, werkend met een gecontroleerde druk, toegepast om het doorgegeven moment aan de rotor aan te passen.

Twee casussen zijn beschouwd in de tijdsdomeinsimulaties voor een hypothetisch hydraulisch windpark onderhevig aan turbulente windcondities. De prestatie- en operationele parameters van individuele turbines zijn vergeleken met die van een referentiewindpark met conventionele-technologieturbines, gebruikmakend van dezelfde windparklay-out en omgevingscondities. De resultaten van de gepresenteerde casus geven aan dat de individuele windturbines kunnen werken binnen de operationele limieten met het concept met de constante-drukregelaar. Het hydraulische windpark is ondanks de stochastische invoer voor de turbulente wind en zogeeffecten in staat om elektriciteit te produceren met een redelijke prestatie zowel onder als boven optimale-windcondities.

PUBLICATIONS BY THE AUTHOR

JOURNAL PUBLICATIONS

- Jarquín Laguna, A. Modeling and analysis of an offshore wind turbine with fluid power transmission for centralized electricity generation. *Journal of Computational and Nonlinear Dynamics: Special issue wind turbine modelling*, 10(4):pp.11–24, 2015.
- Jarquín Laguna, A. Simulation of an offshore wind farm using fluid power for centralized electricity generation. *Wind Energy Science Discussions*, 2016. doi: 10.5194/wes-2016-54. URL <http://www.wind-energ-sci-discuss.net/wes-2016-54/>. (under review).
- Jarquín Laguna, A. and Tsouvalas, A. Transient laminar flow in hydraulic networks based on a semi-analytical impulse response method. *HERON: Special issue dynamics of structures*, 59(1):pp.37–55, 2014.
- Jarquín Laguna, A., Diepeveen, N., and Van Wingerden, J. Analysis of dynamics of fluid power drive-trains for variable speed wind turbines: Parameter study. *IET Renewable Power Generation*, 8(4):pp.398–410, 2014.

CONFERENCE PUBLICATIONS

- Diepeveen, N. and Jarquín Laguna, A. Dynamic modeling of fluid power transmissions for wind turbines. In *Proceedings of the EWEA Offshore 2011 Conference, Amsterdam*. European Wind Energy Association, 2011.
- Diepeveen, N. and Jarquín Laguna, A. Wind tunnel experiments to prove a hydraulic passive torque control concept for variable speed wind turbines. In *Journal of Physics: Conference Series*, volume 555(1), page 012028. the European Academy of Wind Energy, IOP Publishing, 2014a. The Science of Making Torque from Wind 2012.
- Diepeveen, N. and Jarquín Laguna, A. Preliminary design of the hydraulic drive train for a 500kw prototype offshore wind turbine. In *Proceedings of the 9th International Fluid Power Conference*, pages 133–144. RWTH Aachen, 2014b.
- Jarquín Laguna, A. Fluid power network for centralized electricity generation in offshore wind farms. In *Journal of Physics: Conference Series*, volume 524(1), page 012075. the European Academy of Wind Energy, IOP Publishing, 2014. The Science of Making Torque from Wind 2014.
- Jarquín Laguna, A. Simulation of an offshore wind farm using fluid power for centralized electricity generation. In *Journal of Physics: Conference Series*, volume 753(10), page 102004. the European Academy of Wind Energy, IOP Publishing, 2016. The Science of Making Torque from Wind 2016.

- Jarquín Laguna, A. and Diepeveen, N. Performance evaluation of a hydraulic offshore wind turbine. In *Proceedings of the Renewable Energy Research Conference*. Trondheim, Norway, 2010.
- Jarquín Laguna, A. and Diepeveen, N. Dynamic analysis of fluid power drive-trains for variable speed wind turbines: A parameter study. In *Proceedings of the EWEA Offshore 2013 Conference, Vienna, Austria, 4-7 February 2013*. European Wind Energy Association, 2013.
- Jarquín Laguna, A. and Tsouvalas, A. A semi-analytical impulse response method for transient laminar flow in hydraulic networks. In *Proceedings of the XLIII International Summer School Conference of Advanced Problems in Mechanics*. St. Petersburg, Russia, 2015.

CURRICULUM VITÆ

Antonio JARQUÍN LAGUNA

02 June 1984 Born in Toluca, México.

EDUCATION

2002–2007	Diploma in Mechanical Engineering Universidad Nacional Autónoma de México, (México, D.F.) National Autonomous University of Mexico
2008–2010	Master of Science in Sustainable Energy Technology Delft University of Technology Faculty of Applied Sciences
2011–2016	Ph.D. Research Delft University of Technology Faculty of Civil Engineering and Geosciences Department of Hydraulic Engineering Section of Offshore Engineering
2016–present	Researcher at Delft University of Technology

PROFESSIONAL

2007–2008	Analysis Engineer The General Electric Company Engine Dynamics & Structural Systems GEIQ Aviation, Querétaro, México
2010–2012	Solution Development Engineer Bluewater Energy Services BV New energy group, Hoofddorp, the Netherlands